International Scientific-Technical and Production Journal

The Paton WELDING JOURNAL

May 2009 # 5

English translation of the monthly «Avtomaticheskaya Svarka» (Automatic Welding) journal published in Russian since 1948

Founders: *E.O. Paton Electric Welding Institute of the NAS of Ukraine*
International Association «Welding»

Publisher: *International Association «Welding»*

Address:
E.O. Paton Electric Welding Institute,
International Association «Welding»,
11, Bozhenko str., 03680, Kyiv, Ukraine
Tel.: (38044) 287 67 57
Fax: (38044) 528 04 86
E-mail: journal@paton.kiev.ua
http://www.nas.gov.ua/pwj

State Registration Certificate
KV 4790 of 09.01.2001

Subscriptions:
$324, 12 issues per year,
postage and packaging included.
Back issues available.

CONTENTS

ANALYSIS OF CONDITIONS CAUSING INITIATION AND PROPAGATION OF CORROSION CRACKS IN ZONES OF CIRCUMFERENTIAL JOINTS ON MAIN GAS PIPELINES

V.I.MAKHNENKO, V.M. SHEKERA, E.A. VELIKOIVANENKO, O.I. OLEJNIK, G.F. ROZYNKA and **N.I. PIVTORAK**
E.O. Paton Electric Welding Institute, NASU, Kiev, Ukraine

The paper deals with conditions causing formation of corrosion cracks within the zones of circumferential field and longitudinal factory welded joints on main gas pipelines. Described is the case study of force conditions and resistance of material to initiation and propagation of stress corrosion cracks up to a spontaneous fracture.

Keywords: *welded main gas pipelines, circumferential welded joints, initiation and propagation of corrosion cracks, crack resistance diagram, nominal stresses, stress concentration, stress intensity factors*

The most dangerous defects in welded main gas pipelines are corrosion cracks, which are relatively difficult to detect by using the in-pipe diagnostic method. Initiation and propagation of such defects up to critical sizes, when a spontaneous fracture takes place, are determined by a number of factors:

- fracture of corrosion-preventing insulation on the pipeline surface and, hence, formation of contact with the environment (soil);
- time of dwelling of the pipe wall, Δt_c, under stress corrosion conditions;
- degree of aggressiveness of the environment (humidity of soil, its chemical composition, etc.);
- level of tensile stresses in the pipeline wall, and presence of stress concentration zones;
- ability of the pipeline wall material to resist initiation and growth of corrosion cracks.

The presence of the above factors is a precondition for initiation and propagation of corrosion cracks. However, each of them is not sufficient for formation of the given type of defects.

As a rule, the time of reliable operation of a protective coating on a pipeline is markedly shorter than the specified and actual life time of the pipeline itself. Here the probability of fracture (separation) of the coating depends upon its type, deposition and service conditions. The zone of field welded joints may be very vulnerable, depending upon the coating deposition conditions.

Time Δt_c of dwelling of the pipeline wall with a fractured coating in the stress corrosion conditions is hard to estimate by deterministic calculations. Estimation of this value greatly depends upon the periodicity of monitoring of the state of insulation (or re-insulation) on the pipeline, duration of shutdowns of the pipeline, changes in aggressiveness of the environment, etc. A sufficiently conservative estimate of Δt_c made by the reliable methods of monitoring of the state of the insulation coating is an interval between regular inspections (about 2–5 years), providing that they are combined in time with the in-pipe diagnostics of the state of the pipeline wall. It is very important that during time Δt_c the corrosion cracks, allowing for their initiation and growth (coalescence), do not reach their critical sizes, at which the spontaneous fracture takes place.

The degree of aggressiveness of the environment for main gas pipelines is determined primarily by properties of those soils wherein the pipelines are laid down (the issue of corrosion damages on the internal surfaces, which is characteristic of oil pipelines [1], is not considered in this study). In this case, of high importance is the degree of humidity of the soil caused by periodic or continuous inflow of moisture.

As shown by the results of investigations conducted by the E.O. Paton Electric Welding Institute, in the case of periodic moistening of the soil, when it dries out, a film of corrosion products appears on the crack surface. Fracture of this film after an intensive moisture inflow takes some time, this having a marked effect on average values of the rate of crack growth through thickness of the wall at constant stresses induced by a force load. Constant and rather high humidity of the aggressive environment is characteristic of main pipelines laid down in marshland, on the bottom of lakes, rivers and seas. When they are laid down into the firm soil, a high humidity associated with atmospheric precipitates is of a periodic character. Considering the above circumstances, experimental studies of the kinetics of growth of corrosion cracks under laboratory conditions at a constant high humidity (water solutions of extracts of corresponding soils [2]) yield conservative data, which at the given stage of investigation of the problem are fully acceptable to predict remaining safe service life of pipelines.

The level of nominal tensile stresses in the pipe wall is determined by an internal pressure of gas in a pipe, as well as by bending deformations associated most often with subsidence of the soil under the pipe and bending moments due to the dead weight of the pipe and backfilling material. Local geometric peculiarities (e.g. zones of welded joints) causing the con-

centration of nominal stresses are also of high importance. As a rule, these zones in a region of longitudinal (factory) and circumferential (field) welded joints are most vulnerable to formation and propagation of longitudinal and circumferential corrosion cracks, respectively.

As known from practice, corrosion cracks may form and develop in the zone of both longitudinal and circumferential welds, although conditions of initiation of relatively normal stresses responsible for formation and development of such defects are different. Under conventional conditions, where a pipe conforms to the soil and bending deformations are insignificant, the longitudinal welded joints are more vulnerable to the nominal normal stresses (other conditions being equal) than the circumferential ones. However, factory conditions provide in a number of cases a lower stress concentration in the longitudinal welded joints than in the circumferential ones, which may retard initiation and growth of a corrosion crack at the initial stage of its development.

When pipelines are loaded only with the internal pressure, the said factor will take place only if values of the stress concentration coefficient within the zone of a field circumferential weld on the external surface of a pipe are 2 times higher than within the zone of a longitudinal weld made under factory conditions. The latter is confirmed by the known dependencies that relate the sources of stress concentration in the butt welded joints (Figure 1).

Total coefficient α of the concentration of nominal stresses, $\sigma^{n}_{jj} = Q_j/s$, acting across a welded joint, which is related to the geometry (shape) of the butt weld, α_{sh}, via probable edge displacement α_d and angular deformations α_a, can be expressed through the following dependence [3]:

$$\alpha = [1 + (\alpha_d + \alpha_a - 2)]\alpha_{sh}, \qquad (1)$$

where

$$\alpha_{sh} = 1 + \left(\frac{s}{\rho}\right)^{2/3} \left\{\frac{s}{g}\,\mathrm{ctg}\,\theta + 4.0 + \frac{s}{1 + l/s}\right\}^{-2/3}$$

at $0.15 \le l/s \le 2.5$; $0.01 < \rho/s \le 0.1$; $0.1 \le g/s \le 0.2$, and $\theta \le 30°$ (designations in (1) correspond to geometric parameters of the butt joint in Figure 1).

For a butt joint of the longitudinal weld, it can be assumed that $\alpha_d = 1$ and $\alpha_a = 1$. For the circumferential weld, the values of α_d and α_a are more than 1. However, if we assume them to be equal to 1, i.e. that there is no edge displacement and no angularity, then even due to α_{sh} with the s/ρ ratio increased 3 times, other conditions being equal, α increases 2 times. Naturally, with the quality of the circumferential field welded joint at a level of that of the longitudinal factory one, the longitudinal weld zone will be more vulnerable to initiation of corrosion cracks.

Nevertheless, the focus in a number of studies (e.g. [4]) is on corrosion cracks and fracture within the zone of circumferential field welded joints on main gas pipelines, the said phenomena being associated

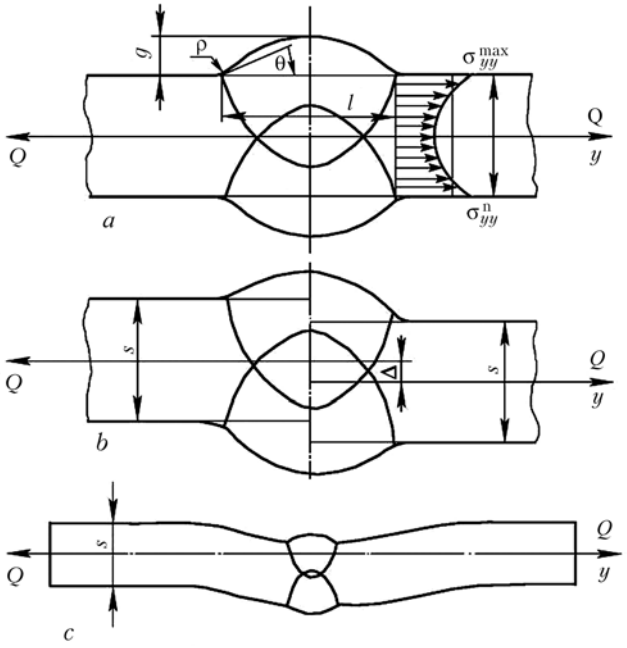

Figure 1. Geometric parameters of the butt joint determining the concentration of stresses caused by the weld shape (*a*), edge displacement (*b*) and presence of angular deformations (*c*)

with the presence of bending moments forming in subsidence of the soil along the length of a pipeline and its corresponding deflection l. The resulting maximal stresses due to internal pressure P of the distributed load (weight of pipe and backfilling material) along axis z of the pipe will be

$$\sigma^{max}_{zz} = P\,\frac{R}{2\delta} + M_{max}\left(\frac{1}{\pi R^2\delta} + \frac{1}{2\pi R^3}\right), \qquad (2)$$

where $M_{max} = \dfrac{(q_p + q_s)l^2}{B}$; q_p is the weight of a unit length of the pipe; $q_p = \gamma_p 2\pi R\delta$; q_s is the weight of the backfilling material per unit length of the pipe; $q_s = \gamma_s A_s$; γ_i is the specific weight of the pipe metal (i = p) or soil (i = s); A_s is the cross section area of the backfilling material (Figure 2) with height h over the upper generating line of the pipeline

$$A_s = \frac{R}{2}\,[4h + R(4 - \pi)]. \qquad (3)$$

The B values vary from 12 (in the middle of span deflection l) to 24 (at the span ends). For the case considered in [4], i.e. for the pipe of X70 type steel ($2R\times\delta$ = 1420×15.5 mm) at γ_p = 7.7 N/cm^3 and γ_s = = 4.9 N/cm^3, h = 120 cm and A_s = 19200 cm^2, we will get that q_p = 52.6 N/cm = 5.26 N/mm and q_s = = 941.8 N/cm = 94.18 N/mm.

Accordingly, the values of maximal nominal stresses determined from (2), depending upon length l of the span deflection at P = 7.5 MPa, are given in Table 1.

As circumferential stresses $\sigma_{\beta\beta}$ due to deflection of the pipe within the limits of the considered values of l vary very slightly and are equal to 343.6 MPa, it follows from the above data that initiation and propa-

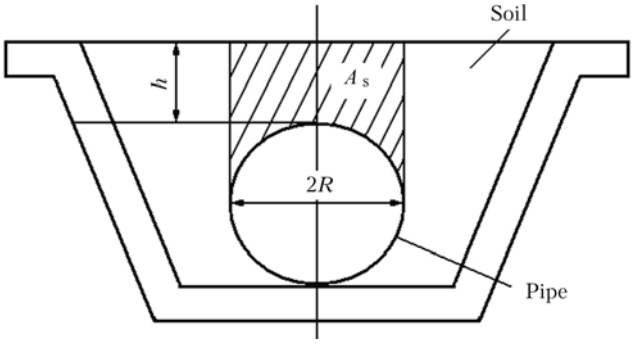

Figure 2. Schematic of cross section of a trench with main pipeline laid down in it

gation of corrosion cracks will be faster in the longitudinal joint at $l < 20$ m and at the identical quality of the factory and field joints (i.e. identical values of α). However, at higher values of α in the circumferential field joint, or at $l > 25$ m and identical values of α, initiation of such defects may occur faster within the zone of this joint. It is particularly from these positions for the specific case under consideration that study [4] explains formation of circumferential corrosion cracks within the zone of the circumferential field weld on the Yamburg–Western Border gas pipeline, which eventually led to fracture of the pipeline. According to the data of the corresponding examination, the fracture was preceded by propagation of a circumferential corrosion crack up to its maximal size (length $2c = 525$ mm, depth $a = 8$ mm).

Modern methods of fracture mechanics for the crack-containing bodies of revolution [3] make it possible to determine that with the said sizes of a crack, $2c \times a$, its spontaneous propagation occurs with a higher probability at $l \approx 20$ m. According to [3], criterion of the spontaneous growth of the given crack can be written down as follows:

$$Y = K_r - f(L_r) > 0, \quad (4)$$

where $K_r = K_I / K_{IC}$ is the ratio of calculated stress intensity factor K_I on a contour of the given crack to the critical value of K_{IC} for a certain pipe material in this zone:

$$f(L_r) = (1 - 0.14L_r^2)\,[0.3 + 0.7 \exp(-0.65L_r^6)] \text{ at } L_r \le L_r^{\max}; \quad (5)$$

$$f(L_r) = 0 \text{ at } L_r > L_r^{\max}.$$

For pipe steels (Fe–Mn–C system), $L_r^{\max} = 1.3$, according to [5], based on the fracture determination diagram (FDD) under static loading of crack-containing bodies (Figure 3); $L_r = \sigma_{ref} / \sigma_y$ (where σ_y is the yield stress of the material, and σ_{ref} is the reference stress corresponding to initiation of plastic instability in the crack zone under the given type of loading). According to [5], it holds for the case under consideration

$$\sigma_{ref} = \frac{1}{3}\left[\sigma_b + \sqrt{\sigma_b^2 + (\sigma_m^{3Z})^2}\right], \quad (6)$$

where σ_b is the purely bending component of stress $\sigma_{zz}^{\max}$ in (2); $\sigma_b = M_{\max}\, 1/2\pi R^3$; σ_m are the membrane stresses, $\sigma_m = P(R/2\delta) + M_{\max}\,(1/\pi R^2\delta)$ (2); and the values of Z are determined from the following relationship:

$$Z = \frac{\pi}{2 \arccos(A \sin\theta) - \frac{a}{\delta}\theta\left[\frac{2 - 2\delta/R + a/R}{2 - \delta/R}\right]}; \quad (7)$$

where

$$\theta = \frac{2c\pi}{8R};$$

$$A = \frac{a}{\delta}\,\frac{(1 - \delta/R)(2 - 2\delta/R + a/R) + (1 - \delta/R + a/R)^2}{2\,[1 + (2 - \delta/R)(1 - \delta/R)]}.$$

Allowing for the above values of a, δ, R and c, we obtain that $A = 0.565$, $\theta = 0.290$, and $Z = 1.177$. The corresponding results of calculations of σ_{ref} for nominal stresses $\sigma_{zz}^{\max}$ in sections at the ends and centre of sag l are given in Table 2. The Table also gives the values of L_r at $\sigma_y = 490$ MPa. It can be seen from the Table that the values of L_r do not exceed $L_r^{\max} = 1.30$. According to [5], the values of K_I at the crack apex at $a/c < 0.01$ can be found from the following relationship:

$$K_I = \sqrt{\pi a}\,(G_0\sigma_m + G_1\sigma_b), \quad (8)$$

where $G_0 = 2.3$, and $G_1 = 1.1$ [5].

The Table also shows the results of calculations of K_I from (8). To calculate $K_r = K_I / K_{IC}$, it is necessary

Table 1. Maximal stresses in different regions of span deflection

Span deflection location	$\sigma_{zz}^{\max}$, MPa, at l, m			
	0	10	20	30
Centre	171.8	206.3	309.8	482.3
End	171.8	189.0	240.8	327.0

Note. Sag $f(1/2) \approx 120(1/20)^2$ [mm] for the pipe at the centre of span deflection.

Table 2. Calculated values of σ_{ref}, L_r and K_I for circumferential crack with size $2c \times a = 525 \times 8$ mm in pipe (1420×15.5 mm) in different regions of span deflection l

l, mm	Span centre			Span end		
	σ_{ref}, MPa	L_r	K_I, MPa·m$^{1/2}$	σ_{ref}, MPa	L_r	K_I, MPa·m$^{1/2}$
0	202.2	0.413	62.6	202.2	0.413	62.6
10	242.8	0.495	75.2	222.4	0.453	68.9
20	364.6	0.744	112.9	283.4	0.578	87.8
30	567.7	1.160	175.8	384.9	0.785	119.2

to know the values of K_{IC} within the crack zone determined for a specific pipe steel of the X70 type at a temperature of the external surface of the pipe.

The authors of study [5] recommend using the corresponding correlation dependencies that relate K_{IC} to integral J_{IC} or impact toughness KCV to calculate K_{IC}, if experimental data are unavailable. In particular, when using the Rolve–Navak correlation dependence [5] in the form

$$K_{IC} = 8.47(KCV)^{0.63}, \quad (9)$$

which corresponds to the minimal level of the K_{IC} values, at which the probability of non-fracture is not lower than 0.05, this yields $K_{IC}(0.05) = 110.8$ MPa·m$^{1/2}$ for the X70 type pipe steel at $KCV^{+20} \approx 59.2$ J/cm^2.

For the probability of non-fracture equal to $p > 0.05$, we will use the following relationship [5]:

$$K_{IC}(p) = 20 + K_d[-\ln(1-p)^{0.25}\ [\text{MPa·m}^{1/2}]. \quad (10)$$

At $K_{IC}(0.05) = 110.8$ MPa·m$^{1/2}$, $K_d = 190.8$ MPa·m$^{1/2}$. Therefore, $p = 0.5K_{IC}(0.50) = 194.1$ MPa·m$^{1/2}$ and $p = 0.94K_{IC}(0.95) = 271$ MPa·m$^{1/2}$. Figure 3, *a* shows the calculated $K_r(L_r)$ curves for the case where a corrosion crack is at a section of the centre of deflection of the span with length l at different values of $K_{IC}(p)$. The points of intersection of these lines with the FDD curve show under what conditions the probability exists of a spontaneous fracture due to the considered corrosion crack depending upon l and p. It can be seen from the Figure that at the brittle fracture resistance of a material equal to $K_{IC} = 110.8$ MPa·m$^{1/2}$ that corresponds to non-fracture probability $p = 0.05$, critical length $l_{cr} = 17.2$ m; $l_{cr} = 23.7$ m at $p = 0.50$; and $l_{cr} = 27.0$ m at $p = 0.95$.

These results were obtained for the field joint located at the centre of the span deflection and subsidence of the soil under a pipe. The results obtained for the joint located in the zone of the span deflection ends at $p = 0.05$ $l_{cr} = 25$ m and $p \geq 0.5$ $l_{cr} < 30$ m are shown in Figure 3, *b*. 2–3 pipes can be accommodated along length $l > 30$ m at a distance between the circumferential welded joints equal to 8–12 m, i.e. there is always a joint near the span deflection centre. Therefore, the data shown in Figure 3 determine the upper and lower bounds of real values. This suggests that in the case under consideration the values of l ranged from 20 to 25 m, which seems to be enough for a spontaneous growth of the considered crack with sizes $2c \times a = 525 \times 8$ mm. However, in terms of its formation, a marked increase in stress concentration α did take place in the zone of the circumferential joint. The process of formation and propagation of a corrosion crack up to its critical size under working pressure $P = 7.5$ MPa and $l = 20$–25 m can be described as follows.

Fracture of the insulation is followed by the process of stress corrosion by the mechanism of anodic dissolution, where the pipe surface is covered by a network of fine cracks elongated in a direction normal to the effect of maximal tensile stresses. Appearance of such cracks depends both upon the level of the said stresses and upon the resistance of a material to their formation. That is why, they may initiate not necessarily

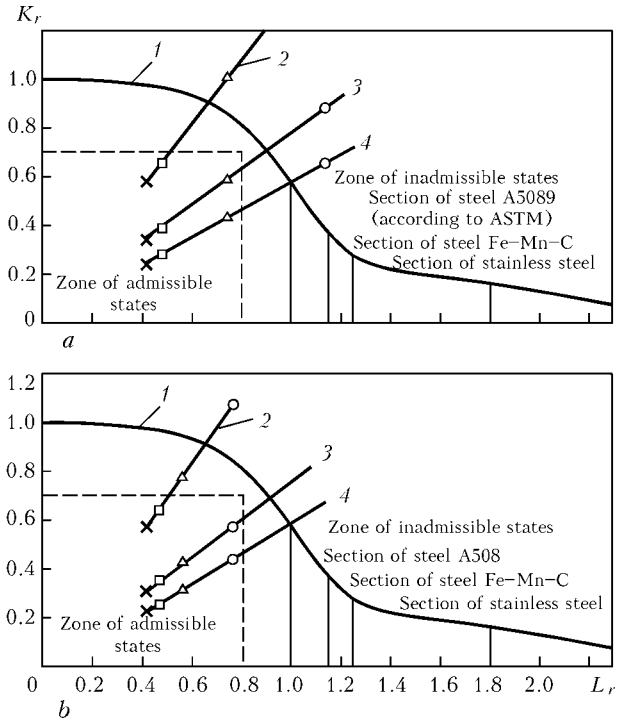

Figure 3. FDD (*1*) and calculated curves $K_r(L_r)$ plotted for a circumferential crack with sizes $2c \times a = 525 \times 8$ mm in pipe with Dn 1420×15.5 mm from steel of the X70 type at $p = 0.05$ (*2*), 0.50 (*3*) and 0.94 (*4*) for sections at the centre (*a*) and ends (*b*) of the span deflection: × ---- $l = 0$; ❐ ---- 10; Δ = 20; ○ ---- 30 m

at the stress concentrator apex (see Figure 1), where the material is hardened due to the thermal-deformation cycle of welding, and where it can acquire a higher resistance to stress corrosion than the material of the peripheral zone affected by this concentrator. As on the free surface across the concentrator extended along axis x (see Figure 1) stresses σ_{yy} are determined by the following relationship:

$$\sigma_{yy}(y) = \sigma_{yy}(y_c) + \int_{y_c}^{y} \frac{\partial \sigma_{xy}}{\partial x}\, dy, \quad (11)$$

where y_c is the coordinate of the apex of the concentrator of stresses σ_{yy}, the process of decreasing of stresses $\sigma_{yy}(y)$ occurs slowly with increase in the y values, compared with $\sigma_{yy}(y_c)$, because σ_{xy} changes but slightly along axis x.

In this connection, the practically observed formation of corrosion cracks in the base metal in parallel to the weld, at some distance from the fusion line [4], where resistance to formation of a defect is lower, is well explainable.

As the fine cracks propagate, they coalesce to form the avalanche cracks, the growth of which can now be determined by the diagram of static corrosion crack resistance for a given material in the aggressive environment [2] (Figure 4). According to this diagram, crack growth rate v is determined by stress intensity factor K_I at the corresponding points along the crack contour. Starting from certain sizes of such cracks, where $K_I > K_{ISCC}$, the main mechanism of their growth changes from anodic dissolution to hydrogen-induced embrittlement, at which the crack growth rate substantially increases.

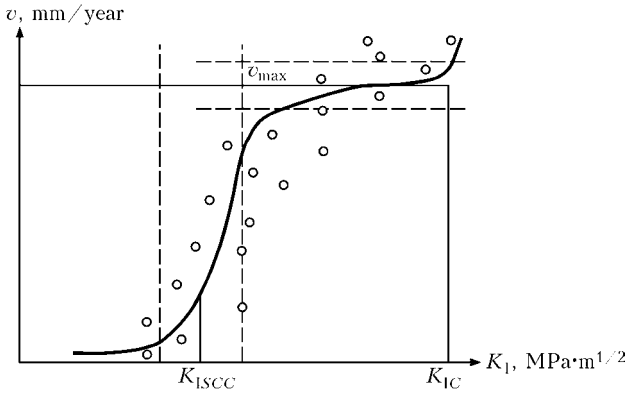

Figure 4. Diagram of static corrosion crack resistance of pipe steel

For shallow cracks extending along the circumferential weld, where $c >> a$, nominal stresses σ_{zz}^{max} are at a level of 300 MPa ($l \approx 20$ m), and $K_{ISCC} \approx 10$–15 MPa·m$^{1/2}$, this change takes place at a crack depth of $a = 0.1$ mm and crack length of $2c = 10$–15 mm [2]. The rate of growth of such cracks along their length is greatly affected by the process of coalescence of the neighbouring cracks, whereas that through the depth is affected by the intensity of removal of corrosion products. These circumstances hamper the estimation of development of a crack under actual conditions. However, if the diagrams of static corrosion crack resistance of the type of those shown in Figures 5 and 6 are available, it is possible to achieve some characteristic estimates with a certain degree of conservatism.

For example, for the considered circumferential crack with size $2c \times a = 525 \times 8$ mm, it is possible to estimate the time of its propagation from the initial size (approximately $2c_0 = 10$ mm, and $a_0 = 0.1$ mm), when it starts growing by the mechanism of hydrogen-induced embrittlement, i.e. from $K_I = K_{ISCC} \approx 12.5$ MPa·m$^{1/2}$ to $K_I^{max} \approx 0.9K_{IC}$, although data of the type of those given in Figures 5 and 6, obtained in short-time tests by the procedure described in [2], are usually limited to the values at a level of $K_I = 30$–40 MPa·m$^{1/2}$. For this we will use the known relationship [2]

$$\frac{da}{dt} = HK_I^2, \qquad (12)$$

where H is the constant proportionality coefficient for the given conditions, which is determined at $K_I > K_{ISCC}$.

Allowing for this approach, integrating (12) with respect to time from t_0 (initial size of crack is 0.1×10 mm) to t ($a = 8$ mm) yields $t - t_0 = 1.2$ year (for this the following experimental data were used: $K_I = 25$ MPa·m$^{1/2}$, $da/dt = 1/4$ mm/year, Figure 7). Accordingly, the average crack growth rate through depth is equal to 6.7 mm/year. The initial length of single crack, $2c_0 = 10$ mm, increases during this time approximately by 5–6 mm, as $K_I(c)$ on the crack surface is lower than $K_I(a)$ in its depth [3], i.e. for a crack to reach its critical length $2c = 525$ mm it is necessary that n single cracks with initial sizes $2c_0$

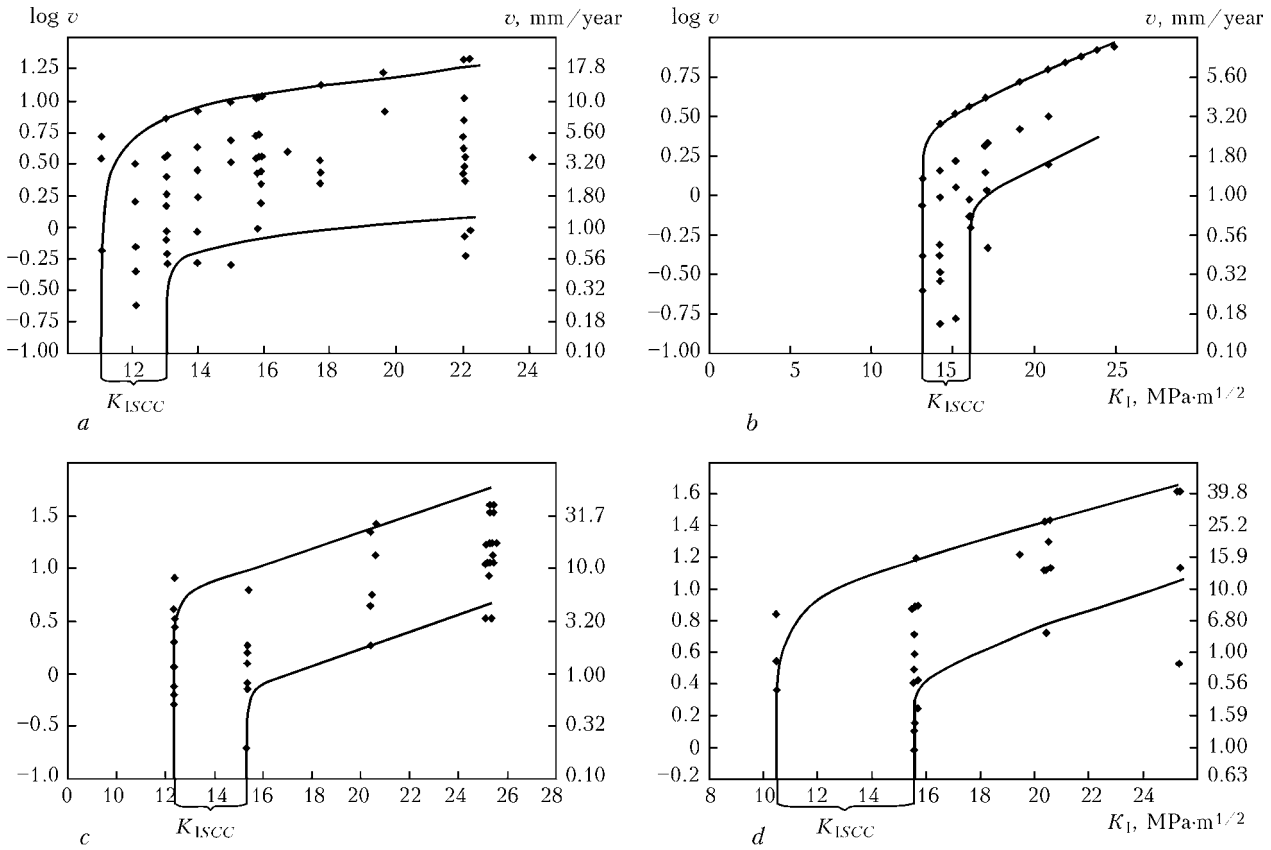

Figure 5. Diagrams of static corrosion crack resistance plotted for pipe steel 17G1S in short-time tests: *a* ---- 3 % NaCl solution, test time $t = 534$ h, average crack growth rate $v_{av} = 3.16$ mm/year; *b* ---- water extract of black soil, $t = 265$ h, $v_{av} = 2.12$ mm/year; *c* ---- water extract of loamy soil, $t = 271$ h, $v_{av} = 3.1$ mm/year; *d* ---- water extract of sand soil, $t = 163$ h, $v_{av} = 7.25$ mm/year

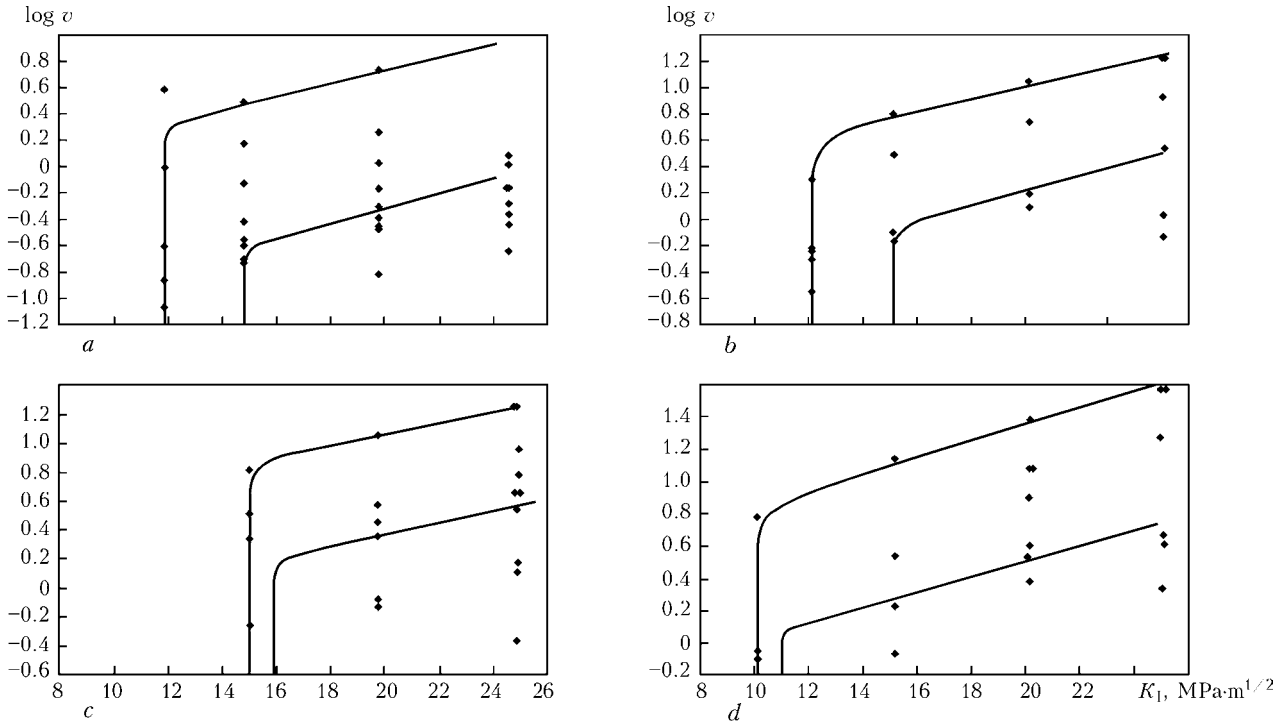

Figure 6. Diagrams of static corrosion crack resistance plotted for pipe steels X60 (*a, b*) and 13G1SU (*c, d*) in short-time tests: *a* ---- 3 % NaCl solution, t = 449 h, v_{av} = 0.41 mm/year; *b* ---- water extract of loamy soil, t = 167 h, v_{av} = 1.84 mm/year; *c* ---- 3 % NaCl solution, t = 168 h, v_{av} = 2.24 mm/year; *d* ---- water extract of loamy soil, t = 134 h, v_{av} = 4.2 mm/year

coalesce, where $n = 525/(2c_0 + 6) \approx 33$ at $2c_0 = 10$ mm, which is quite realistic.

Note the characteristic feature of growth of corrosion cracks, following from the results obtained by using the procedure described in [2] in three-point bend tests of the Charpy type specimens with a preliminarily grown fatigue crack about 100 mm long along the entire front of crack propagation. In analogy with cyclic loading [3], the registered increments of the crack, Δl (see Figure 7), correspond to a uniform distribution of increment Δa along the entire front of crack propagation. In Figure 7, such data are given for a constant value of K_I = 25 MPa·m$^{1/2}$ for a test time of about 168 h, during which 17 acoustic emission signals were fixed, i.e. each signal corresponding approximately to Δa = 0.0016 mm. Considering a high selectivity of the crack growth rate along the front, we have every reason to assume that, unlike the fatigue crack growth, the process of propagation of this crack occurs not simultaneously along the front, i.e. in this case each signal corresponds to crack area increment $\Delta S = 10\Delta a = 0.016$ mm^2 at its average size of $\Delta a > 0.0016$ mm and $2\Delta c < 10$ mm. However, this issue requires special investigations.

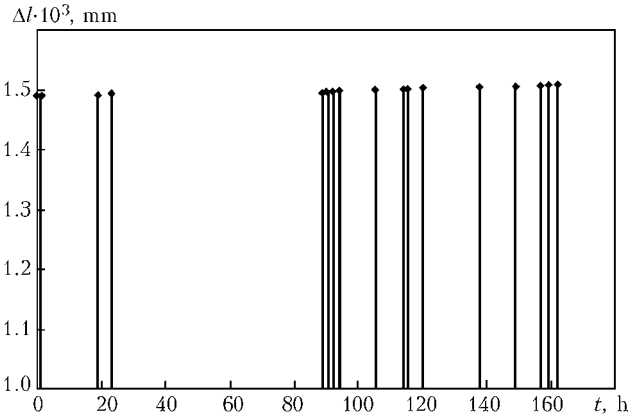

Figure 7. Increments Δl of a crack corresponding to one acoustic emission signal in test of the X60 type steel specimen in 3 % NaCl solution at K_I = 25 MPa·m$^{1/2}$

CONCLUSIONS

1. Subsidence of the soil in a trench under the main pipeline along a length of 20–30 mm is a source of extra nominal axial stresses in the pipe wall, which cause a substantial increase in the sensitivity to stress corrosion cracking in the zone of circumferential welds, compared with the longitudinal welds.

2. Approaches of fracture mechanics for crack-containing bodies, and availability of corresponding diagrams of static corrosion crack resistance allow an in-depth analysis of the process of kinetics of development of the said defects with time, which is very important for prediction of safe service life of main pipelines.

1. Andrejkiv, O.E., Kushnir, R.M., Tsyrulnyk, O.T. (2006) Determination of residual life of oil pipeline allowing for defects present in its wall and real service conditions. In: *Problems of life and service safety of structures, constructions and machines*. Kiev: PWI.
2. Makhnenko, V.I., Shekera, V.M., Onoprienko, E.M. (2008) Determination of parameters of simplified diagram of static corrosion crack resistance for pipe steels in soil corrosion. *The Paton Welding J.*, **10**, 26–30.
3. Makhnenko, V.I. (2006) *Safe service life of welded joints and assemblies on current structures*. Kiev: Naukova Dumka.
4. Romanenko, S.V. (2008) Analysis of the causes of fracture of main gas pipeline in transverse direction. *Gaz. Promyshlennost*, **1**, 55–57.
5. (2000) *Fitness-for-service:* Recommended practice 579. Washington: American Petroleum Institute.

TECHNOLOGICAL FEATURES OF ELECTRON BEAM WELDING OF DRILL BITS

V.M. NESTERENKOV, N.E. PROTOSEJ and **Yu.A. ARKHANGELSKY**
E.O. Paton Electric Welding Institute, NASU, Kiev, Ukraine

The peculiarities of electron beam welding of drill bits applied in oil production industry are considered. It is shown that the best quality of weld is achieved using elliptical scanning of electron beam at ratio of axes 2:1 and maximum amplitude equal to two radii of concentration of electron beam. To improve the quality of weld in a rotary part of drill bits, it is recommended to use inserts of modifying materials in the form of foil of up to 0.2 mm thickness.

Keywords: *electron beam welding, rotary drill bits, hardening steels, keyhole, through penetration, electron beam scanning, modifier*

To drill oil and gas wells the rotary drill bits are used, which are the main tool of a high speed drilling of earth rocks. Nowadays the total volume of rotary bit drilling reaches tens of millions of meters per year and further constant increase of this volume is required. Therefore, the problem of this updating the existing tool is challenging. The rotary bits are operating under severe conditions of influence of high abrasive liquid at high static and dynamic loads, therefore, the high requirements are specified to strength and service characteristics.

Nowadays, the electron beam welding (EBW) is widely used to join three elements of a bit into one structure (Figure 1). This method provides minimal deformations of bits at the lowest thermal effect on elements of rotary bearings. However, conventional materials, mainly steels 14KhN3A and 20KhN3A which are applied in the design of drill bits, have a restricted weldability and properties of metal of welded joints on these steels do not correspond in some cases to the conditions of high speed drilling. With the increase in sizes of bits and simultaneously in thicknesses being welded the probability of formation of small cracks in welded joints arises, thus leading to violation of their water-tightness and reduction in service life.

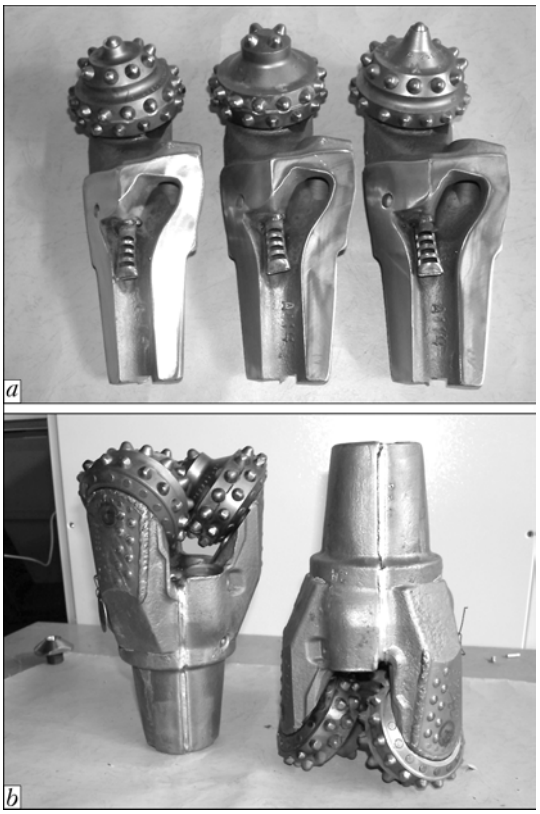

Figure 1. Appearance of three elements of a bit before assembly and welding (*a*) and a bit welded by electron beam (*b*)

To increase the service characteristics of welded joints it is possible either to select other materials for manufacture of bits or to modify the weld metal. In our opinion, the second method is more preferable from the point of view of its possibility to achieve the positive results at relatively small costs. It can be performed through feeding the alloyed filler wire into a weld pool or applying the foil produced of a material-modifier, which can be inserted into butts of bit being welded before welding. There are certain difficulties in feeding filler wire in welding of welds in a rotational area of a bit and violations in welds formation can be expected using inserts-modifiers, which increase a gap in the butt. The largest difficulties for quality formation is a weld region where electron beam is practically parallel to the metal being welded (Figure 2, region 2).

Due to the design features of a bit its welding is performed using electron beam positioned at angle of 23° to the horizon. This angle allows obtaining the required penetration depth (it is shown in the Figure 2 by hatching) in a rotary part of a bit without destruction of heads (see Figure 1). According to technical specifications for drill bits a nipple part of bits should be welded using complete penetration and with formation of a reverse bead. In the transition to a rear part the penetration depth decreases and is 1/3 of thickness of workpiece being welded. The same ratio of penetration depth to the thickness of workpieces is preserved also on the rotary part of a bit. At the same time, the presence of projection in transition from a nipple to a rear part of a bit deteriorates abruptly the

conditions of weld formation, as the direction of gravity force and dynamic pressure of vapors of weld pool coincide in this area, resulting in flowing out of molten metal from the pool and formation of large defects in a weld. The task to achieve the quality weld formation becomes far more complex in connection with the fact that during transition from a nipple part of a bit to a rear part the required penetration depth decreases from a complete penetration across the whole thickness of workpiece being welded to a partial penetration for a depth equal to 1/3 of thickness of a workpiece being welded. And if during through penetration the evolution of vapors occurs on both sides of keyhole, then at a partial penetration the evolution of vapors on the side of a weld root closes, the pressure of vapors in the channel increases and the conditions of weld formation are changed. In the examined case when the electron beam passes a projection in a rear part of a bit the keyhole is opened in a certain moment from below and the increased pressure of vapors, typical of a partial penetration, contributes to flowing out of metal from the weld pool (Figure 3). Thus, there is a necessity to examine technological peculiarities of EBW of drill bits more in detail with account for a weld formation in problematic areas providing the stability of production and improvement of service characteristics.

Peculiarities of conditions of EBW of drill bits. The difficulties in compiling of EBW program mode are intricate profile of penetration of bit components, changing abruptly the angle of electron beam incidence on the surface of metal being welded. So, to provide geometry of penetration of a nipple part of a bit it is necessary to use heat input of welding 22.5 kJ/cm, whereas for welding of a rotary area 15 kJ/cm is required. It was established in the process of investigations that along with the determination of heat input and focus position of a beam relative to the surface of a workpiece it is necessary to determine the mode of technological oscillations of electron beam as well. The welding using static beam did not allow obtaining the required repeatability of geometry and quality of welded joints.

The earlier investigations [1] showed the high efficiency of use of oscillations of a beam in EBW technology. It was established in the present work that application of longitudinal or transverse scanning of electron beam in case of EBW of drill bits using inclined beam «upwards» does not contribute to a stability of welding process proceeding, as during the longitudinal scanning the oscillations of molten metal are excited in the plane of welding in parallel with the movement of electron beam. This leads to flowing out of molten metal from the weld pool and, as a consequence, to the violation of the welding process stability. During the transverse scanning of electron beam the keyhole increases in diameter, that also causes the flowing out of molten metal from the keyhole and formation of defects in a weld (Figure 4). Thus, it is unreasonable to use scanning of given configuration in EBW of workpieces with a vertical orientation of a weld.

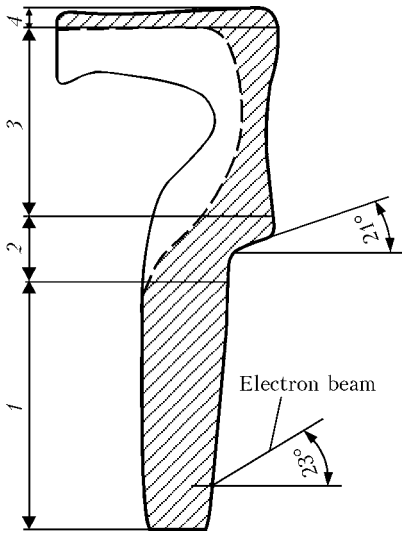

Figure 2. Scheme of bit section welded by electron beam: *1* ---- nipple part of a bit; *2* ---- transition from a nipple part to a rear part; *3* ---- rear part; *4* ---- under-rotary bit part

At the same time, the application of a circular scanning with a radius of somewhat higher than the radius of concentration of electron beam R ($r \geq R$) allows the capillary forces to maintain the melt in keyhole without its flowing out. However, at a circular scanning there is one more problem: instability of keyhole as regards to axially-symmetric oscillations of molten metal on the keyhole walls.

Due to symmetry of the problem, stipulated by a shape of scanning, the circular scanning of electron beam can excite a zero mode ($m = 0$) of melt oscillations, corresponding to axially-symmetric oscillations of the inner surface of keyhole of the type of constrictions and expansions. In particular, frequency of zero

Figure 3. Splashes of pool metal (marked by arrows) in EBW of projection at the rear part of a bit

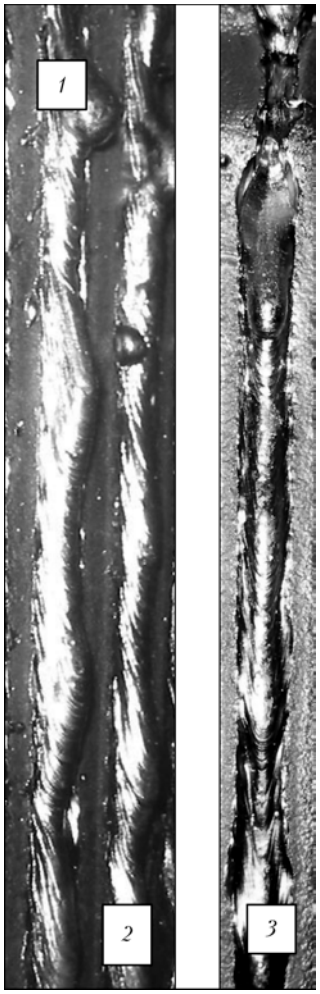

Figure 4. Non-uniformity of welds formation in use of transverse (area *1*), longitudinal (*2*) and circular (*3*) beam scanning

mode of oscillations of melt in keyhole, $\omega_0(k)$, is determined according to dispersion relation from [2]:

$$\omega_0^2(k) = \frac{\sigma}{\rho}\frac{k}{R^2}(k^2R^2 - 1)C_0(k), \qquad (1)$$

where k is the wave vector of oscillations; σ, ρ are the coefficient of surface tension and density of molten metal, respectively; $C_0(k)$ is the coefficient, depending on the wave vector and sizes of the keyhole.

For through keyhole, formed at the area *1* (see Figure 2) of drill bit, the length of wave of melt oscillations is equal to the depth of keyhole, which varies at this area approximately from 25 up to 30 mm. Consequently, the wave vector of oscillations $k = 2\pi/H$ changes from 2.5 to 2.0 cm^{-1}. For the keyhole radius 1.0--1.5 mm, formed in welding of a nipple part of a bit, kR is obtained of about 0.20--0.38, that is less than unity ($kR < 1$). This means that application of circular scanning results in instability of a keyhole even at the initial region of bits welding.

As the practice showed, to suppress the instability of keyhole are possible using a combining scanning of electron beam providing its scanning simultaneously along two axes X and Y, i.e. parallel and normal to the direction of welding. The instantaneous distribution of power of electron beam $q(r, t)$ in projection to the plane XY (normal to electron beam) has the following form [2]:

$$q(r, t) = q_0 \exp\left(-\frac{\mathbf{r}(t)^2}{R^2}\right) = q_0 \exp\left(-\frac{|\mathbf{r}_{xy} - \mathbf{r}_e(t)|^2}{R^2}\right), \qquad (2)$$

where q_0 is the maximum power on the axis of electron beam; $\mathbf{r}_{xy}$, $\mathbf{r}_e$ are the current radius-vector in the plane XY and instantaneous radius-vector of axis of electron beam, respectively (in the formula (2) vector equality $\mathbf{r} = \mathbf{r}_{xy} - \mathbf{r}_e$ was used).

It is obvious that for sufficiently high frequencies of scanning of electron beam the averaging of a value $q(x, y, t)$ according to the period T allows replacement of time dependence by spatial one. In other words, the process of scanning of electron beam can be considered as spatial dispersal of a beam, leading to reduction in its peak power.

Thus, for two periodical functions $f(t) = f(t + T_1)$ and $g(t) = g(t + T_2)$ of arbitrary form, describing the scanning of electron beam (with a Gaussian distribution) along two mutually normal axes X and Y, the beam power $<I(x, y)>$, averaged by a period, can be written in the following form:

$$<I(x, y)> = \frac{I_0}{T}\int_0^T \exp\left\{-\frac{(x + f(t))^2 + (y + g(t))^2}{R^2}\right\} dt, \qquad (3)$$

where I_0 is the peak power of a beam; T is the least general period of functions $f(t)$ and $g(t)$.

Thus, formula (3) for arbitrary functions $f(t)$ and $g(t)$ allows eliminating the time dependence by its replacement by spatial one.

In case of application of scanning of a beam along the ellipse the functions $f(t)$ and $g(t)$ can be given in the form: $X(t) = A\cos\omega t$ and $Y(t) = B\sin\omega t$, where ω is the frequency of scanning of electron beam; A, B are the amplitudes of scanning of electron beam along the axes X and Y, respectively. For this scanning the Figure 5 presents a spatial distribution of normalized density of power of 2D electron beam, averaged by a period, designed for different amplitudes of scanning $A = (0\text{--}3)R$ at fixed ratio of amplitudes $A:B = 2:1$.

The main axis is directed along the axis X. All distributions of power in the Figure are normalized in such a way that volume under each of the 2D surfaces was equal to $1:\int q(x, y)dxdy/q_0 = 1$, and distances are measured in radii R of concentration of electron beam.

The static electron beam, shown in the Figure 5, *a*, has the Gaussian distribution of power density. It is seen from the Figure that with the increase in the amplitude of scanning the redistribution of power of electron beam occurs along the axis X and it becomes not to be Gaussia. In addition, the maximum density of beam power is also decreased, which at $A = 3R$ is about 25 % of peak power of static electron beam.

As is seen from the Figure, at small amplitudes of scanning ($A \le 2R$) the distribution of power of electron

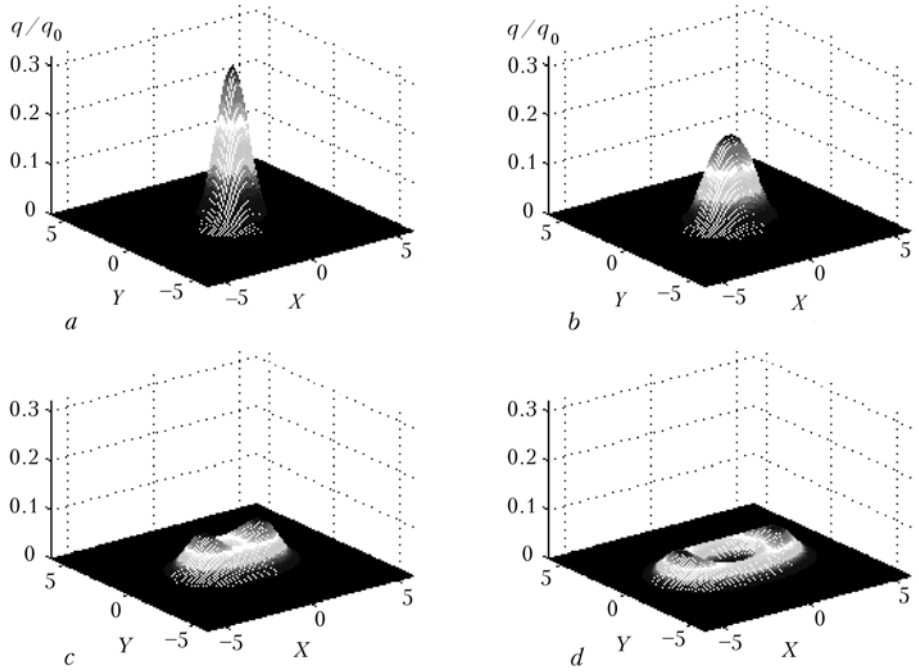

Figure 5. Distribution of normalized density of power of electron beam q/q_0 in use of combined scanning of electron beam: $X(t) = A \cos \omega t$ and $Y(t) = B \cos \omega t$ at different amplitudes of scanning: *a* ---- 0; *b* ---- 1*R*; *c* ---- 2*R*; *d* ---- 3*R*

beam is slightly differed from similar distribution of power in use of 1D cosinusoidal scanning along the axis X. However, beginning from the amplitudes of scanning $3R$ and higher ($A \geq 3R$), the distribution of power acquires a clearly expressed shape of oval (or ellipse) with a dip in its central part.

The experiments showed that application of oval scanning of electron beam with amplitude of scanning $A \geq 3R$ leads to violation of stability of welding process and, as a result, to formation of different types of defects in welds of drill bits. The best quality of a weld is achieved at small amplitudes of beam scanning ($A = 2R$, $B = R$ and $B{:}A = 1{:}2$), i.e. at such amplitudes when dip in the centre of distribution of power has not been yet become apparent.

Due to the symmetry, the elliptical scanning corresponds to the second mode of oscillations ($m = 2$) of melt in keyhole, which corresponds to alternating compression and expansion of keyhole along two mutually perpendicular directions (Figure 6). Therefore, when elliptical scanning of electron beam in keyhole is used, the stable second mode of oscillations is excited ($m = 2$), thus suppressing here both the unstable zero mode ($m = 0$), and also the first mode of oscillations ($m = 1$) corresponding to the longitudinal melt shifting. The oscillations of the second melt mode in keyhole are realized at higher frequencies than those of the first or zero modes of molten metal oscillations. According to data of [2], the dispersion relation for the second mode of oscillations has the following form:

$$\omega_2^2 = \frac{\sigma}{\rho} \frac{k}{R^2} (k^2R^2 + 3)C_2, \qquad (4)$$

where C_2 is the coefficient, depending on the wave vector and sizes of keyhole, is determined using the following formula:

$$C_2(k) = \frac{[K'_2(kR_1)\, I'_2(kR_2) - I'_2(kR_1)\, K'_2(kR_2)]}{[I_2(kR_1)\, K'_2(kR_2) - K_2(kR_1)\, I'_2(kR_2)]}, \qquad (5)$$

where R_1, R_2 are the inner and outer radii of the keyhole, respectively; I_2, K_2 are the modified functions of Bessel of the 1st and 2nd kinds; I'_2, K'_2 are the appropriate derivatives from these functions according to their argument.

For through keyhole of depth $H = 3$ cm with inner and outer radii $R = 0.08$ and 0.12 cm, respectively, the coefficient C_2 for the first harmonics of oscillations is approximately $C_2 \approx 32$. Then, the natural frequency of the second mode of oscillations is approximately equal to $\omega_2 \approx 1230$ rad/s, which corresponds to the frequencies of scanning $f \approx 195$ Hz. In practice, the frequency of scanning is selected higher, i.e. $f \approx 200$--300 Hz to reduce the amplitude of resonance oscillations of melt in the keyhole.

Capillary effect in EBW of butts with gaps. As was mentioned above, the angle of inclination of electron beam to the surface of workpiece being welded should remain constant during the whole welding process not to damage the rotary bits of a drill bit.

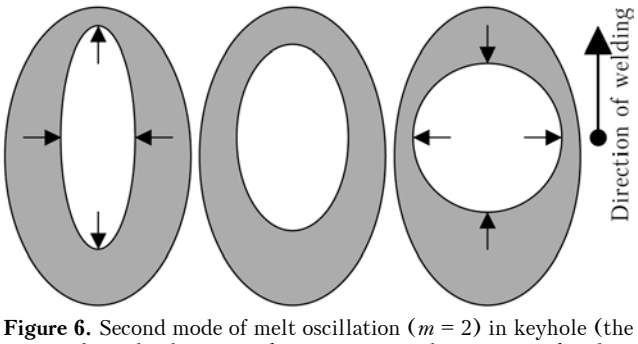

Figure 6. Second mode of melt oscillation ($m = 2$) in keyhole (the arrows show the direction of compression and expansion of molten metal in the keyhole)

Here, certain difficulties arise in formation of weld in under-rotary part of a weld. So, in horizontal area of a weld the microcracks are initiated due to a partial penetration, predetermined by a low angle of inclination of electron beam to the drill surface (about 23°).

To increase the service characteristics of welded joints and to eliminate defects in under-rotary part of a weld the Γ-shaped inserts, made of a material-modifier in the form of foil of stainless steel or titanium, were used, being placed into butts of a bit. The presence of inserts of foil leads to a gap formation between the composite parts of a bit along the entire length of a butt. The appeared gap creates some more difficulties in formation of a weld. According to the experiments too large gap results in flowing out of molten metal and, as a consequence, in formation of defects in a weld. At the same time, a small gap does not influence the weld formation, however the effect of modifying in application of thin foil is reduced to zero. It is obvious that to make a proper selection of thickness of inserts it is necessary to make evaluation of maximum admissible gap, at which a metal will not flow out from the pool and, consequently, will not violate the stability of welding process.

To evaluate the gap the known problem from hydrodynamics about capillary rising of liquid between two parallel plates, positioned on a certain distance $d < a$, where a is the capillary constant of a substance [3], can be used. As is known the capillary constant is defined by the formula

$$a = \sqrt{2\sigma/\rho g}, \qquad (6)$$

where g is the acceleration of gravity force.

For steel ($\sigma = 1500 \cdot 10^{-5}$ N/cm, $\rho = 7.8$ g/cm^3) the capillary constant $a = 0.63$ cm. Consequently, the keyhole of radius R = 1–2 mm, formed in EBW of metals, represents a capillary, in which the capillary forces exert a great influence on molten metal spreading along the keyhole walls. Moreover, in the gap between segments of a bit, the size of which is less than diameter of keyhole, the capillary effect can become apparent even more distinctly than in the keyhole itself.

According to data of [3] for the plates immersed into the wetting liquid, the height of a column of rising the liquid between the plates Z_0 and height of capillary near-wall layer of liquid Z_1 can be defined from the following formulae:

$$Z_0 = a\sqrt{A - 1}, \quad Z_1 = a\sqrt{A_\sigma - \sin\theta}, \qquad (7)$$

where θ is the angle of wetting; A_σ is the coefficient, which is defined by the formula

$$A_\sigma = \frac{a^2}{d^2}\cos\theta, \qquad (8)$$

where d is the distance between the plates.

When the distance between the plates is essentially smaller than the capillary constant of liquid ($d << a$), then $A_\sigma >> 1$ and, consequently, the height of rising of liquid Z_0 and Z_1 are the values of the same order:

$$Z_0 \approx Z_1 = \frac{a^2}{d}\cos\theta. \qquad (9)$$

For melt on the surface of metal the angle of wetting is practically equal to zero (complete wetting), therefore, the condition $\cos\theta \approx 1$ is fulfilled. For example, at gap of 0.3 mm the formula (9) gives the height of melt rising up to $Z_0 \approx 4$ mm.

In practice the molten metal during the welding process is not able to rise for this large height in the narrow gap, as it will be instantly cooled by side walls and solidify in the space of a gap. Therefore, the formula (9) presents a somewhat exaggerated evaluation for the height of melt rising in the gap of butts of bits.

In general case the problem of capillary rising of melt in a gap with account for its cooling on gap walls does not have precise solution and should be solved using numerous methods. The similar solution is too cumbersome and is beyond the limits of consideration of the present article. The evaluation of maximum admissible gap, at which the stability of welding process is not violated, can be performed coming from the following physical considerations. It is obvious that the presence of a gap results in decrease of metal amount, taking part in the formation of a weld. At small gap the given effect has no almost influence on the weld formation, however with increase in a gap the balance of a metal transfer on the front wall of keyhole begins to violate. Besides, at a sufficiently large gap the capillary retraction of melt into a gap takes place, thus leading to the additional decrease in amount of melt, spreading along the keyhole walls. It is evident that this leads even to a greater violation of balance of transfer of metal mass during the welding process. In this conception the typical size for evaluation of admissible thickness of a gap can be a thickness of melt layer on the front wall of the keyhole. To preserve the balance of metal it is necessary that gap d did not exceed the thickness of the melt layer D ($d << D$). Coming from the analysis of macrosections of longitudinal sections of welds the thickness of melt layer on the front wall of a keyhole can lie within the limits of 0.2–0.4 mm. The experiments showed that satisfactory quality of welded joints is achieved at the gap of 0.1–0.2 mm, that is well correlated with the above-made evaluation.

As it was mentioned above, one of the peculiarities of EBW of drill bits is the electron beam passing through the rear part of a bit where a projection of more than 1 cm is available. In EBW of vertical butts the column of melt in a gap is maintained due to the Laplace pressure in the gap P_L, and also due to the pressure of gas and vapours of metal in keyhole P_V and output pressure on the front wall of the keyhole P_R (Figure 7). Therefore, in EBW of a nipple part of a bit even at the presence of a gap in butts the flowing out of melt from the weld pool does not occur.

When passing through the stepped part *2* the keyhole is opened in the upper part and, consequently, pressure P_V disappears. As a result the balance of melt column is violated and, consequently, the in-leakage of excessive molten metal from a step under the electron beam may occur. To eliminate the effect of in-leakage at welding beam approaching the rear area, it is necessary to provide the conditions of laminar flowing of molten metal in the penetration channel. With this purpose it is necessary, first of all, to reduce smoothly the welding speed at the area considered, that is usually done in the technological cycle of EBW of drill bits.

Experimental results. In Figure 8, *a* the crack is clearly seen, formed in a weld, produced in EBW without a material-modifier. The use of modifier allows prevention of cracks in welded joints (Figure 8, *b*), that increases service characteristics of welded product. The welding was performed using the scanning of electron beam along the ellipse at the frequency 300 Hz and ratio of ellipse axes 2:1 (mm). Such scanning of beam provides the uniform weld formation along the entire length (see Figure 1, *b*).

In the present work the modifiers were used in the form of plates of titanium or stainless steel 10Kh18N10T of 0.2 mm thickness. The width and length of plates depended on the type of bits being welded and could vary within the limits of 15--20 mm in width and 45--70 mm in length. Such inserts do not violate welds formation, do not require alteration of existing electron beam equipment and devices for assembly and welding and do not create obstacles in automatic tracking of butts during EBW.

Material-modifier is inserted into three rotary bit butts and into butts of the bit rear part where the crack ignition is most probable.

To study the effect of modifiers on the properties of welded joints the metallographic examinations of structures in the microscope «Neophot-32» were carried out. It was established that at a thermal cycle, typical of EBW, the transformation of austenite of weld metal of region of overheating of HAZ metal takes place in the bainite and martensite regions. Here the characteristic dendrite structure of weld with direction of growth of crystallites from the fusion line to weld centre is revealed. It is these places where the

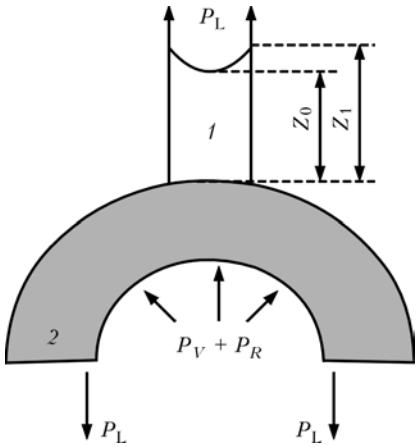

Figure 7. Scheme of capillary rising of melt in the gap between the segments of drill bits (*1*) and melt on the front wall of keyhole (*2*)

crystalline cracks of size of 0.5--0.7 mm are most often initiated.

Microstructure of weld metal and region of HAZ metal overheating represents mixture of bainite and low-tempered martensite and has the same hardness (*HV* 418) that is a somewhat higher than the hardness of parent metal (*HV* 385--396). At the area of overheating a negligible grain growth takes place (Figure 9, *a*).

The comparative analysis of structures of welds, made without modifiers and after their adding into the weld pool, indicates that in the second case the grain refinement takes place during crystallization of the weld metal (Figure 9, *b*). Here the hardness of weld metal is decreased to *HV* 280--300. The hardness of near-weld zone is remained at the level of hardness of zone of welds, made without modifier.

In connection with change in grain size of weld metal at a titanium insert the increase in weld resistance a against formation of crystalline cracks was expected. However, it was established during the further study of microstructures of welds with titanium inserts that in the middle part of cast zone the crystalline cracks often appear. The general appearance of such cracks is presented in Figure 9, *c*. The cracks are located at the boundaries of primary grains along the lines of meeting the columnar crystallites. X-ray spectral microanalysis of joints with a titanium insert showed the presence of a significant amount of inclu-

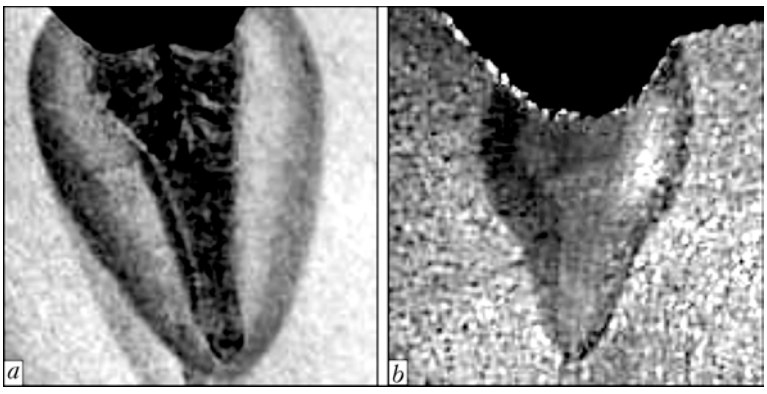

Figure 8. Macrosections of welds in a drill bit rotary part welded without application of a material-modifier (*a*) and with use of foil of stainless steel (*b*)

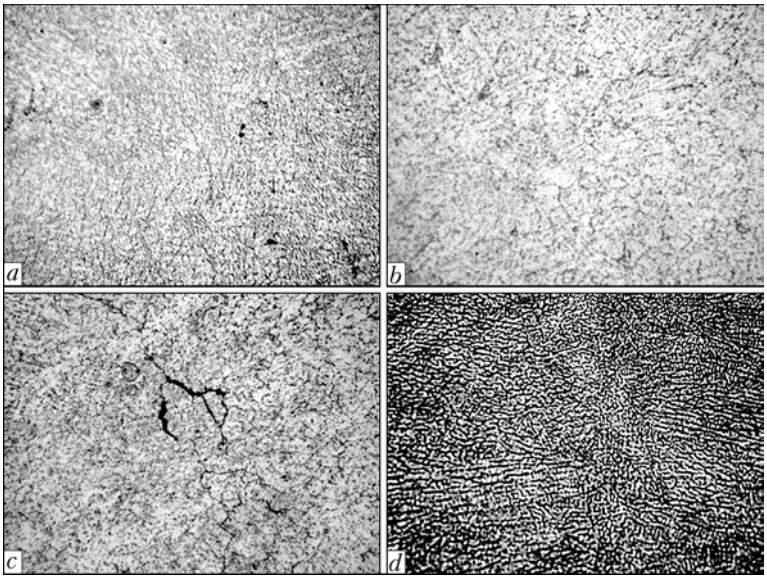

Figure 9. Microstructures (×320) of a central part of weld metal welded without a modifier (*a*), with insert of titanium (*b*) or steel 10Kh18N10T (*d*), and crack in modifying by titanium (*c*)

Mechanical properties of welded joints of drill bits

Type of joint	σ_t, MPa	σ_y, MPa	δ, %	ψ, %	α_n, J/cm^2
Steel 14KhN3A	960	822	8.1	49.2	74.31
Welded joint without modifier	862	--	--	--	84.45
Welded joint with insert of titanium of 0.2 mm thickness	690.3	--	--	--	12.10
Welded joint with insert of 10Kh18N10T of 0.2 mm thickness	918	--	--	--	51.35

sions in the form of carbides of titanium both along the section of a weld and also at fusion boundary with the base metal. Here, in the weld eutectics there is 2–3 % of titanium, while in the composition of inclusions ---- 10–11 %. Probably, this non-uniform distribution of inclusions is the cause of decrease in strength characteristics of a weld.

During the analysis of structures of welded joints performed after adding inserts of stainless steel 10Kh18N10T, it was established that grain refinement in weld structure is similar to welds with titanium, but without cracks. X-ray spectral microanalysis shows that distribution of modifying elements in a weld is far more uniform as compared with distribution in use of titanium (Figure 9, *c*).

The performed mechanical tests of welded joints of drill bits, the generalized results of which are represented in the Table, show that in use of titanium in the form of a modifier the characteristics of strength and especially impact toughness of weld metal are abruptly deteriorated. This is caused by the formation of a large amount of titanium carbides in the weld metal. All tensile specimens are fractured in weld, impact test specimens have a brittle fracture.

In use of insert-foil of steel 10Kh18N10T the fracture takes place along the HAZ metal area, the fracture of impact test specimens is tough.

Mechanical properties of welded joints with insert of steel 10Kh18N10T are greatly superior to the properties of welded joints with a titanium insert and approach the properties of parent metal in strength.

In conclusion it is necessary to note that in this work the effect of shape of scanning of electron beam and capillary effect in the gap between segments of drill bits of complex configuration on the quality of weld in EBW at a variable speed of electron beam movement in the vertical plane was investigated. It is shown that application of a combined scanning of electron beam simultaneously along two axes X and Y (parallel and normal to the EBW direction at scanning amplitudes ratio 2:1) in the frequency range f = = 250–300 Hz allows decreasing the disturbances of melt surfaces in keyhole and, consequently, achieving the significant improvement of quality of welds of drill bits.

It was established that the use of a material-modifier in the form of foil of stainless steel of thickness up to 0.2 mm allows avoiding the crack initiation in welds that improves the service characteristics of welded products.

The obtained theoretical results are well correlated with experimental data.

1. Nazarenko, O.K., Kajdalov, A.A., Kovbasenko, S.N. et al. (1987) *Electron beam welding*. Kiev: Naukova Dumka.
2. Nesterenkov, V.M. (2003) Special features of capillary waves in the vapour-gas channel in electron beam welding of thick metal. *The Paton Welding J.*, **4**, 7–12.
3. Landau, L.D., Lifshits, E.M. (1986) *Hydrodynamics*. Moscow: Nauka.

STRESS-STRAIN STATE OF WELDED JOINTS ON POLYMER PIPES PRODUCED BY BUTT WELDING AT AN ANGLE

E.S. NIKONOVA, N.G. KORAB and **V.Yu. KONDRATENKO**
E.O. Paton Electric Welding Institute, NASU, Kiev, Ukraine

The stress-strain state of butt welded joints made at different angles was studied, and distribution of equivalent stresses across the weld section was calculated. The ranges of angles to the lower generatrix in butt welding were determined, within which it is necessary to mount additional hold-down devices to level the existing gradient of stresses in the weld. A new technological solution was found in the form of a device for welding thermoplastic pipes, for which a patent of Ukraine was granted.

Keywords: *polymer products, welded joints, butt welding, fittings, welded structure strength, investigation of stress-strain state, device for welding thermoplastic pipes*

At present three main welding processes are used to join pipes from polymer materials: thermoresistor, hot tool and spigot welding. Hot tool welding of spigot joints is mainly used for joining small diameter pipes, for instance, in mounting water and gas supply, and heating systems, etc. Pipes with more than 63 mm outer diameter are usually joined using thermoresistor or butt welding. Here even comparative surface analysis shows the obvious advantages of using butt welding: absence of the need for additional fittings, simplicity of welding performance and high reliability of the produced welded joints. In addition, the cost of thermoresistor fittings is relatively high and with increase of pipeline diameter the price of such parts rises in proportion. Earlier, minimizing of the so-called human factor and, consequently, higher quality of the produced welded joints, was a strong argument in favour of thermoresistor welding. Now, however, the situation has drastically changed with appearance in the territory of Ukraine of an ever larger number of modern automated welding equipment for butt welding, capable of precisely controlling all the welding process parameters. Butt welding became a process providing a practically 100 % quality of the produced welded joints and capable of competing with thermoresistor welding on equal terms. Taking into account the economic factors, it may be assumed that for more than 160 mm diameter pipes there is no alternative to butt welding [1, 2].

At the same time, there is a problem of prohibition in the territory of Ukraine of application of welded fittings in gas pipeline construction ---- more expensive cast fittings are used instead (no such limitations are applied in construction of water supply, drainage and collecting systems).

It was earlier believed that welds used in manufacture of fittings always reduce the strength of the structure as a whole. Even special lowering coefficients were introduced, and it was assumed for calculations that the welded structure strength was from 30 to 70 % of that of the base material without welds. At present in practical design of polymer pipelines a coefficient of lowering of welded joint strength is introduced, and welded fittings are made from pipes with a greater wall thickness than that of the pipelines. All this is due primarily to lack of understanding and ignoring the features of structure and formation of polymer welded joints [3, 4].

At present there is practically no research or publications on fittings for polymer pipelines, produced by butt welding at an angle. Welding equipment for manufacture of such parts mostly is foreign-made and has several disadvantages, the main of which is the inability of the technology to level out the stress gradient at pipe edges, which form the butt in welding at an angle [5]. This may result in poor quality of the produced welded joint. Moreover, there are no standards on the applicability of such parts in construction, which would take into account the features of modern polymer materials and modern concepts of their structure. In view of the above, several experiments were staged and empirical calculations were made to study the stress-strain state of polyethylene welded joints produced by butt welding at an angle.

APROX computational system was selected to study the stress-strain state of the polymer welded joint, as this complex is aimed at investigation of the stress-strain state of various systems and structures in physically and geometrically non-linear definitions, exposed to static and dynamic load. It enables studying in the classical and refined definitions such characteristic features of operation of structures and systems as large displacements, process of plastic deformation of structure material layers, crack initiation and propagation both across the thickness, and in the structure plane under force, stationary and non-stationary dynamic load, determination of the spectrum of system inherent vibration forms and frequencies.

APROX computational system is based on application of finite element method, with which it is difficult to determine the calculation error, so that test

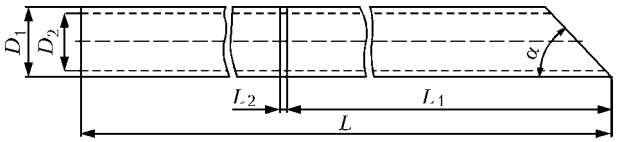

Figure 1. Schematic of a model sample of polymer pipe welded using butt welding process

problem method was used for evaluation of the latter. Values derived when solving such a test problem using APROX system, differ from the analytical ones derived from the classical formulas of material strength by less than 5 %, which is indicative of the effectiveness and accuracy of the selected numerical method of solving such a problem [6].

Process of butt welding at an angle of polymer pipes with welds was simulated in APROX system. This model implements maximum close process conditions of producing welded fittings from polymer pipes (of the type of tee-joint, segmented pipeline branch, single- and multisection) by butt welding.

The following calculation data were used to assign parameters in APROX system (Figure 1): D_1 = = 110 mm ---- pipe outer diameter; D_2 = 90 mm ---- pipe inner diameter; L_1 = 600 mm ---- pipe segment length; L_2 = 10 mm ---- weld length; L = 2000 mm ---- total pipe length; 2α = 30, 45, 60, 90° ---- angle of welding polymer pipe segments in fitting manufacture, respectively (welding dimensions and angles are selected proceeding from the data of typesizes of the main fittings provided by Barbara Kaczmarek Company, Poland). Pipe material is high-pressure polyethylene of PE80 grade; Young's modulus E = = 690 MPa; Poison's ratio k = 0.35.

Axial load of 0.147 MPa is applied to the pipe from the end face. Pipe section cut at angle α was considered to be fastened in all directions.

Results of calculations of the posed problem in APROX system are given in the Table, from which it is seen that the design distribution of stresses across the section is from 15 to 55 %. This is indicative, primarily, of the fact that strength will be different in different points of the weld. It should be noted

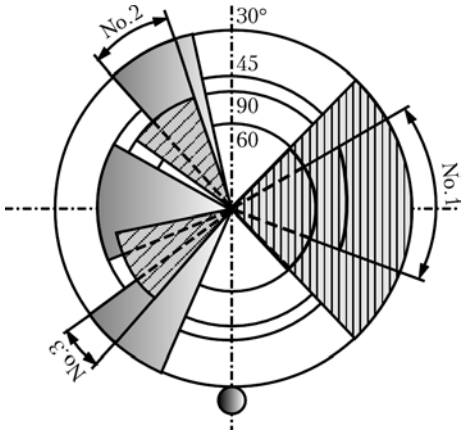

Figure 2. Diagram of distribution of equivalent stresses across the section of welding surface (ranges of angles of stress gradient relative to lower generatrix in butt welding: No.1 ---- 65--120; No.2 ---- 195--225; No.3 ---- 305--320°)

Results of calculation of stress-strain state of welded polymer joint in APROX system

Angle of welding pipe segments 2α, deg	Equivalent stress across the welded surface section $\sigma_{eq} \cdot 10^3$, MPa	Range of distribution of equivalent stresses, deg
30	129.8	43--136
	150.5	193--222
	151.7	307--336
45	126.1	242--291
60	0.7282	41--140
90	74.03	65--120
	151.9	283--318
	156.8	199--234

that the regularity of distribution of the specific force of clamping over the butt surface is of special interest.

Figure 2 shows the ranges of stress gradient angles relative to the lower generatrix in butt welding, which simultaneously are the ranges of angles relative to the lower generatrix, within the limits of which it is necessary to mount additional clamping devices, so as to level the existing stress gradient: 65--120, 195--225, 305--320°.

Proceeding from the above considerations, a new process solution was developed in the form of a device for welding thermoplastic pipes, for which a patent of Ukraine for a useful model was granted [7]. According to this patent a useful model pertains to the field of plastics welding, namely devices for welding thermoplastic pipes.

Schematic of a device for thermoplastic pipe welding is given in Figure 3.

To improve the design it was necessary to create the conditions for uniform clamping of the pipes to be welded by installing hydraulic cylinders on the aligning device, with the capability of moving in the

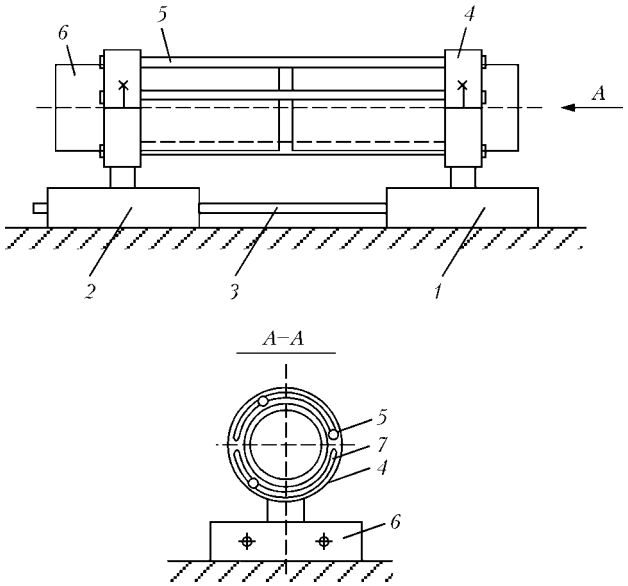

Figure 3. Schematic of a device for welding thermoplastic pipes (for designations see the text)

range of angles of 65--120, 195--225, 305--320° relative to the pipe lower generatrix. The defined problem is solved as follows: a device for welding thermoplastic pipes *6* contains a welding block ---- an aligning device in the form of two plates mounted on guides *3*: mobile *2* and stationary *1*, which through a hinged connection support binding clips *4* with replaceable inserts (not shown in the drawing), drive for pipe alignment, displacement and applying welding pressure, heater and electronic control module. Hydraulic cylinders *5* are mounted in the aligning device with the capability of their displacement in the set range of angles or their mounting on the aligning device with initially different length. Hydraulic cylinder fasteners are made in the form of mounting bores of «lug» type *7*.

Presence of hydraulic cylinders located in the above range of angles relative to the pipe lower generatrix provides conditions for uniform clamping of the pipes to be welded and, consequently, approximately equivalent strength of the welded joint in individual sections of the weld.

Application of a useful model allows a significant improvement of welded joint quality in butt welding at an angle and wider application of welded fittings in pipeline construction.

CONCLUSIONS

1. It is rational to replace cast fittings from polymer materials by butt welded ones.

2. It is necessary to allow for the stress-strain state of butt welded joints made at different angles, range of angles relative to the lower generatrix in butt welding, within the limits of which additional clamping devices should be installed, so as to level the existing stress gradient in the weld.

3. A new technological solution was developed in the form of a device for welding thermoplastic pipes, for which a patent of Ukraine for useful model was obtained.

4. Work results can be applied in further studies of strength characteristics of welded fittings and evaluation of the prospects for a wide acceptance of such fittings in pipeline construction in the territory of Ukraine.

1. Esaulenko, G.B., Kondratenko, V.Y. (1992) Morphologie und Eigenschaften von Stumpfschweissungen an polymeren Werkstoffen. In: *Kunststoffschweissen und Kleben'92*. Dusseldorf: DVS, 3--5.
2. Nikonova, E.S. (2006) Ensuring service reliability of pipeline transport systems. In: *Proc. of 4th Sci.-Pract. Seminar on Welds of Polymer Materials as a Reinforcing Element of Pipeline Structure* (Kiev, 11 April, 2006). Kiev: Ekotekhnologiya.
3. Nikonova, K.S., Kondratenko, V.Yu., Goncharenko, V.V. et al. (2007) Experimental investigations of physico-mechanical properties of butt welded joints of polymer materials and recommendations for welding process optimization. In: *Proc. of 2nd Sci.-Pract. Seminar on Welding and Related Processes in Industry* (Kiev, 17 April, 2007). Kiev: Ekotekhnologiya.
4. (1985) *Recommendations on calculation and design of pipelines from thermoplastic materials:* TsNIIE of engineering equipment: NPO Plastic. Moscow: Strojizdat.
5. Shestopal, A.N., Mineev, E.A. (1986) *Reference book on welding and adhesion bonding*. Ed. by A.N. Shestopal. Kiev: Tekhnika.
6. Gondlyakh, O.V., Sakharov, O.S., Sivetsky, V.I. et al. (2006) *CAM. Program complex APROX in calculations of machines and apparatuses of chemical productions*. Kyiv: Poligraph Consulting.
7. Goncharenko, V.V., Kovalenko, I.V., Nikonova, E.S. *Device for welding of pipes from thermoplastic materials*. Pat. 24692 Ukraine. Publ. 10.07.2007.

PECULIARITIES OF UTILIZATION OF HYDROGEN-OXYGEN FLAME IN FLAME TREATMENT OF MATERIALS

V.N. KORZH and **Yu.S. POPIL**
NTUU «Kiev Polytechnic Institute», Kiev, Ukraine

Peculiarities of utilization of hydrogen-oxygen flame in flame treatment of materials are generalized, the flame being formed by combustion of a mixture produced by electrolysis-water generators. The study shows that it is possible to regulate the reduction potential of the combustion product flame with respect to iron, and control the overall thermal power due to saturation of the mixture with hydrocarbon additions.

Keywords: *flame spraying of coatings, hydrogen-oxygen mixture, gas jet, laminar and turbulent flow, plume core, afterburning zone, flame geometry, temperature distribution, jet velocity*

Despite of the fact that electric fusion and pressure welding methods dominate in welding production, gas welding, brazing, gas-thermal cutting and flame spraying of coatings are also used widely enough. The ever increasing deficiency of calcium carbide and hydrocarbon combustible gas-substitutes of acetylene, propane, butane, natural and other gases results in the problem of searching for alternative combustible gases for flame treatment of materials (FTM).

One of the gas-substitutes of acetylene is hydrogen ---- ecologically clean and renewable energy source. Its utilization, however, as an acetylene substitute has not received wide acceptance so far due to restricted data on technological capabilities of the hydrogen-oxygen flame (HOF). Utilization of this gas

was restricted by a lower caloric power and temperature of the hydrogen flame in comparison with the acetylene-oxygen one, as well as by its explosion hazard and service and transportation costs incurred to maintain cylinder facilities. Emergence of mobile electrolysis-water generators (EWG), which permit producing the combustible mixture directly on site without any costs for maintenance of cylinder facilities and with a significant reduction of transportation costs, initiated investigations of the possibility of utilization of hydrogen in FTM.

The results of many year's work of the personnel of the Welding Department of NTUU «Kiev Polytechnic Institute» in the area of development of new resource-saving technologies and, in particular, development and introduction of the processes of flame welding, cutting, brazing and spraying of coatings with replacement of acetylene by the hydrogen-oxygen mixture (HOM) produced by EWG, are summarized in the present work.

The peculiarity of HOM is that the ratio of the volume of oxygen, V_{O_2}, to that of hydrogen, V_{H_2}, in the mixture produced by electrolytic water dissolution $2H_2O = 2H_2 + O_2$, is constant and equal to $\beta = V_{O_2}/V_{H_2} = 0.5$. At such a ratio of the mixture components the flame has the oxidation potential. Devices, wherein HOM produced by EWG is separated into two flows, one of which remaining pure and the other being passed through a bubbler with a liquid hydrocarbon compound (for example, gasoline, alcohol, etc.), is proposed in [1, 2]. They are meant to achieve a normal or carbonizing character of flame combustion. Both flows of the mixture are supplied to connectors of the welding torch; the character of flame combustion is regulated by changing the ratio of these flows with the help of corresponding torch valves.

Investigations of composition of HOM combustion products were carried out by using the experimental setup of the Gas Institute of the NAS of Ukraine through taking samples with the help of the Grey probe from the plume core, at the boundary of the core and behind the core, allowing for gas temperatures. Depending on the composition and consumption of the initial combustible mixture, growth of the reduction potential of the combustion products in comparison with molten metal is possible due to increase in their content of hydrogen and carbon oxide [3].

Oxidizing power of the flame for the neutral one relative to the iron melted in the weld pool, which is determined by the equilibrium charts of hydrogen and carbon oxide with iron oxides and iron, corresponds to the proportions of hydrogen (43 vol.% H_2 and 57 vol.% H_2O) and carbon (83 vol.% CO and 17 vol.% CO_2) in the combustion products of the flame [4].

In composition of the EWG generated HOM combustion products with a constant proportion of oxygen to hydrogen in the mixture equal to $\beta = 0.5$, the total content of hydrogen $H_2 + [H]$ in the dissociated combustion products is less than 40 vol.%, that proves the oxidizing character of the flame combustion. Addition of vapors of hydrocarbon compounds (from the total volume of a mixture the gasoline vapors equal to about 4--5 %), ethyl alcohol (more than 14--16 %) or acetone (14--25 %) to those in HOM provides the total content of hydrogen $H_2 + [H]$ in the system H_2--45--50 vol.% H_2O and that of carbon oxide in CO--84--90 vol.% CO_2 in the dissociated combustion products. At such a content of hydrogen and carbon oxide in the dissociated combustion products the possibility exists of reduction of iron oxides in the weld pool. At the same time, the dissociated combustion products of the EWG generated mixture, saturated with vapors of hydrocarbon, contain free oxygen formed as a result of air inflow and thermal dissociation of the combustion products. The total content of free oxygen $O_2 + [O]$ in the dissociated combustion products of the normal HOM welding flame with the gasoline vapors makes up 7--12 vol.%, with the alcohol vapors is 12--16 % vol.%, with the acetone vapors is 5--7 vol.%. The presence of free oxygen in the combustion products requires additional alloying of filler wire with deoxidizers.

By adding the vapors of hydrocarbon compounds to HOM at its constant consumption it is possible to regulate the thermal power of HOF (at combustion of 1 m^3 it makes up 6.75 MJ). Addition to HOM of 5.5 % of the gasoline vapors at combustion of the same volume of combustible mixture increases the thermal power to 17.15 MJ, which is almost 2.7 times higher in comparison with the flame of pure HOM. In the case of addition to HOM of 16 vol.% of the ethyl alcohol vapors at combustion of the same volume of combustible mixture, the thermal power makes up 14.7 MJ. Therefore, the character of combustion of the flame can be regulated and its thermal power can be increased by adding the vapors of hydrocarbon compounds to HOM.

The plume method of combustion of chemically homogeneous gas mixtures is used, as a rule, in FTM, which is attributable to availability of special welding torches and cutting torches of the injector and injectorless types. The plume combustion is characterized by the presence of a stationary flame of a less or more regular form, which depends on the torch type, level of mixing of a fuel and oxidizer, and character of the jet flow.

Figure 1 shows a scheme of the acetylene-oxygen flame plume of a gas welding torch. Area L_c taken by the initial boundary of the flame is called the jet ignition zone or plume core, and area $L_{a\text{-}b}$, where the process of combustion finishes, is called the after-burning zone.

It is known from the combustion theory [5] that in the case of a laminar flow the plume core should be clearly defined and width of the normal flame front should be small. This is area λ_n, which is situated between the two surfaces, where chemical reactions occurring as a result of the presence of oxygen in the mixture start and finish, and where temperature in-

creases from its initial value T_{in} up to the maximum adiabatic combustion temperature T_{comb}. Thus, it equals 0.128 mm when using HOM 2H--O_2, 0.24 mm with the methane-oxygen mixtures CH_4--$2O_2$, and 0.71 mm with the acetylene-air mixtures C_2H_2--air [6].

In welding production, the normal flame propagation zone λ_n is called the middle flame zone. At the end of this zone the temperature of the combustible products reaches its maximum, and then it starts falling.

At a turbulent flow the middle flame zone λ_n is diffused. It is characterized by a significant thickness, which complicates calculation of L_c as its values depend on the process of propagation of the flame from the periphery to center, i.e. on the velocity of propagation of the turbulent flow front.

The length of the after-burning zone $L_{a\text{-}b}$ situated between the middle zone and end of the flame plume (boundary of complete burning) depends, in general, on the kinetic properties of the combustible mixture.

Efficiency of the combustion process is determined, as a whole, by the total length of the flame plume

$$L_{pl} = L_c + \lambda_n + L_{a-b}. \quad (1)$$

In a case of the laminar character of flow $\lambda_n \approx 0$

$$L_{pl} = L_c + L_{a-b}. \quad (2)$$

The working zone is determined by a specific character of the process in FTM. In gas welding and brazing of metals, the working zone of the flame is an end of the flame middle zone λ_n, and the flame combustion temperature is maximal. In gas-oxygen cutting, the working zone of the flame is an end of the flame plume core and after-burning zone. The influence of temperature distribution in the after-burning zone is especially pronounced in cutting of metals of big thicknesses.

In flame spraying of a powdered material, the working zone, in general, is an after-burning zone, in which, as a rule, heating of particles up to their melting temperature or plastic state takes place. In wire rod or flexible cord spraying, melting occurs at the end of the flame plume core or in the middle zone of the flame.

Investigations were conducted to study the mode of flow of gas jets from the torch nozzle in the plume core and combustion products in the flame after-burning zone, as well as distribution of temperature along the flame plume length, in order to evaluate the possibility of utilization of HOF produced during combustion of HOM as a heat source for different FTM processes.

A set of interchangeable tips with diameters of outlets of the nozzle channel equal to 0.6--3.5 mm for standard welding torches G2-04 and G3-03 (Nos. 0--7) was used to study the mode of flow of the gas jets from the torch nozzle within the flame core zone, and a standard set of tips for the flame spraying EUROJET XS-7 torch with nozzle diameters of 1.6--2.2 mm (No. 1--3) was used to study that in the flame after-

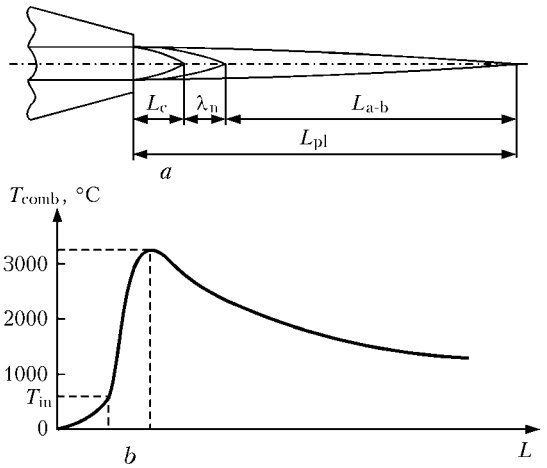

Figure 1. Scheme of plume of acetylene-oxygen flame (*a*) and distribution of temperature along the plume length (*b*): *L* ---- distance along the flame plume axis; see other designations in the text

burning zone. The experiments were carried out by using EVG A1803 with a gas mixture efficiency of 1.6 m^3/h.

The HOM jet (Figure 2, *a*) and jet of the combustion products (water vapor) (Figure 2, *b*) flowing from standard tips (Nos. 0--2) of the welding torches that limit consumption of the mixture to 0.6 m^3/h

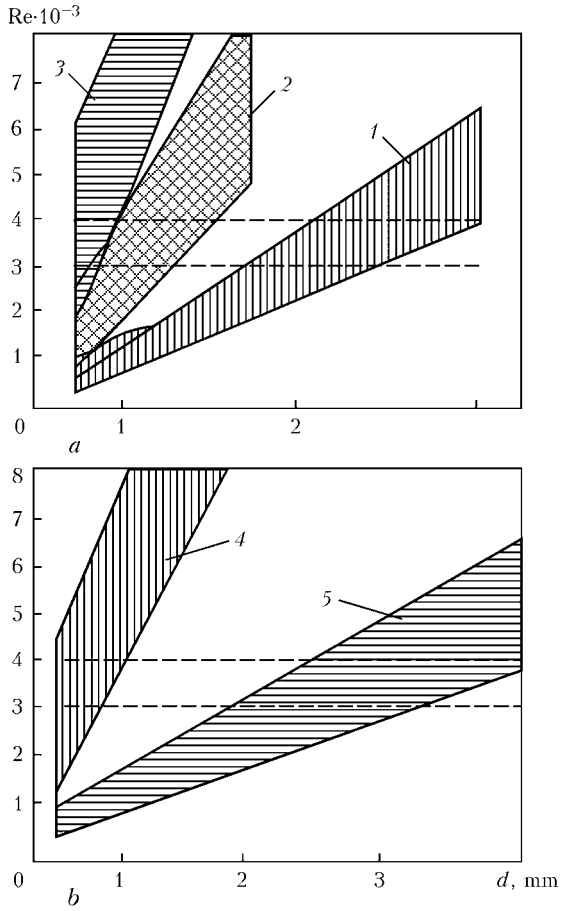

Figure 2. Gas-dynamic characteristics of the gas jet flowing from the nozzle of standard tips of the G2-04 and G-03 type torches under standard conditions: *a* ---- hydrogen (*1*), 30 % O_2 + 70 % H_2 (*2*) and oxygen (*3*); *b* ---- water vapor at pressure of 0.1 MPa and temperature of 107 (*4*) and 577 (*5*) °C, respectively; dashed ---- area of transfer from laminar to turbulent mode of flow of the HOM (or water vapor) jet; *d* ---- torch tip diameter

are characterized by a laminar flow in the plume core and immediately behind the core, whereas when using tips No. 3 and 4 that limit consumption of the mixture to 1.8 m^3/h the above jets are characterized by a slightly turbulent flow. With distance from the plume core the gas flow temperatures decrease, the coefficient of viscosity falls, and a gas jet has a turbulent flow.

The laminar mode of flow of the HOM jet combustion products in the zone of the flame plume core reduces width of the normal front of its flow and, consequently, surface area of combustion.

Achievement of an increased flame calorific intensity and concentrated heat generation in the welding working zone confirms the efficiency of utilization of HOF for metal welding and brazing, compared with other gas-substitutes of acetylene [7], and provides the possibility of using the acetylene to hydrogen replacement factor equal to 2 for calculations [8].

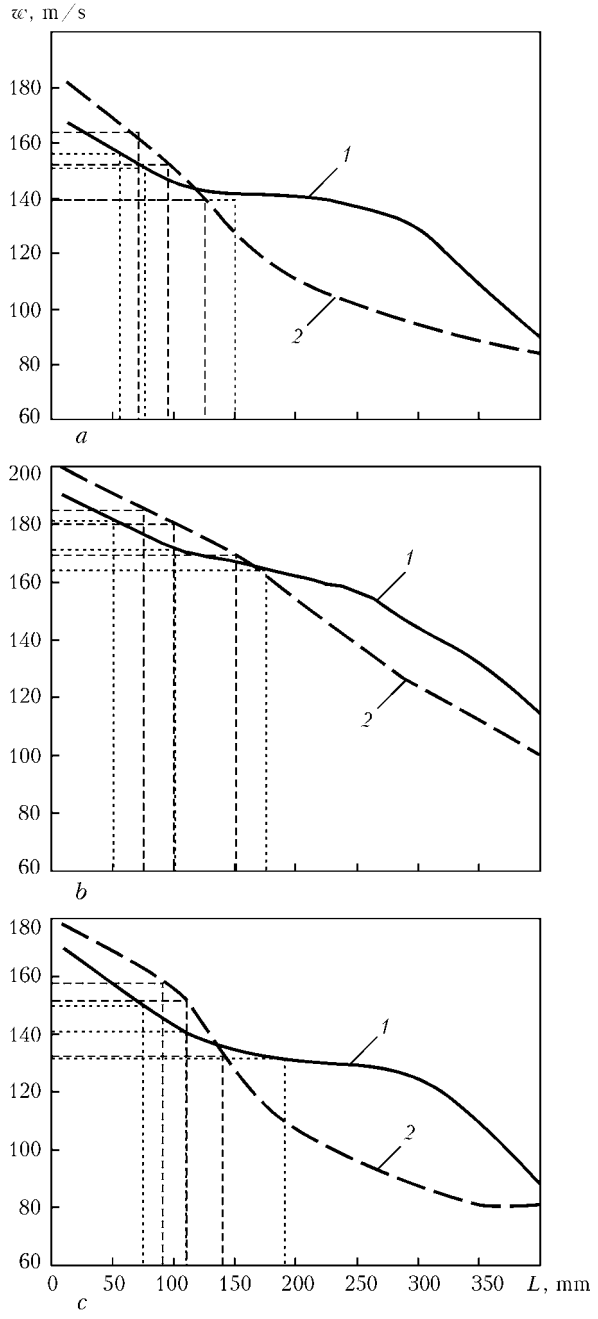

Figure 3. Distribution of the velocity of flow of the combustion products jet along the plume length in the laminar (*1*) and turbulent (*2*) mode: *a* ---- HOM generated by EWG; *b* ---- HOM + 5.5 vol.% of gasoline vapors; *c* ---- HOM + 16 vol.% of alcohol vapors

The temperature of flame in the core and near-core zone was determined by an experimental-calculation method using gas enthalpy, which depends on the heat flow taken up by the probe in extraction of gas through an internal capillary. Its values are found by means of calculations using the heat balance equation by method developed by the Gas Institute of the NAS of Ukraine. The mean specified temperature in the plume core and near-core zone when using pure HOF made up approximately 3117 °C (3390 K), in combustion of a mixture of HOM + 5 vol.% of the gasoline vapors it was around 3108 °C (3381 K), extreme deviation from the mean specified temperature ranging from --5.4 up to +6.5 %, and in combustion a mixture of HOM + 16 vol.% of the alcohol vapors it was 3088 °C (3360 K) (the deviation ranging from --2.3 to +3.3 %).

Utilization of HOF is indicated for welding of steel parts up to 3 mm thick. Welding of parts up to 2 mm thick is carried out by flanging without a filler, or with a filler without edge preparation. Steel parts of 2--3 mm thickness can be butt welded by using a filler. For welding low-carbon low-alloy steels, it is recommended to use HOF with additions of the gasoline vapors (normal flame). Electrode wires of the Sv-08G2S, Sv-08GS and Sv-10GS grades are used as a filler material.

Gas welding with HOF produced by combusting the EWG generated mixture is successfully used for joining brass up to 4 mm thick. In this case the use is made of the oxidizing flame, i.e. pure HOM without hydrocarbon additions. Specific consumption of the combustible mixture is 250--300 $dm^3/(h \cdot mm)$. Brass of the LOK-59-1-0.3 grade, or that similar to the base metal, is used as a filler wire. The use of fluxes containing borax $Na_2B_4O_7 \cdot 10H_2O$, boric acid H_3BO_3, or their mixtures, is imperative. Also, it is convenient to use liquid flux BM-1.

As proved by the experience, HOF can be used for flame soldering of copper and copper alloys, e.g. copper-zinc solders with liquid flux BM-1, and fluxes based on calcined borax and boric acid, are used for soldering copper pipelines of refrigerating systems with a diameter of 25 mm and wall thickness of 2 mm.

Utilization of HOF as a heating flame is also appropriate for cutting of steel parts up to 40 mm thick. In this case, HOM enriched with the gasoline vapors is recommended. Consumption of the combustible mixture for the heating flame in performing the work by using a machine cutting torch of the RM type with a removed injector unit, depending on the thickness of metal to be cut, ranges from 1.1 to 1.8 m^3/h.

The quality of coatings in flame spraying depends on the temperature and velocity of spraying material particles, which, in turn, in spraying of powder materials depend on the distribution of temperature and

velocity of combustion products jet in the flame after-burning zone.

If the mode of flow of the combustion products changes from laminar to turbulent, the so-called transient flows are formed, in which the laminar and turbulent forms of flow combine in different areas of the flame.

At a relatively low velocity of the combustible mixture jet, the length of the plume after-burning zone increases proportionally to the Reynolds number (Re), which corresponds to the laminar character of the flow that persists up to Re ≈ 3000–3500. As the velocity of the combustible mixture jet increases at high Reynolds number values, the deviation of the above dependence from the linear one takes place. Pulsations form at the flame apex, which grow with increase in the velocity of the mixture jet and result in fracture of the laminar front and flame turbulization. Further increase in the velocity of the combustible mixture jet leads to decrease in the length of the plume after-burning zone.

Effective heating of metal particles up to a melting temperature in convective heat exchange between the flame combustion products and spraying particles is possible if temperature of the combustion products in the plume is 250–300 °C higher than the metal melting temperature [9]. Taking into account the above-said, length of the active temperature interval of the flame plume for metals melted at a temperature of 1250 °C (brass, bronze, powders of self-fluxing alloys, exothermically reacting powders and composites) will be determined by the isotherm corresponding to 1500 °C.

Investigations of variations in temperature along the length of flame plume [10] showed that length of its regions with a combustion temperature above 1500 °C is bigger at a turbulent character of flow of the combustion products, and that with a temperature below 1500 °C is bigger at a laminar character of the flow. With introduction of hydrocarbon compounds to HOM a tendency to increase of the length of the flame active zones is observed.

Mode of the jet flow influences the distribution of velocity of the gas jet along the length of the flame plume. At a turbulent character of the jet flow the velocity in initial regions situated closer to the nozzle is maximal, whereas at a laminar character its reduction takes place more monotonously (Figure 3, *a*).

Addition to HOM of 5.5 vol.% of the gasoline vapors increases the gas jet velocity in comparison with pure HOM (Figure 3, *b*), and addition of 16 vol.% of the alcohol vapors has almost no influence on the jet velocity (Figure 3, *c*).

Results of the investigations conducted were used for the development and implementation of the processes of gas welding of copper output wires of electromagnet coils to their winding wires, sheet steel casing parts, brass pipelines of refrigerating systems, brazing of capillary pipelines of stainless steels, copper radiator tubes, spraying of axles of electric drill shafts, repair of dies, and other gas-thermal processes of metals treatment at Kiev and Moscow enterprises.

CONCLUSIONS

1. The investigations showed that the mode of flow of the HOF combustion products jet at stable burning of combustible mixture is of a laminar and turbulent character. A change in the character of flow of the combustion products influences the flame geometry, distribution of temperature and velocity of the gas jet along the flame plume length. At that it is possible to control the oxidation-reduction processes in the weld pool by regulating composition of the combustible gas mixture through saturation with vapors of liquid hydrocarbon compounds by means of bubbling.

2. The calorific intensity of HOF is higher compared with other hydrocarbon fuels due to a laminar flow of the combustion products in the core and near-core zone, which allows welding steel parts up to 3 mm thick. In this case, the coefficient of acetylene to oxygen change is equal to 2. The thermal capacity of HOF produced by combustion of the EWG generated mixture can be increased in 2–3 times through saturation of the mixture with vapors of hydrocarbon compounds.

1. Korzh, V.N., Starodumov, A.I., Matveev, I.V. et al. *Device for flame treatment of metals*. USSR author's cert. 967704. Int. Cl. B 23 K 5/00. Publ. 23.10.82.
2. Korzh, V.N., Matveev, I.V., Tuzenko, Yu.M. et al. *Device for flame treatment of metals*. USSR author's cert. 1164017. Int. Cl. B 23 K 5/00. Publ. 30.06.85.
3. Korzh, V.M., Popil, Yu.S. (2002) Control of parameters of hydrogen-oxygen flame burning process in flame treatment of materials. *Nauk. Visti NTUU KPI*, **4**, 59–64.
4. Shashkov, A.N. (1946) Principles of control of gas welding flame composition. *Avtogennoe Delo*, **7**, 1–3.
5. Khitrin, L.N. (1957) *Physics of burning and explosion*. Moscow: MGU.
6. Kryzhanovsky, V.N. (1984) Determination of normal flame front width for stoichiometric and thin mixtures with various chemical compositions. *Promyshl. Teplotekhnika*, **3**, 39–45.
7. Korzh, V.N., Tuzenko, Yu.M., Matveev, I.V. (1984) Hydrogen-oxygen flame welding of parts from low-carbon steel. *Avtomatich. Svarka*, **1**, 70–71.
8. Korzh, V.N. (1985) Calculation of consumption of hydrogen used instead of acetylene in flame treatment of metals. *Ibid.*, **10**, 76–77.
9. (1964) *Application of gas-substitutes in flame treatment of metals*. Ed. by I.A. Antonov. Moscow: Mashinostroenie.
10. Korzh, V.N., Popil, Yu.S. (2004) Influence of hydrocarbon additives on the structure of hydrogen-oxygen flame and temperature distribution along the plume length. *The Paton Welding J.*, **11**, 32–36.

NONVACUUM ELECTRON BEAM WELDING OF STRUCTURAL STEELS

Fr.-W. BACH, A. BENIYASH, K. LAU and **R. KONYA**
Institute of Materials Science, Leibniz University of Hannover, Germany

Given are experimental results of application of nonvacuum electron beam welding for joining structural and high-strength steels up to 20 mm thick. It is shown that no machining of edges prior to welding is required after plasma and laser cutting. The high quality of welded joints was proved by comprehensive tests.

Keywords: *nonvacuum electron beam welding, welding unit, stainless steel, high-strength steels, penetration depth, filler wire, weld root formation, welding speed, metallography, mechanical properties*

The first publications on successful practical application of atmospheric (nonvacuum) electron beam welding (EBW) date back to the 1960s [1–3]. High productivity of the process and possibility of integrating it into existing production lines generated interest in it, first of all, among auto makers. A new wave of interest in the electron beam technology has emerged since the early 1990s, which is attributable to new tendencies in modern motor-car construction, which are related, in particular, to the development of lightweight structures of car bodies by using aluminium alloys [4, 5].

It should be noted that nonvacuum EBW is applied at present exclusively for joining thin-sheet materials in motor-car construction, which is practically the only industry that extensively uses this process. However, the capabilities of this technology are far from being exhausted only to this industry. Application of new materials and required increase in labour productivity make the manufacturers look for new advanced technological processes. Recently, a high interest in nonvacuum EBW is expressed by crane construction and shipbuilding industries, as well as other engineering sectors. This study presents estimation of the prospects of application of nonvacuum EBW for joining thick-plate materials.

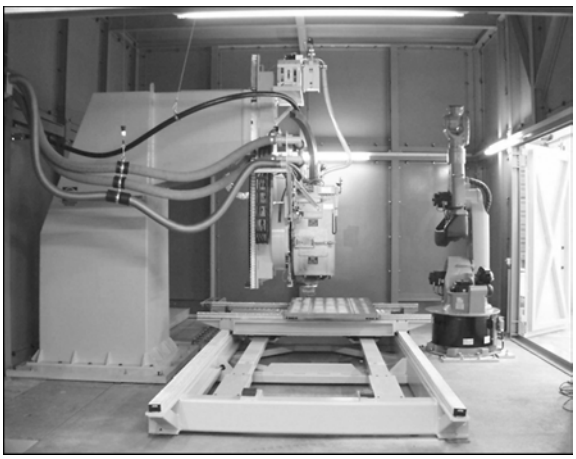

Figure 1. Unit for nonvacuum EBW at the Institute of Materials Science, the Leibniz University of Hannover

Experimental. Nonvacuum EBW was performed by using the «PTR Praezisionstechnik GmbH» welding unit of the NV-EBW 25-175 TU model (Figure 1). It has much in common with the widely applied units for welding in vacuum, and consists of a high-voltage power supply with a working voltage of 175 kV, and an electron beam gun with a maximum beam current of 140 mA. The beam is led out to the atmosphere by means of the three-stage evacuation system with helium being fed to the outlet stage to decrease scattering of the beam. The «Siemens» CNC positioning table is used to move the parts being welded. The unit comprises the «Kuka» industrial robot, which performs auxiliary operations. Specifications of the unit are as follows:

Working voltage, kV	175
Maximum beam current, mA	140
Table dimensions, mm	800 × 1200
Travel of table along coordinate X (Y), mm	3000 (800)
Vertical travel of gun along axis Z, mm	1200
Gun inclination angle, degree	0–90
Maximum welding speed, m/min	20

Preliminary experiments for evaluation of dependence of the penetration depth upon the welding parameters, which were conducted on samples of different alloys, proved a wide potential of application of the NV-EBW 25-175 TU unit for welding thick-plate materials. Figure 2 shows a typical dependence of the penetration depth upon the beam current, and Figure 3 ---- a transverse macrosection of the penetration

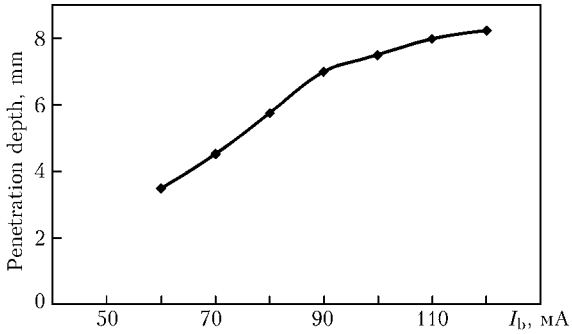

Figure 2. Penetration depth versus beam current for steel X2CrNi 18 9

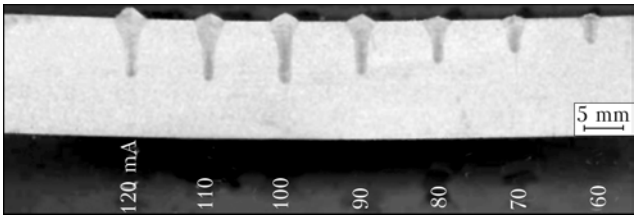

Figure 3. Transverse macrosection of penetration depth for steel X2CrNi 18 9 at different beam currents

depth for steel X2CrNi 18 9 at different beam currents (10 mm working distance, and 3 m/min welding speed). Figure 4 shows dependence of the penetration depth upon the welding speed.

An important difference of nonvacuum EBW from traditional vacuum EBW is the substantial dependence of the penetration depth upon the working distance, which can be explained by a considerable scattering of the beam in atmosphere (Figure 5).

As shown by preliminary investigations, the NV EBW 25-175 TU unit allows welding a thick-plate material at a high productivity. A drawback of nonvacuum EBW is a dramatic drop of the power density in the beam spot with increase of the working distance, this imposing certain limitations on the choice of geometry of the parts to be welded. Advantages of nonvacuum EBW can be best realised in making long horizontal welds, e.g. in welding of panels applied in shipbuilding, making of longitudinal welds in manufacturing of pipes, etc.

Welding of high-strength steels in crane construction. One of the possible application fields of nonvacuum EBW is crane construction. Requirements for increase in lifting capacity with a simultaneous decrease in weight of lifting cranes made it necessary to use high-strength steels with tensile strength of up to 1300 MPa. Experiments on nonvacuum EBW of high-strength steels applied to manufacture telescopic booms of high-capacity (up to 500 t) truck-mounted cranes were carried out by a request of the «GEC Ehingen» Company. The above steels of the bainitic-martensitic grade are supplied in the heat-treated condition. To avoid a dramatic decrease of their mechanical properties in tempering, welding of such materials should be performed at sufficiently high speeds. The experiments were conducted on plates of ESAB steels S960QL, S1100QL and S1300QL, the mechanical properties of which are given in Table 1.

Samples $500 \times 200 \times 6$ mm in size were butt welded without additional edge preparation after laser cutting. Part of the samples was welded by using the 1.2 mm diameter Draht Union X90 (GMn4Ni2CrMo) (EN 12534) filler wire. Welding speed was 2.5--3.0 m/min, beam current was 100--130 mA, working distance was 15 mm, and wire feed speed was 8 m/min.

Table 1. Mechanical properties of steels for crane construction

Material	σ_t, MPa	$\sigma_{0.2}$, MPa	ε, %
S960QL	980--1150	960	12
S1100QL	1200--1500	1100	10
S1300QL	1400--1700	1300	8

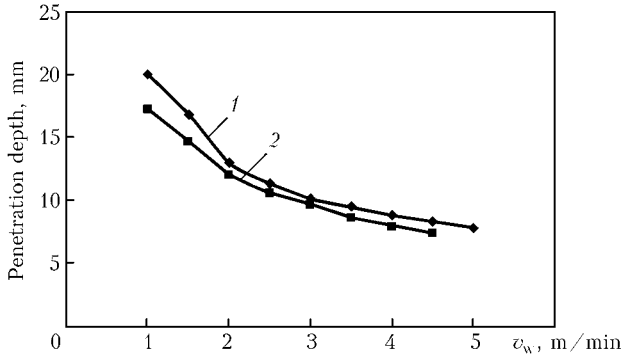

Figure 4. Penetration depth versus welding speed for steel X2CrNi 18 9 (10 mm working distance): *1* ---- I_b = 140; *2* ---- 120 mA

Specimens made from the welded samples were subjected to tensile tests. Results of mechanical tests are given in Table 2, which, for comparison, also gives mechanical properties of the joints made by hybrid plasma + MIG welding at a speed of 0.6--0.8 m/min [4]. For steel S96QL an increase in microhardness by *HV*0.2--50 was observed on the weld axis in a cross section of the weld, compared with the base metal. For steels S1100QL and S1300QL, the drop of microhardness by *HV*0.2--50 took place in the HAZ metal. In hybrid welding, the drop of microhardness in the HAZ metal increased to *HV*0.2--100. The data obtained are in good agreement with the mechanical test results. The experiments showed that the use of nonvacuum EBW instead of hybrid welding allows improvement of mechanical properties of the joints, in addition to a substantial increase in the welding speed.

Welding of shipbuilding steel D36. A promising field of application of nonvacuum EBW is shipbuilding, which is characterised by the use of thick-plate materials and long linear welds. Investigations were conducted in collaboration with the HDW-Gaarden GmbH shipyard and the shipbuilding equipment manufacturing company «ISU-GmbH» to evaluate the possibility of replacement of submerged-arc welding, which is traditional for shipbuilding, by nonvacuum

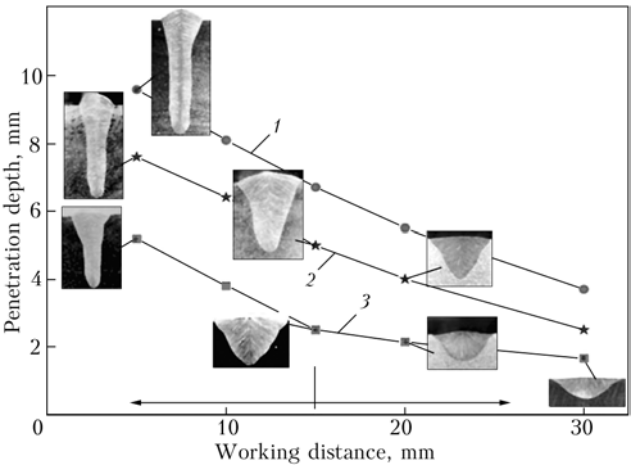

Figure 5. Penetration depth versus working distance for steel X2CrNi 18 9 at 5 m/min welding speed: 1 ---- I_b = 140; *2* ---- 100; *3* ---- 60 mA

Table 2. Results of mechanical tensile tests of 6 mm thick welded joints

Material	v_w, m/min	σ_t, MPa	$\sigma_{0.2}$, MPa	Filler	Character of fracture	Welding method
S960QL	3.0	1190	1037	Without filler	Base metal	EBW
S1100QL	3.0	1310	1250	Same	HAZ	Same
S1100QL	2.5	1485	1420	X90	Same	»
S1300QL	3.0	1315	1300	Without filler	»	»
S1300QL	2.5	1440	1385	X90	»	»
S1100QL	0.6	1265	1207	X90	»	Plasma+MIG
S1300QL	0.8	1235	1160	X90	»	Same

Table 3. Welding parameters used for samples of steel D36

Sample No.	Sample thickness, mm	Beam current, mA	Welding speed, m/min	Working distance, mm	Feed speed, m/min	Pass No.	Type of filler
66	4	110	4.5	10	--	1	--
59	10	140	2.2	10	--	1	--
59	10	50	1.4	15	10	2	Autrod 12.58
36	15	140	1.5	10	--	1	--
36	15	65	1.0	10	7	2	G3Si
25	20	135	1.0	10	2.2	1	G3Si

EBW. The task was to produce one-sided welds with a quality reverse bead formation without additional edge preparation after thermal cutting. In this case, substantial scattering of the electron beam, which is usually considered to be a drawback of nonvacuum EBW, is a very useful property, making it possible to reliably overlap the weld edges. Experiments were carried out on samples of shipbuilding steel D36 of the ferritic-pearlitic grade, 500 × 150 mm in size and 4--20 mm thick. Edge preparation after plasma cutting consisted in removal of a thin scale layer by using a metal brush.

Material 4 mm thick was welded without a filler wire. The technological bend (Figure 6) and static tensile tests, according to standard DIN EN 10002, showed a good quality of the joints.

Materials 10, 15 and 20 mm thick were welded with a filler wire. Typical configuration of the joint prior to welding is shown in Figure 7.

Owing to a large diameter of the beam, for the 20 mm thick material the gap in the upper part of a joint was 3.4 mm, which was not an obstacle for welding, in contrast to the sharp-focused laser or vacuum electron beams. Filler wire was used in welding the 10, 15 and 20 mm thick material to compensate for the gaps in the joints. The 10 mm thick steel was welded in one pass by simultaneously feeding the 1 mm diameter Autrod 12.58 (EN 440, G2Si) wire to the welding zone. The 10 and 15 mm thick materials were welded in two passes. Welding of the main section of the joint and formation of the reverse bead took pace during the first pass made without a filler wire. During the second pass the lacking section of the joint was filled up, and the weld surface was formed by using the 1.6 mm diameter G3Si (EN 440) filler wire. Welding parameters are given in Table 3.

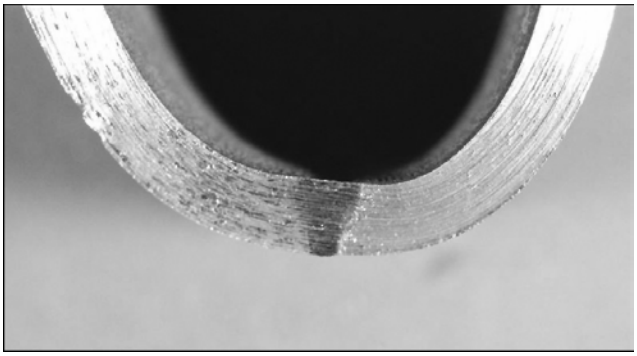

Figure 6. Appearance of a welded sample of 4 mm thick material after bend tests

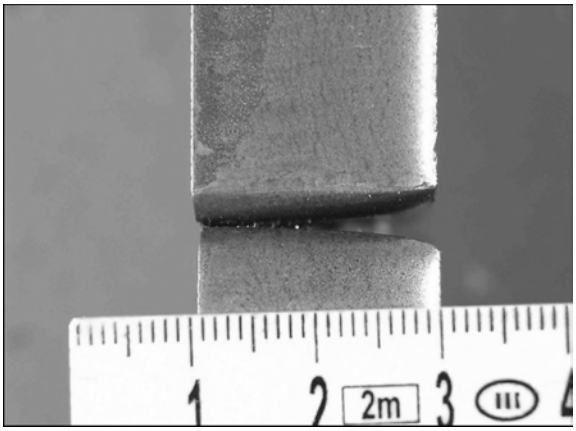

Figure 7. Configuration of the butt joint between 20 mm thick plates prior to welding

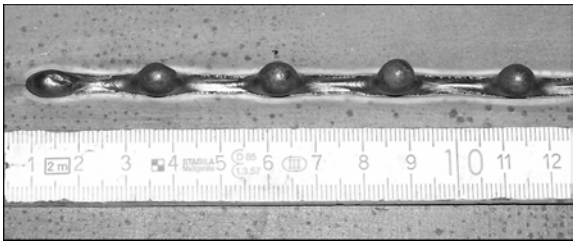

Figure 8. Defects in the weld root in welding of 20 mm thick material without backing

Welding of the 10 mm thick material caused no difficulties, whereas in welding of thicker materials (15 and 20 mm thick) the main problem was to provide a reliable formation of the weld root. As shown by the experiments, careful selection and strict observance of the welding parameters allow a free formation of the weld root for the 15 mm thick material. For the 20 mm thick material, the free formation of the weld root leads to defects in the form of periodic deflection of liquid metal (Figure 8).

To eliminate these defects, welding was performed on a backing. In this case, the first pass was made by EBW with a backing of the OERLIKON flux OP 122, and the second pass was made by EBW with a filler wire, or by submerged-arc welding. Appearances of the reverse beads made by different welding methods are shown in Figure 9.

Metallography revealed no defects in the form of pores or cracks. Figure 10 shows macrosections of the 15 mm thick sample made by EBW in two passes by using the G3Si filler wire. Maximal values of microhardness $HV0.2$--374 were detected in a transverse section of the weld on its axis with a gradual decrease along the line of the transverse section of the weld to microhardness of the base metal equal to $HV0.2$--232. No drops of microhardness were observed in the HAZ metal.

Figure 11 shows transverse macrosections of the weld on the 20 mm thick material after the first pass made by EBW and second pass made by submerged-arc welding. Both passes were made without any edge preparation. Static tensile tests in compliance with

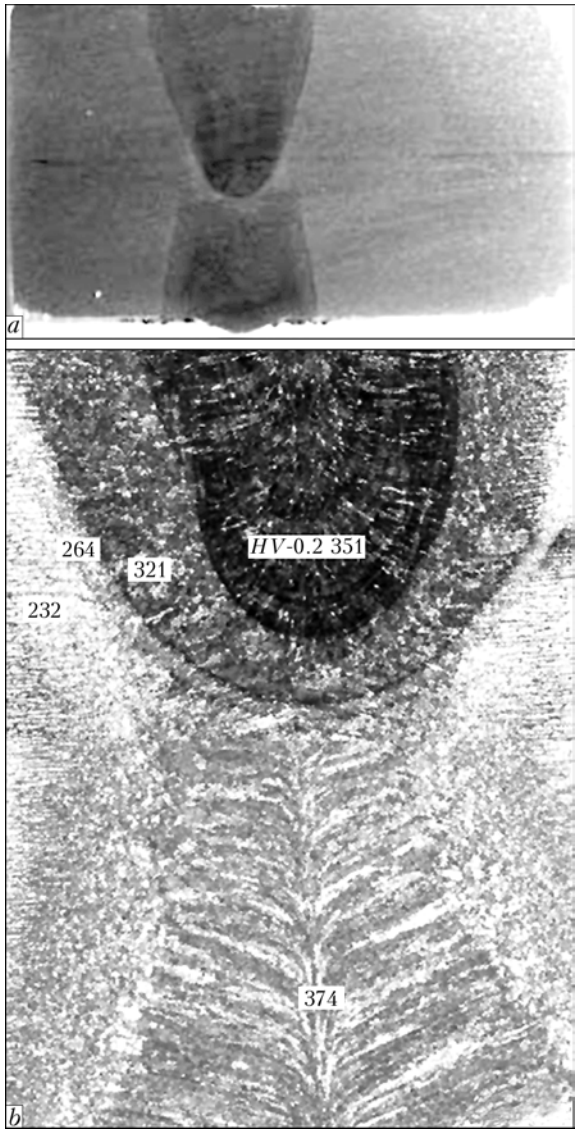

Figure 10. Transverse macrosections (*a* ---- ×1.5; *b* ---- ×16) of the 15 mm thick sample made by EBW in two passes with the G3Si filler wire

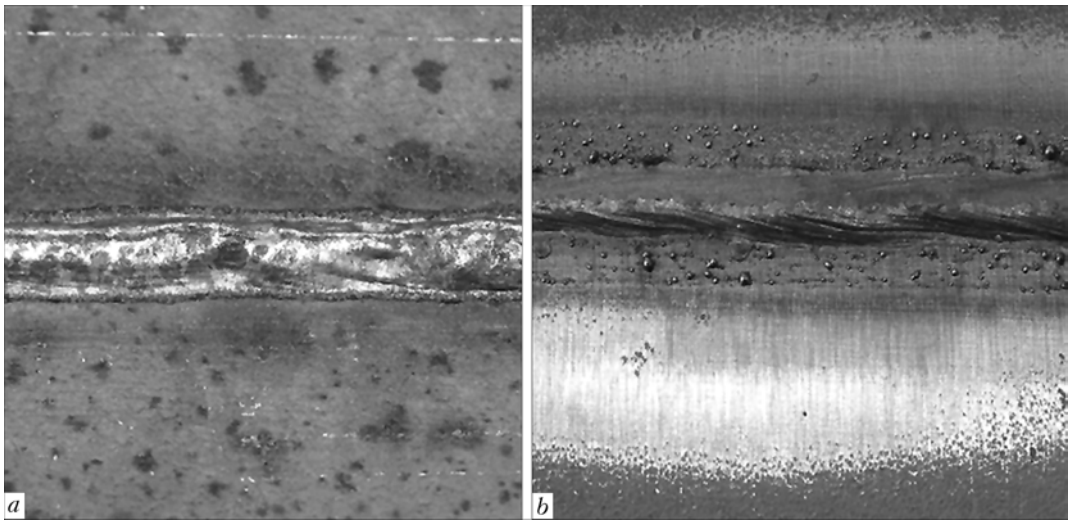

Figure 9. Appearances of the root part of the 20 mm thick weld made on the OP 122 flux backing (*a*) and 15 mm thick weld made with free formation (*b*)

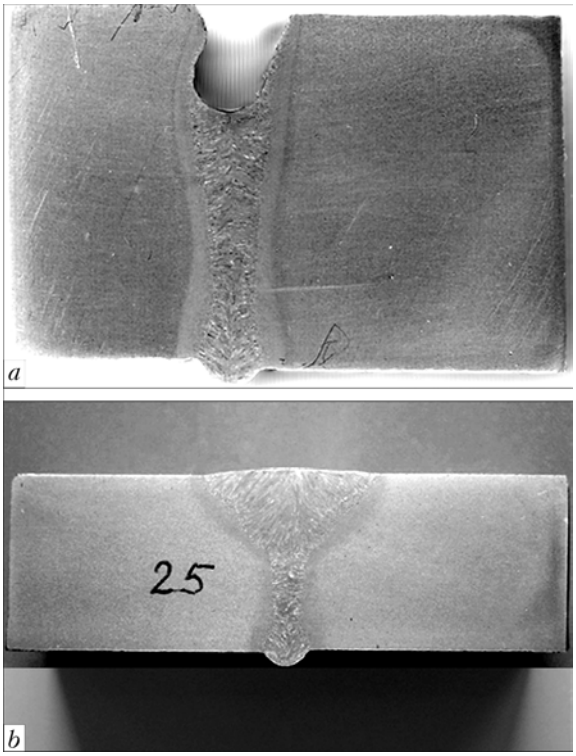

Figure 11. Transverse macrosections of the weld on the 20 mm thick sample after the first pass made on the OP 122 flux backing (*a*), and after the second pass made by submerged-arc welding using the OP 122 flux (*b*)

standard DIN EN 10002 showed a good quality of the joints. All the samples fractured in the base metal during the static tensile tests (Figure 12). Mechanical properties of the welded joints are given in Table 4.

In addition to the static tensile tests, the samples were subjected also to the impact toughness tests in compliance with the German Lloyd and standard DIN EN 10045. Impact energy on the standard Charpy test piece at –20 °C was 83 J for the weld metal and 64 J for the HAZ metal, which is much higher than the value of 47 J required by the standard.

The investigations conducted proved the high efficiency of nonvacuum EBW for welding thick-plate materials.

CONCLUSIONS

1. The welding unit of the NV-EBW 25-175 TU model allows welding of steels up to 20 mm thick.

2. Large diameter of the beam in nonvacuum EBW provides reliable welding at the presence of substantial fit-up gaps.

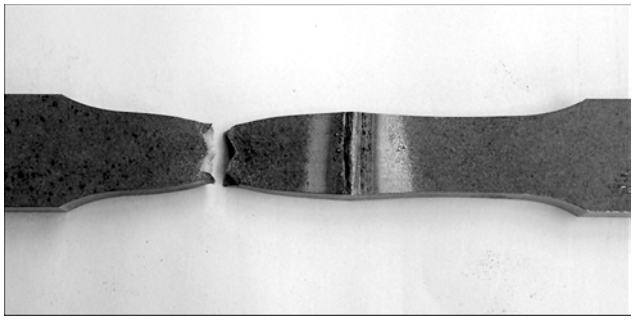

Figure 12. Appearance of the 15 mm thick welded sample after tensile tests

Table 4. Mechanical properties* of welded samples of steel D36

Metal thickness, mm	σ_t, MPa	$\sigma_{0.2}$, MPa	ε, %
4	513	357	14
10	552	379	11
15	581	386	11

*Mechanical properties of the base metal: σ_t = 490–630 MPa; $\sigma_{0.2}$ = = 355 MPa; ε = 21 %. The samples fractured in the base metal.

3. The thermal cycle of welding does not lead to a marked deterioration of properties of high-strength steels of the bainitic-martensitic grade.

4. Replacement of hybrid welding by nonvacuum EBW allows improvement of mechanical properties of the welds on high-strength steels for crane construction, in addition to a substantial increase in the welding speed.

5. Welding of shipbuilding steel 4–20 mm thick requires no additional edge preparation after thermal cutting, and provides mechanical properties of the joints that meet requirements of standard DIN EN 10045 and German Lloyd.

1. Bennet, M.G. (1970) Out-of-vacuum electron-beam welding. *Welding and Metal Fabr.*, **3**, 105–113.
2. O'Neil, F.P. (1967) High speed electron beam welding of tube. *Can. Welding and Fabr.*, **11**, 26–28.
3. Duhamel, R.F. (1965) Non-vacuum electron beam welding technique development and progress. *Welding J.*, **6**, 465–474.
4. Schubert, G., Holdgruben, H., Gomes-Buco, J. (1996) Non-vacuum electron beam welding of aluminium structural beams. In: *Proc. of Int. Body Eng. Conf.* (Detroit, Michigan, 1996), 58–61.
5. Bach, Fr.-W., Beniyash, A., Flade, K. et al. (2004) Non-vacuum electron beam welding: a beam process for welding zinc coated high strength steels and steel-aluminium hybrid structures. In: *Proc. of 4th Conf. LANE* (Erlangen, Germany, 2004). Vol. 1. Bamberg: Meisenbach, 247–258.

INFLUENCE OF JOINT GEOMETRY AND FIT-UP GAPS ON QUALITY OF CORNER JOINTS IN NEW MODIFIED SHORT ARC GMAW

P. KAH[1], **J. MARTIKAINEN**[1], **P. JERNSTROM**[2] and **J. UUSITALO**[2]
[1]Lappeenranta University of Technology, Lappeenranta, Finland
[2]Kemppi Company, Lahti, Finland

The effect of process parameters on the fit-up gaps in new modified short arc gas metal arc welding (GMAW) and the conventional short arc GMAW for steel plates is described. The modified short arc GMAW offered a number of advantages over the conventional short arc GMAW of fillet weld between two sheet plates in a corner joint in vertical downward welding direction. It was found that a higher welding speed and a smaller HAZ are reached using less energy with the modified short arc GMAW than with the conventional GMAW process. It was noticed that the modified short arc GMAW possesses approximately 25 % less heat input than the conventional GMAW, and modified short arc is 10 % faster than in conventional GMAW.

Keywords: *modified short arc GMAW, conventional GMAW, root gap, sheet metals, torch angle, electrode extension, joint quality*

GMAW is commonly used in most fabrication processes in industry due to its essential advantages such as deep penetration, smooth bead, low spatter and high welding speed. These advantages can be achieved due to various types of special equipments available for joining different types of metal of various thicknesses and with weld characteristics that suit the application requirements. [1, 2]. Nevertheless, weld defects may occur due to the welding process control parameters as a result of incorrect positioning of the torch, an incorrect root gap, and the placement of the sheet plates [3].

Research has shown that industries need to gain productivity and quality in sheet plate welding because the current method used in shielded metal arc welding (SMAW), gas tungsten arc welding (GTAW) and conventional GMAW methods are not specialized enough to be used with sheet plates [2]. This paper outlines the recent results of the potential advantages of the new modified short arc (MSA) GMAW technique over the conventional GMAW technique when welding sheet plates. The first section discusses the process principle which shows the current curve of the MSA GMAW process of different arc modes, the materials and consumables used in our investigation. The second section discusses the results of our experiments which provide an overview of an effort to develop and implement the MSA GMAW technique and conventional GMAW technique for the joining of sheet plates in a corner joint with different fit-up gaps.

The experimental study includes the welding of a $300 \times 50 \times 1.5$ mm sheet plate in a corner joint, in a single pass with different manipulation patterns of air gaps with the MSA GMAW technique and the conventional GMAW method. The welding equipment used was an inverted 500 A power source, a wire feeder and a cooling unit. The method of welding was automatic, but it can also be applied in mechanized methods.

Two base materials (structural and stainless steels) were used in this study. To determine their weldability, the formulas for the carbon equivalent and the units of crack susceptibility for cold and hot cracking were applied to the structural steel. It was found that the structural steel (Table 1) was free from cold cracking ($C_{eq} = 0.07$) and hot cracking (UCS = 9.8). For stainless steel, the most suitable way to make out the effect of a variety of elements on the basic structure of chromium-nickel stainless steels is the use of the Schaeffler diagram, which is frequently employed in welding. It plots the compositional restrictions at the room temperature of austenite, ferrite and martensite, in terms of nickel plus chromium equivalents (see Table 1). It was noticed that the stainless steel was free from hot cracking. In addition, the welding was carried out in ambient temperature and without any foreign material left in the groove [4].

In the study, the weld quality was based on the appearance of the weld bead with a different root gap. With a view to achieve an aesthetic weld, the process parameters were changed many times and the best parameters were chosen. In this work, the heat-affected zone (HAZ) was visually observed for different processes and the heat input was also calculated. Macrographs were taken after the welded pieces were cut, grinded, polished and etched with regard to observing the effects of process parameters on the penetration profile with different fit-up gaps.

This investigation is based on a dip-transfer arc which is characterized by the arcing period followed by a short-circuiting phase in which the transfer of metal takes place. This phase can be fine-tuned to the quality and diameter of the wire and the shielding gas used. When proper combinations of variables are applied, the outcome is less spatters and an obviously

Table 1. Chemical composition (wt.%) and weldability indicators for steels used

Steel	C	Si	Mn	P	S	Al
Structural	0.04	0.01	0.17	0.007	0.011	0.039
Stainless	0.05	0.42	1.58	0.031	0.003	--

Table 1 (cont.)

Steel	Cr	Ni	N	C_{eq}	UCS	Cr_{eq}/Ni_{eq}
Structural	--	--	--	0.07	9.8	--
Stainless	18.2	8.1	0.059	--	--	20.4/9.63

more stable arc, even when welding stainless steels. The main problem in short arc and pulse-arc welding has been the amount of spatter and the somewhat unstable arc when welding stainless steels.

Experimental procedure. *Welding equipment*. The welding machine used has a wide range of weld programs supporting most filler wires and gas combinations. This welding machine is a direct current (DC) power source which is used for other GMAW processes and for the MSA GMAW process. Figure 1 [5] shows the phases in the MSA GMAW and the conventional short arc GMAW process.

In the conventional short arc process, droplet detachment occurs at a high current value, which depends on voltage control. After that, the current slowly decreases before the arc period ends and the next short-circuit begins. In the modified short arc, the material transfer occurs at a low current value, which results in a soft transmission to the weld pool. Once the drop has been transmitted to the weld pool, the second current-rising phase begins and this initiates the arc stage. Subsequent to the two upslope phases of the modified short arc, the current is reduced to a desired base level. The use of a specified base current (BC) level ensures that the next filler drop will be transmitted during the next short-circuit. The highly controlled arc of the modified short arc process reduces spatter in the droplet detachment phase and decreases the heat input in the arc phase to be comparable with that in the conventional short arc process.

In the MSA GMAW process, the current and voltage are synchronized by the power source. The modified process as a GMAW process falls in the category 131, 135, 136, or 137 as classified in the EN ISO 4063 standard.

The total cycle last for approximately 5 ms consequently the power supply does not have enough time to dissipate the energy, thus, using enough energy to melt the metal to create a continuous weld. Since this energy is brought so fast to melt the metal, it is obvious that the travel speed can be increased with the modified short arc process.

The MSA GMAW process allows the adjustment of the wire feed, the level of the second upslope stage (forming pulse) level and the BC [5]. The forming pulse (FP) gives the control of the energy to the arc and droplet detachments do not occur at this point, whereas in the conventional pulse welding processes every pulse detaches a droplet. At the FP the arc force is greater than in the short arc processes because it pushes droplets to the molten pool. After the FP, the arc energy goes much lower than where the short arc level is at this point, and this facilitates the modified process to go faster in the next short-circuit. In general, the FP is needed because the droplet detachment happens at low current values.

Materials and consumables. Tables 1 and 2 give the elements of the various constituents that make up the base metals and their tensile properties at room temperature.

The consumable electrodes used in the experiment were 1 mm in diameter, and their compositions corresponded to the base metals. The electrodes were EN 440: G 3 Si1 (OK Autrod 12.50) and EN 12072: G 19 12 3 L Si (OK Autrod 16.32) for structural and stainless steels, respectively.

Gas selection was based on the metal to be welded. The shielding gases used in the study met the requirements of the EN 439 standard for the welding of steel metals. The shielding gas composition was Ar +

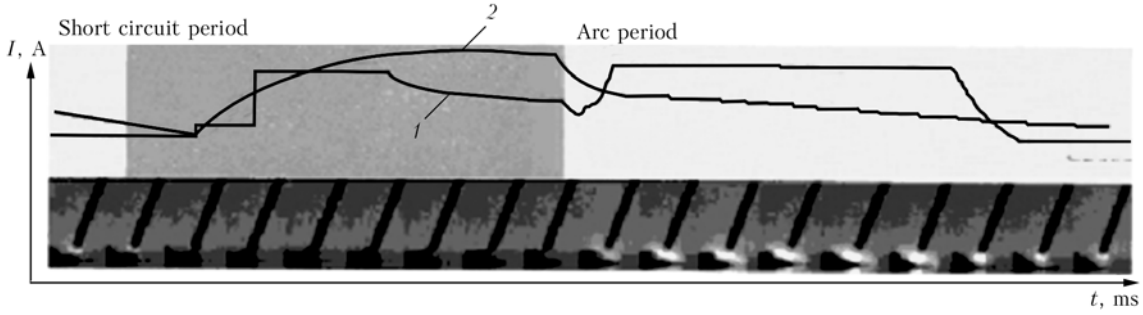

Figure 1. Current curve of the MSA (*1*) and conventional short arc GMAW (*2*) at different arc modes

Table 2. Room temperature tensile properties of base metals

Steel	$\sigma_{0.2}$, MPa	σ_t, MPa	*HB* 30	δ, %	ψ, %
Structural	177	305	--	80	41
Stainless	304	341	173	67	61

8 % CO_2 + 0.03 % NO used to weld structural base metals, and Ar + 2 % CO_2 + 0.03 % NO used to weld stainless steel base metals. The flow rate of the shielding gas used in all the stages of the experimental study was 15 l/h.

Welding parameters. Two welding variables were considered in this study: primary and secondary adjustable variables. The primary adjustable variables were travel speed, arc voltage, welding current and FP. Secondary adjustable variables are more difficult to measure and control accurately. They are assigned values and are usually included in welding procedure schedules. They include the tip-to-work distance (stick out), electrode position and electrode or nozzle angle.

When all the variables are in proper balance, the welder will have control over the molten metal and will deposit high-quality weld metal. The following section will explain how these welding variables interrelate and how some of them are more easily changed and are useful for control.

Experimental results and discussion. The experimental study was carried out with steel plates that had been degreased and wire brushed with a stainless steel brush. This guarantees both a minimum and an even oxide layer thickness.

The procedure is required for a clamping joint in fixtures (Figure 2) including setting welding parameters. First, one parameter was changed and the others were kept constant until the best quality of one group was attained. This procedure was repeated for different parameters until a high-quality joint was achieved. The quality of the joint was determined by inspecting the bead for a smooth surface and the absence of any visible defects, e.g. lack of penetration. The gap between the end of the consumable electrode and the workpiece was maintained at approximately 1 mm throughout the experiment. The air gap and joint design determine the weld parameters [6].

Case 1. *Zero root gap*. In this case with the conventional GMAW method, it was realized that the electrode extension (the length of the electrode that is out from the torch) is 6–7 mm and the gun angle is perpendicular to the workpiece and pointing at the line of the joint (Figure 3, *a*). The torch angle is of great importance when welding the fillet weld in corner joints. When making a fillet, the welding torch should be held so that it bisects the angle between the plates and is perpendicular to the line of the weld [4].

When the parameters were altered, it was realized that when the welding speed was 16 mm/s, the feeding speed 3.2 m/min, voltage 15.7 V, the electrode

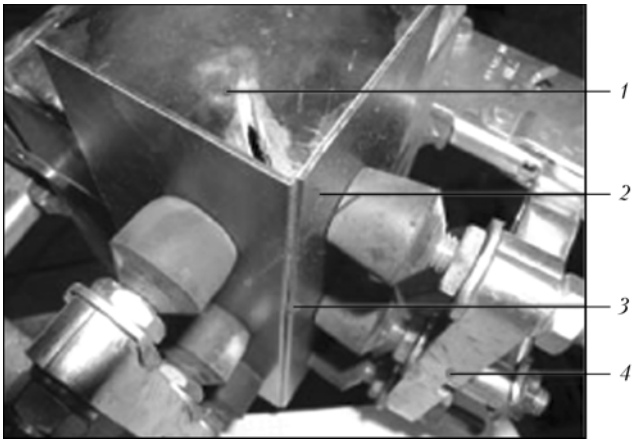

Figure 2. Set-up of metal plate before the welding process: *1* ---- support for the sheet plates; *2* ---- sheet plates; *3* ---- corner joint; *4* ---- hold-down clamp

extension (stick-out) 6 mm, inductance zero, and the intensity of the welding current 102 A, a very good quality weld could be achieved with the conventional GMAW process (Figure 3, *c*). When the parameters were maintained and the electrode was altered to point to the tip of one of the plates (Figure 3, *b*), it was noticed that the quality of the weld was identical. It was also noticed that the parameters used for a zero root gap could also be applied for 0.1 to 0.3 mm air gaps which also yield good quality welds. If these parameters are not properly selected, weld discontinuity will occur, including incomplete fusion, undercuts, burn-backs and an irregular bead surface.

When the welding speed is increased, the wire feed rate should also be increased so that the weld will have a sufficient weld puddle. With a low inductance setting, the welding was relatively cold and this helped the electrode to freeze in the weld pool [4].

The MSA GMAW method, as in case 1, revealed that the electrode extension should be 13 mm and the torch angle should be in a 97° pushing angle and perpendicular to the axis of the weld (Figure 4, *a*).

When the parameters were altered, it was found that a good quality weld could be achieved with structural steel (Figure 4, *c*) with a welding speed of 15 mm/s, wire feed rate of 3.5 m/min, voltage of 15 V, arc length of 15 mm, welding current of 95 A

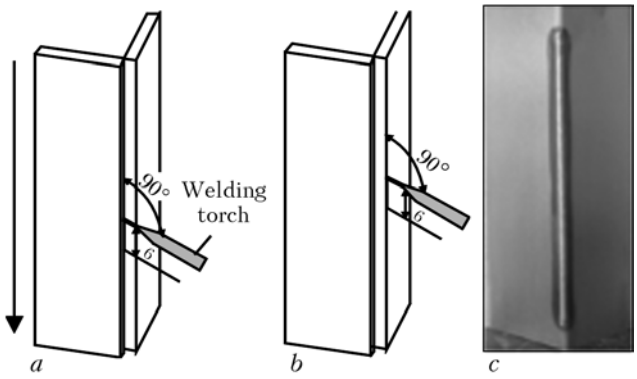

Figure 3. Conventional GMAW of the structural steel corner joint with zero root gap (*a, b*) and appearance of a welded joint (*c*): *a* ---- torch is directed along the joining line; *b* ---- same along the edge of one of the plates

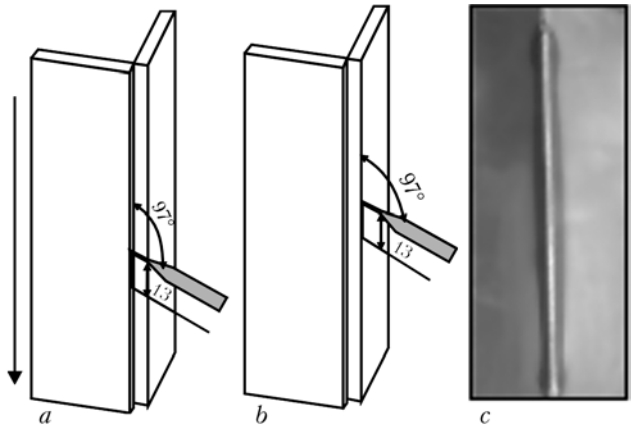

Figure 4. MSA GMAW of the structural steel corner joint with zero root gap (*a, b*) and appearance of a welded joint (*c*)

and FP of 0. A good quality joint resulted with stainless steel with a welding speed of 19 mm/s, feeding rate of 3.5 m/min, voltage of 16 V, welding current of 101 A, arc length of 20 mm, and the FP could be maintained at 0 or 20. Usually, the arc voltage increases slightly as the current increases.

On the other hand, maintaining the variables and changing the electrode to point to the tip of one of the plates (Figure 4, *b*) did not change the quality of the weld. The parameters that were used for zero root gaps are also suitable for root gaps of 0.1 to 0.3 mm.

The electrode extension is one of the important parameters to be considered in the new modified welding process in order to obtain a stable arc. It was found that a length in the range of 12 to 14 mm in the electrode extension is optimal for achieving a stable arc. A greater extension will increase spatters and the difficulty to start the arc. A shorter electrode extension will result in the arc burning underneath the workpiece. In the new modified process, just as in the conventional GMAW process, the GMAW torch feeds in the welding wire to strike the main arc with the workpiece. To ensure that the arc is ignited in a proper manner, the consumable electrode has to be close enough to the workpiece: the distance should be ≤ 1 mm.

The angle of the torch to the workpiece is also a significant parameter to be considered when welding

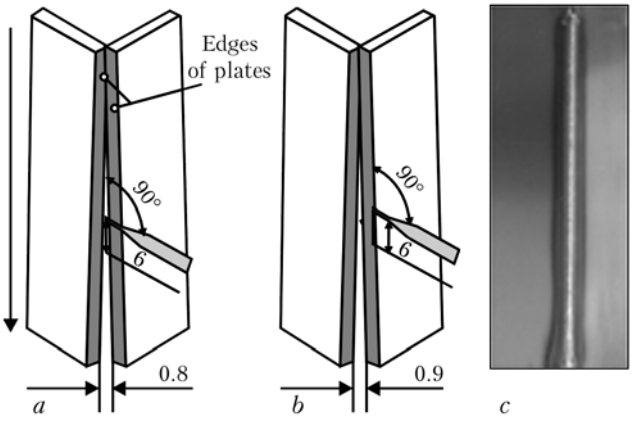

Figure 5. Conventional GMAW of structural steel with increasing root gap (*a, b*) and appearance of a welded joint (*c*)

with the new modified short arc welding process; it determines the behaviour and the stability of the arc. It was found that the angle in the range of 95 to 105° downward in the vertical direction is the most favourable; if this is taken into account, the arc stability is significantly improved.

A study carried out to see the effect of FP showed that when the FP is zero, the weld looks much better than when a negative FP is used with a zero root gap. With a negative arc length and zero FP, there is a slight influence on the quality of the weld. When the arc length is positive, there is a negative change in the superiority of the weld.

Case 2. *Increasing root gap*. A study carried out with conventional GMAW in this case shows that the stick-out should be 6 mm and the torch angle should be perpendicular to the base metal and pointing to the line of the joint or to the tip of one of plates (Figure 5, *a, b*, respectively).

With the set-up, described in Figure 5, *a*, a good quality joint with an increasing root gap of 0.8 mm with conventional GMAW can be realized (Figure 5, *c*) with a feeding rate of 3.2 m/min, welding speed of 13 mm/s, voltage of 15.7 V, inductance of 0, and current of 103 A. Changing the electrode to point to the tip of one of the plates (see Figure 5, *b*) it was noticed that good quality welds were produced in root gaps of 0.8 mm, and it was also possible to fill root gaps of 0.9 mm but with a negative effect on the weld quality.

When the direction of welding was changed to a vertical upward direction with the same parameters, there were negative changes in the weld quality.

The inductance had little or no effect on the weld puddle when welding thin plates with a little root gap, and negative inductance had some advantages in the smoothness of the weld as compared to positive inductance when the root gap is increasing [1].

As in case 2, with the new modified short arc method, the electrode extension and the torch angle were maintained at 13 mm and 97°, respectively, due to the advantages they demonstrated on the quality of the weld. The torch angle pointed either to the line of the joint or to the tip of one of the plates (Figure 6, *a, b*, respectively).

When the consumable electrode was pointed to the line of the joint (see Figure 6, *a*) it was possible to obtain a good quality weld with a root gap of up to 0.8 mm, but when the electrode extension was pointed to the tip of one of the sheet plates (see Figure 6, *b*) it was most likely that a good quality weld (Figure 6, *c*) with a root gap of up to 1.25 mm could be achieved with the following parameters: welding speed of 13 mm/s, wire feed rate of 3.7 m/min, voltage of 16.5 V, arc length of 15 mm, current of 104 A, and an FP of –20. With an FP of –20, the arc burned with a spreading manner, and this helped the weld puddle to spread over a large area, enabling the gap to be filled in the joint.

Once more, when the torch angle ranged from 92 to 95° vertically downward to the line of the joint of

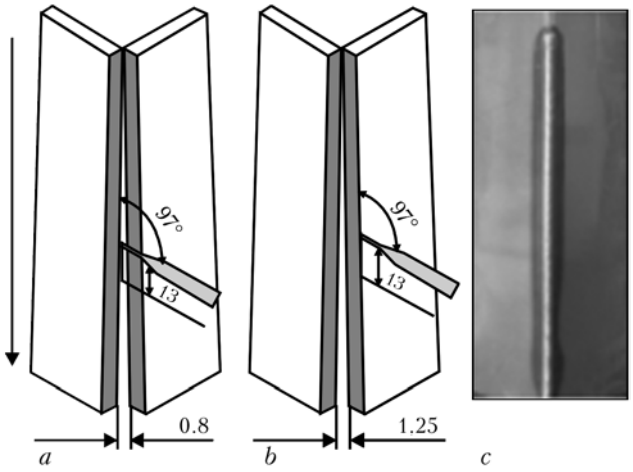

Figure 6. MAS GMAW of structural steel with increasing root gap (*a, b*) and appearance of a welded joint (*c*)

the workpiece, and the direction of welding was pushed or dragged, it was realized that the quality of the welded joint tended to decrease compared to when the angle of the torch was increased to 97 or 100°.

A good quality weld was achieved with a root gap of 0.7 to 0.8 mm with a welding speed of 13 mm/s and a feeding speed of 3.5 m/min, and the electrode pointing to the line of the base metal joint (see Figure 6, *a*). Keeping all the parameters constant and changing the position of the electrode to the tip of one of the metal plates, the weld results were the same as when the electrode was pointing to the line of the joint with a root gap of 0.7 to 0.8 mm.

Case 3. *Root gap in the middle*. With the conventional GMAW method in this case, the electrode extension was also maintained at 6 mm and the torch was perpendicular to the workpiece and pointing either to the line of the joint or to the tip of one of the workpieces (Figure 7, *a, c*, respectively).

When the consumable electrode was pointed to the line of the joint (see Figure 7, *a*) it resulted in a good quality weld (Figure 7, *b*) with a root gap of 0.8 mm using a welding speed of 13 mm/s, voltage of 15.7 V, current of 98 A and feeding rate of 3.3 m/min with conventional GMAW. When the consumable electrode was pointed to the tip of one of the workpieces (see Figure 7, *c*) it was possible to achieve a good quality weld (Figure 7, *d*) with a root gap of 1 mm,

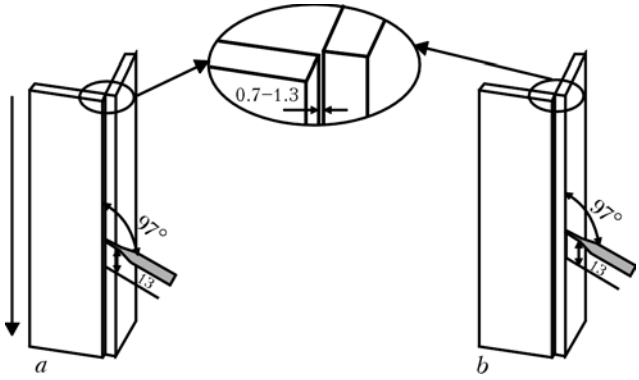

Figure 8. MSA GMAW of structural steel with a root gap in the middle (for explanations see the text)

welding speed of 13 mm/s, voltage of 15 V, current of 92 A, and feed rate of 3.0 m/min.

When the welding speed was increased to 18 or 20 mm/s, a good quality weld could be achieved with a voltage of 19.7 or 20 V with a root gap of 0.6 or 0.5 mm, respectively. For an aesthetic weld to be achieved, the inductance should be set to zero once the travelling speed is increased.

An experiment was also carried out with the MSA GMAW process in case 3 with the sheet plates placed perpendicularly (Figure 8). The torch angle was maintained at 97° vertically downward, and the electrode extension was maintained in 13 mm and pointing closely to the line of the joint or to the tip of one of the plates (see Figure 8, *a, b*, respectively).

When the consumable electrode is pointed closely to the tip of the upper plate and the plates are placed approximately 0.7–1.1 mm apart (Figure 8, *b*) the quality of the joint is good compared to when the consumable electrode is pointed closely to the line of the joint (Figure 8, *a*) with the same parameters: welding speed of 15 mm/s, feed rate of 3.7 m/min, voltage of 15.6 V, arc length of 15 mm, amperage of 101 A, and FP of 20 with a 0.8 mm root gap with structural steel. Using the same set-up to join stainless steel, it was realized that a root gap of up to 1.35 mm could be welded (see Figure 8, *a*) with a welding speed of 17 mm/s, feed rate of 3.8 m/min, and voltage of 15.7 V. The arc length and FP were kept at 20, while the current was 104 A. This is due to the ability of the welding machine to continuously analyze

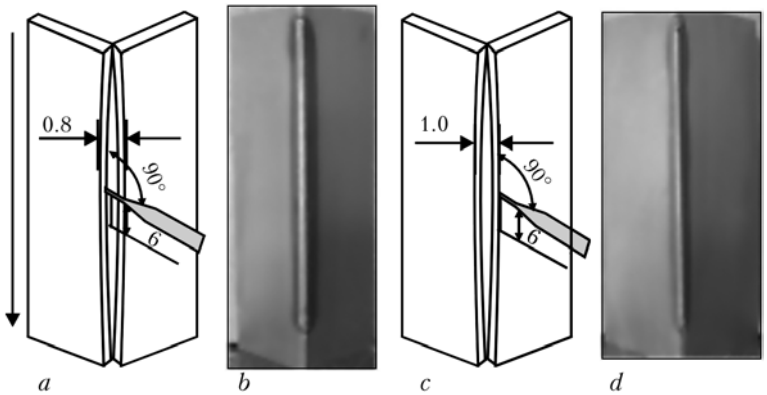

Figure 7. Conventional GMAW of structural steel with a root gap in the middle (*a, c*) and appearance of welded joints (*b, d*)

Table 3. Macrographs of weld cross sections in various GMAW of plates 1.5 mm thick

Conventional GMAW	Gap width variables	Zero root gap Structural steel Welding along the joining line	Zero root gap Structural steel Welding along the edge of plate	Root gap of 0.8 mm in the middle Structural steel	Root gap of 1.0 mm in the middle Structural steel
	Profile	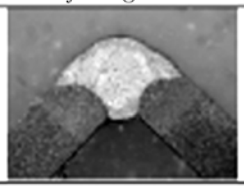	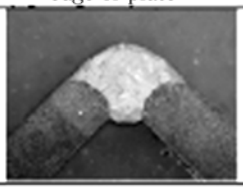	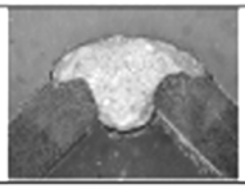	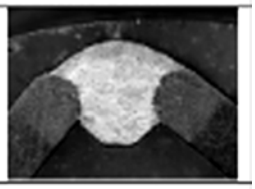
MSA GMAW	Gap width variables	Zero root gap Structural steel Welding along the joining line	Zero root gap Stainless steel Welding along the joining line	Increasing root gap of 1.25 mm Structural steel	Root gap of 1.35 mm in the middle Stainless steel
	Profile	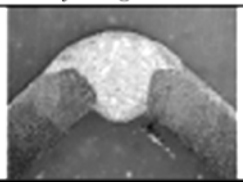	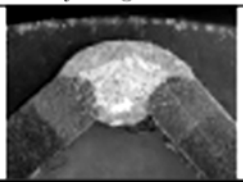	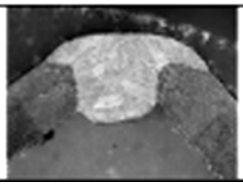	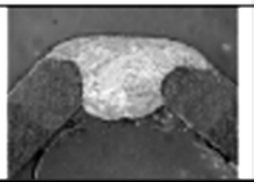

the changes in the arc and compare them to the pre-set value.

When the process parameters were maintained and the consumable electrode pointed to the line of the joint (see Figure 8, *a*) it was only possible to weld a 1.0 mm root gap with stainless steel. Again, a root gap of 1.25 mm could be also welded when welding structural steel when the angle of the torch is increased to approximately 100° and the electrode points to the tip of the upper plate.

With the MSA GMAW method, a very high welding speed can be achieved as compared to conventional GMAW due to the fact that the process checks and corrects the times of the separation of the weld bead metal droplets from the wire into the weld pool [5].

The manipulation pattern of the root gap has an important role in welding a larger root gap in a corner joint because with the location of the electrode to the part and the plates placed (see Figure 8) it is possible to weld larger root gaps.

Evaluation of welded joint performance. The external appearance of the welded joints was visually inspected and evaluated for the presence of welding defects such as non-fusion zones, blowholes and a lack of penetration. Specimens for optical metallography were obtained from the transverse direction of the weld, followed by mechanical polishing with a standard technique and etched with a 4 % nital [7].

The shape of the photomacrographs showed that correct process parameters were chosen for the realization of good quality joints. The shapes of the bead also depend on the placement of the workpieces and the position of the torch. The depth and width of the molten pool are extremely important for a high-quality weld. Table 3 presents macrographs which demonstrate changes in the weld cross section with different manipulations of air gaps and different types of steel with a thickness of 1.5 mm.

Evaluation of energy and heat input in welding of sheet metal. In GMAW, a sufficient amount of power (energy transferred per unit time) and energy density are supplied to the electrode to produce melting. Heat is an important characteristic because it influences the cooling rate which may affect the mechanical properties and metallurgical structure of the weld and HAZ metal. Another factor relates to the alloying in the weld pool, especially if the analysis of the welding rod is different from the base metal [5].

In this study, the wire feed rate and welding speed were maintained for a given length of the workpiece, and the following evaluation was conducted by applying the formula for calculating the heat input Q [4]:

$$Q = \frac{60EI}{1000v},$$

where Q is the heat input; E is the voltage; I is the welding current, and v is the welding speed.

With the conventional GMAW process, the outcome was as follows: v = 13 mm/s = 780 mm/min, E = 15.6 V, I = 113.5 A. Replacing the values in the formula resulted in Q = 0.109 kJ/mm.

Finally, using the MSA GMAW technique, the outcome was as follows: v = 13 mm/s = = 780 mm/min, E = 14.9 V, I = 90 A. Replacing the values got after the weld to the formula led to Q = = 0.082 kJ/mm.

In principle, all of the heat generated in the arc does not enter the base metal. Some energy is lost through radiation and some is used to melt the electrode. The loss varies from as low as 20 % to as high as 75 %, based on the welding process and other conditions [4].

CONCLUSIONS

This is a comparison of the effect of types of power supplies in achieving a good weld. Referring to the

above-mentioned results and discussion, the conclusions are as follows:

• the new modified short arc GMAW process allows the welding of structural and stainless steels in a corner joint in a vertical downward position;

• the manipulation pattern of the root gap and the location of the electrode extension have a great deal to do with the welding of a root gap greater than 0.5 mm;

• the new technique possesses a heat input (0.082 kJ/mm) of approximately 25 % lower than the conventional GMAW process. This creates a lower effect on the metallurgical properties of the weld piece. One can even perceive that the area on the weld metal affected by heat is smaller with the modified technique than with the conventional GMAW process;

• with the modified GMAW technique, it is possible to weld larger root gaps with higher travel speeds, with electrode extension ranges from 12 to 14 mm and the torch angle ranges from 95 to 105° vertically in the push direction;

• when the electrode extension is placed at the tip of one of the metal plates, larger root gaps can be welded with high quality, compared to those when the electrode is placed on the line of the joint of the base metal;

• when the wire feed rate with the new technique is low, it causes melt back, and when it is high it causes the arc to extinguish through short-circuiting;

• the results obtained from the photomicrograph show that the parameters chosen for the different processes with regard to the different aspects were sufficient for a good quality weld;

• the new modified short arc technology offers an alternative to all automated or robot-assisted GMAW processes for joining thin sheets.

Acknowledgments. *This work was carried out at Lappeenranta University of Technology, with collaboration with the Kemppi Company in Lahti, Finland. The authors wish to thank the following people: Esa Hiltunen, Tero Kontiainen, Harri Rotko and Antti Heikkinen who contributed in one way or the other in the realization of this study.*

1. Kah, P.C., Martikainen, J. (2007) Welding of sheet metal using modified short arc MIG/MAG welding process (FastROOT). In: *Proc. of 3rd Int. Conf. on Total Welding Management in Industrial Application* (Lappeenranta, Finland).
2. Uusitalo, J. (2007) Modified short arc process — a new way of welding root passes. *Ibid*.
3. Murugan, V.V., Gunaraj, V. (2005) Effect of process parameters on angular distortion of gas metal arc welded structural steel plates. *Welding J.*, **11**, 165–171.
4. Howard, B.C. (2002) *Modern welding technology*. 5th ed. AWS, 123, 134, 135, 142, 151, 193.
5. Uusitalo, J. (2008) The WiseRoot welding process for root passes welding. In: *Proc. of Symp. on Joining of Materials* (2008), 109–117.
6. Zhang, G.J., Chen, S.B., Wu, L.J. (2005) Intelligent control of pulsed GTAW with filler metal. *Welding J.*, 9–15.
7 *EN 10112-1*: Welding recommendation for welding of metallic materials.

EVALUATION OF RESIDUAL LIFE OF WELDED JOINTS ON TANK VERTICAL WALL AFTER 20–25 YEARS OF SERVICE

A.Yu. BARVINKO
E.O. Paton Electric Welding Institute, NASU, Kiev, Ukraine

The paper presents the results of experimental investigations of the residual service life of shop vertical butt welded joints of 16G2AF steel on a coiled tank wall after 20–25 years of service. No changes of mechanical properties with time were found, including their cold resistance. It is established that the studied welded joints have the residual service life sufficient for their further operation for not less than 20 more years.

Keywords: *oil storage tanks, 16G2AF steel, shop butt welded joints, residual life*

Starting from 1984, OJSC «Ukrtransneft» has had four floating roof tanks each of 50,000 m^3 volume in operation for oil storage. Tanks were constructed with application of coiled blanks butt welded in the plant by two-sided automatic submerged-arc welding from separate 1.5 × 6.0 m sheets. Lower rings of the wall of 17–10 mm thickness are made of high-strength 16G2AF steel (C440). Tanks are operating under the conditions of low-cycle loading. Having operated for the specified service life of 20 years [1], they require overhauling in most of the cases. In keeping with the acting norms of Ukraine [1], the tanks after overhauling should have the guaranteed residual life of not less than 20 years at the maximum technically possible level of oil filling.

Taking into account the actual technical condition of the tanks during overhauling in most of the cases the bottom, central part of floating roof bottom, entire first ring and vertical site butt joint of the wall are to be replaced. After repair the tank service life is mainly determined by the residual life of vertical butt welded joints of the wall.

Evaluation of tank residual service life after overhauling should be considered in terms of ensuring their performance under the conditions of cyclic and static loading. It may be assumed that the butt joints of the wall over the past 20 years of tank operation have withstood $20 \cdot 300 = 6 \cdot 10^3$ cycles of oil draining-filling, where 300 is the number of cycles per 1 year [2]. It is natural that this leads to the question of residual service life of shop welded joints during the subsequent guaranteed service life of the tanks.

Joints cut out of the tank first ring during its repair are taken as the initial welded joints. Current (final) welded joints were produced in the laboratory by artificial loading of the initial joints in the pulsator-machines up to cycle number $N = 1.2 \cdot 10^4$ at stress amplitude $\sigma = (0.10–0.67)\sigma_y$. Produced samples to a certain extent reflect the tank wall performance after their operation for the next 20 years in the main pipeline system [2].

Fatigue analysis of the butt welded joint for steel of strength class C440 made in keeping with the recommendations of [3] at cycle number $N = 10^5$ showed the maximum admissible stress for the given welded joint $\sigma = 546$ MPa at specified value $\sigma_y = 440$ MPa.

Four samples of this welded joint were tested with the above stress amplitude as additional evaluation of the obtained data on prediction of the fatigue life of the initial welded joint. Testing showed that no visible

Table 1. List of the performed testing and investigations of the initial and current welded joints on 16G2AF steel

Description of investigations and tests	Initial welded joints			Current welded joints		
	BM	Weld	HAZ	BM	Weld	HAZ
In-coming radiographic inspection	+	+	+	+	+	+
Determination of the composition	+	–	–	–	–	–
Determination of mechanical characteristics	σ_y; σ_t δ_5; ψ	σ_t	σ_t	σ_y; σ_t δ_5; ψ	σ_t	σ_t
Metallographic investigations of microstructure: microstructure examination	+	+	+	–	+	+
HV hardness measurements	+	+	+	–	+	+
Determination of *KCU* and *KCV* impact toughness (T = +20; 0; –20; –40 °C)	+	+	+	+	+	+

cracks developed on the basis of $N = 10^5$ loading cycles. Therefore, in terms of cyclic loading the residual service life of the tanks is guaranteed for the next 20 years after overhauling.

The list of testing and investigations to be performed for assessment of possible lowering of mechanical properties of welded joints is given in Table 1, and schematic of sample cutting out ---- in Figure 1.

Before the start of investigations X-ray inspection of the quality of welded joints was performed on four plates taken as the initial and current welded joints. No inadmissible defects were found taking into account the codes [4]. Mechanical properties of rolled sheets from high-strength 16G2AF steel supplied to the plant in 1982 for fabrication of coiled blanks, should comply with the specification [3, 5].

As is seen from Table 2, composition of 16G2AF steel corresponds to GOST 19282--73 [5] and is the same for the initial and current samples.

Table 3 gives the results of testing the initial and current rolled sheets.

Results of tensile testing of butt welded joints without removing the weld reinforcement are as follows: for initial joint σ_t = 640.5--672.3; for current joint ---- 630.1--650.0 MPa. The fracture site is the base metal. Conducted testing showed that the strength properties of the rolled sheets meet the requirements of GOST 19282--73 ($\sigma_t \geq 590$ MPa) [5].

Results of impact toughness testing of the initial and current welded joints (base metal, weld and HAZ metal) are given in Figure 2. Note that the code [3], which was in force during tank design and coiled blank fabrication (1982--1984), as well as in the code currently in force [6], impact toughness (*KCU*) of not less than 40 J/cm^2 at T = --40 °C is required for rolled sheets of 18G2AF steel 10--32 mm thick. Considering that the Russian codes [7] specify a more strict evaluation of cold resistance of the rolled sheets, additional testing of samples, also with a V-shaped notch, was performed for the studied welded joints.

Analysis of the results of impact toughness testing (*KCU*) of the samples did not reveal its change in the current welded joint compared to the initial one. A rather high scatter of values is noted, which is characteristic for 16G2AF steel. It is established that the base metal, weld and HAZ metal in the initial and current condition satisfy the requirements of impact toughness (*KCU*) of the codes [3], by which they were designed.

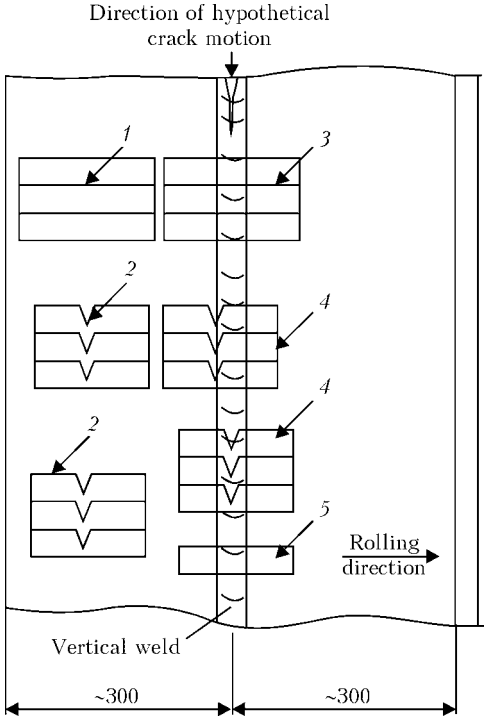

Figure 1. Schematic of sample cutting out of the welded butt: *1, 3* ---- samples for strength testing of base metal and welded joint, respectively; *2, 4* ---- samples for determination of base metal impact toughness, as well as metal of the weld and HAZ with a round (*KCU*) and sharp (*KCV*) notches; *5* ---- samples for metallographic examinations

Impact toughness testing of samples with a sharp notch (*KCV*) did not reveal any change in the properties of the initial and current welded joint. However, for both the welded joints *KCV* values for the weld and HAZ did not satisfy the requirements of the standard [7]. It should be noted that taking into account the characteristics of weldability and cold resistance

Table 2. Composition of the initial and current rolled stock of 16G2AF steel, wt.%

Kind of rolled sheets	C	Si	Mn	Ni	V	S
Initial sample	0.16	0.39	1.41	0.22	0.11	0.024
Current sample	0.18	0.47	1.55	0.21	0.10	0.031
GOST 19282--73	0.14--0.20	0.3--0.6	1.3--1.7	≤ 0.3	0.08--0.14	≤ 0.035

Table 3. Mechanical properties of initial and current rolled sheets

Kind of rolled stock	σ_y, MPa	σ_t, MPa	δ_5, %	ψ, %
Initial sample	490.8--507.7	640.0--663.0	29.0--30.6	65.1--69.1
Current sample	421.3--513.2	663.4--680.4	27.6--28.2	68.6--70.8
GOST 19282--73	≥ 440	≥ 590	≥ 20	--

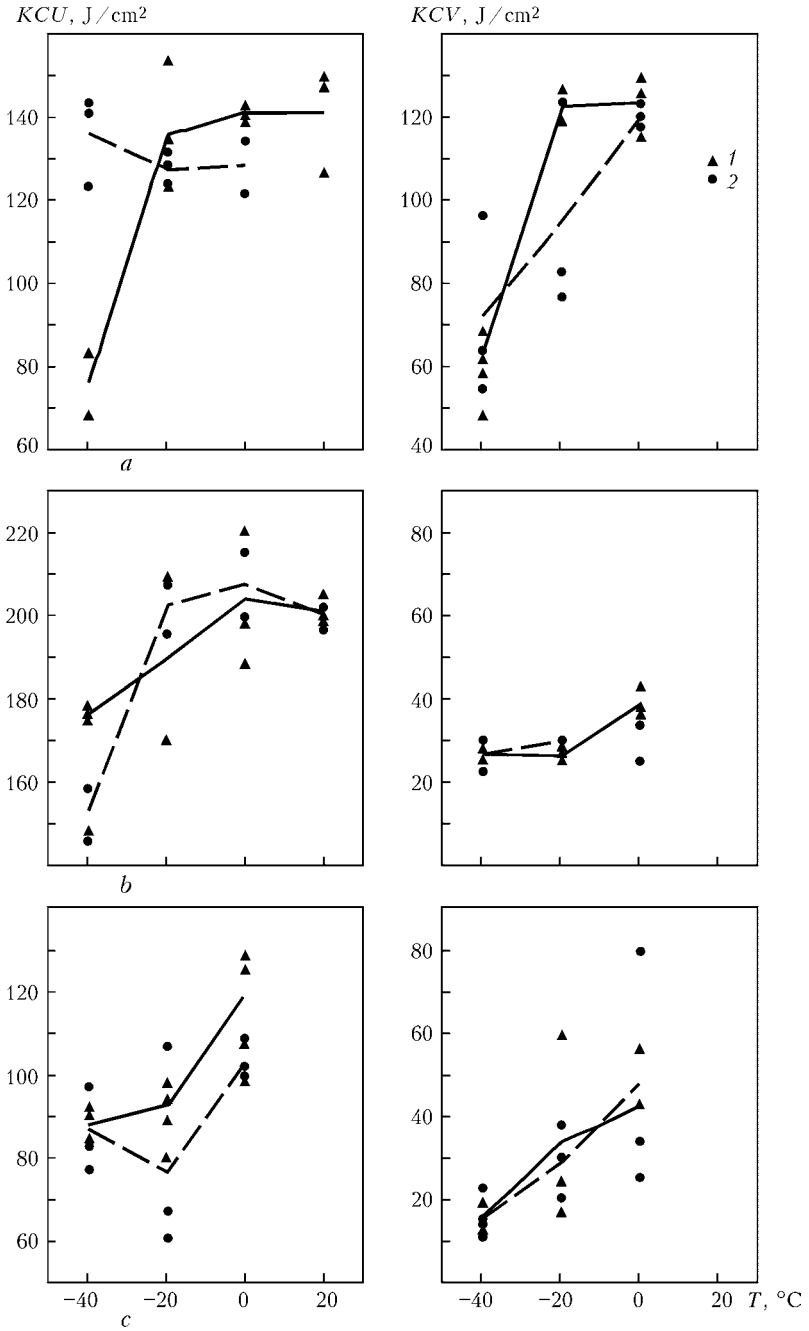

Figure 2. Results of testing samples of initial (*1*) and current (*2*) welded joint from 16G2AF steel on impact toughness with round (*KCU*) and sharp (*KCV*) notches: *a* ---- base metal; *b* ---- weld metal; *c* ---- HAZ

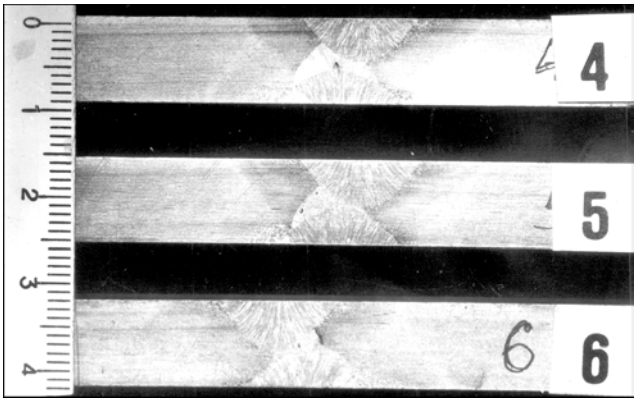

Figure 3. Macrosections of shop butt welded joints of 16G2AF steel with lacks-of-fusion and slag inclusions

the codes currently in force [1, 7] do not recommend 16G2AF steel for application for oil tanks and it can be successfully replaced by new generation steels 10G2FB [7] or 06G2B (C440) [8].

Metallographic investigations of the initial and current welded joints were performed in addition to the obtained results on the mechanical properties of 16G2AF steel welded joints. Base metal is a ferritic-pearlitic mixture with a pronounced rolled stock structure. Metal grain point was #8, ferrite hardness *HV*0.05-210--221, that of pearlite ---- *HV*0.05-244. Base metal and welded joint HAZ feature a great number of sulphide stringer inclusions both at a distance from the weld and in direct vicinity from the fusion line.

During metallographic examination also indirect assessment of crack resistance of welded joints was performed, allowing for presence of slag microinclusions and lacks-of-fusion in the HAZ (Figures 3, 4). Investigation results show that no initiation of new or development of the existing microcracks was revealed at the ends of crack-like microinclusions after artificial low-cycle loading equivalent to 20 years of tank operation. However, presence of crack-like microinclusions and lacks-of-penetration in the welded joints gives rise to the assumption that the welds can also have similar macroinclusions, development of which can be observed with time. To ensure guaranteed performance of such welded joints it is proposed at each complete examination of the tanks to perform ultrasonic or radiographic testing of the quality of plant vertical welds with application of only vertical X-ray films on the five lower rings of the wall.

The need to perform the proposed scope of research is confirmed by the conclusions on examination of a number of tanks of 20,000 and 50,000 m^3 volume. Analysis of the results shows that at each next examination of plant welds inadmissible defects are revealed, which are to be repaired.

CONCLUSIONS

1. Shop vertical joints of the tank wall built with application of coiled blanks from 16G2AF steel, preserved their high performance after 20–25 years of operation in the low-cyclic loading mode, and their residual life guarantees further safe operation of tanks for not less than 20 years, which meets the requirements of the standards of Ukraine for new tanks.

2. During periodical full examination of tanks it is necessary to perform ultrasonic and radiographic inspection of vertical shop welds on not less than five lower rings of the wall.

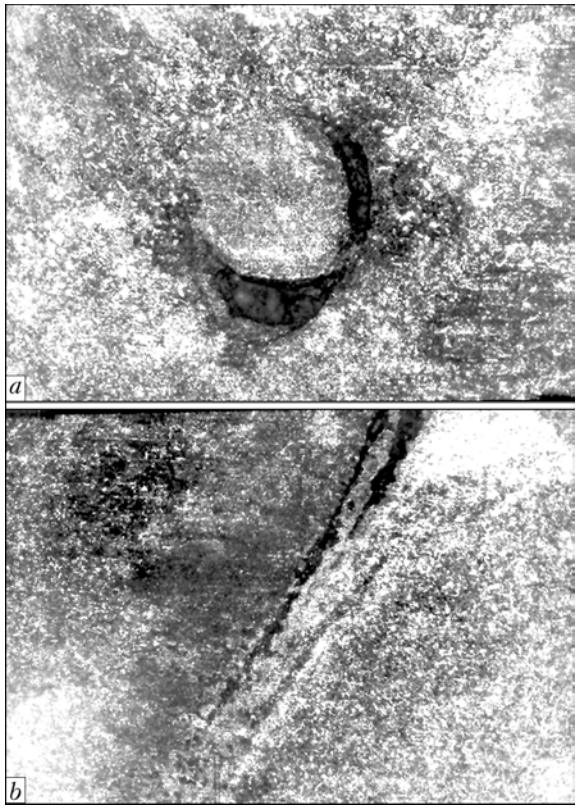

Figure 4. Microstructure (×100) of weld metal (*a*) and HAZ (*b*) of welded joint (after $N = 1.2 \cdot 10^2$ cycles) of 16G2AF steel

1. *VBN V2.2-58.2–94*: Vertical steel tanks for storage of oil and mineral oil. Valid from 01.10.1994.
2. *RD 16.01-60.30.00-KTN-026-1–04*: Norms for design of oil storage steel tanks of 1000–5000 m^3 volume. Introd. 21.06.04.
3. *SNiP II-23–81*: Steel structures. Introd. 01.01.1982.
4. *SNiP 3.03.01–87*: Load-carrying and enclosing structures. Introd. 01.06.1988.
5. *GOST 19282–73*: Low-alloy plate steel and wide strip universal shape steel. Introd. 01.01.75.
6. *GOST 19281–89*: Increased-strength steel rolled stock. Introd. 01.01.89.
7. *PB 03-605–03*: Rules for design of vertical cylindrical steel tanks for oil and petroleum products. Introd. 09.07.2003.
8. *TU U 27.1-05416923-085:2006:* Rolled sheets welded of quality steel of 355–590 strength grade for machine-building. Introd. 02.04.2007.

NEW FLUX-CORED WIRE ENSURING THE EFFECT OF STRAIN HARDENING OF THE DEPOSITED METAL IN OPERATION

L.S. MALINOV[1], **V.L. MALINOV**[1], **L.N. ORLOV**[2] and **A.A. GOLYAKEVICH**[2]
[1]Priazovsky State Technical University, Mariupol, Ukraine
[2]OJSC «TM VELTEK», Kiev, Ukraine

The paper gives information on a new flux-cored wire, not containing expensive alloying elements. Wire application ensures production of a metastable austenite structure in the deposited metal and realization of deformation martensite transformation during operation. This results in an essential increase of the surfaced part fatigue life. New wire can become widely accepted in manufacture of rapidly wearing parts for the most diverse applications.

Keywords: *arc surfacing, flux-cored wire, deposited metal, metastable austenite, deformation martensite transformation, self-hardening at loading*

The problem of resource saving is becoming ever more urgent now. One of the directions of its solving is improvement of fatigue life of parts reconditioned by automatic arc surfacing, in particular, heavily loaded crane wheels of metallurgical shops.

A considerable improvement of the residual life of reconditioned parts is achieved using surfacing consumables. They enable producing in the deposited metal the structure of strongly hardening metastable austenite, which transforms into martensite under the influence of deformation at loading in operation, which is classified as the effect of self-hardening at loading [1].

The first surfacing consumables ensuring formation of metastable austenite in the deposited metal were developed by M.I. Razikov with a team of associates at the start of the 1960s [2] based on cavitation-resistant 30Kh10G10 steel developed by I.N. Bogachev and R.I. Mints [3]. These surfacing consumables were applied mainly to improve the fatigue life of parts of hydraulic units, and later for surfacing various rapidly wearing parts operating under the conditions of dry friction, in particular, crane wheels.

A feature of surfacing by such materials, is the fact that failure to satisfy a number of conditions may result in embrittlement of the deposited layer because of formation of austenitic-martensitic structure, characterized by a high hardness. To prevent it, surfacing should be performed at relatively low values of current, arc voltage, but at an increased speed, formation of narrow beads, their intermittent nature, thus making the technology more complicated. In addition, deposited metal has poor cuttability [4] as a result of an intensive formation of martensite under the tool impact (deformation martensite).

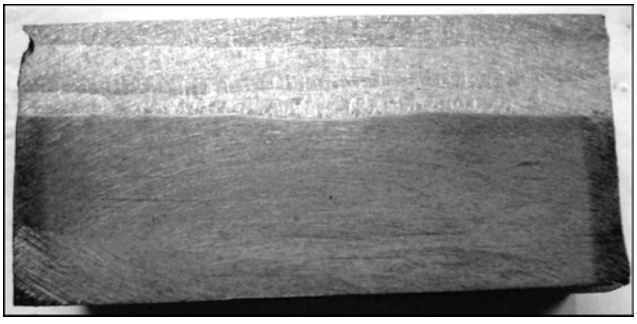

Figure 1. Macrostructure (×16) of deposited metal produced with new flux-cored wire

Under the conditions of friction wear resistance of high-alloyed deposited metal of Fe--Cr--Mn system is largely determined by hardening ability of austenite proper, which depends on its carbon content and intensity of formation of deformation martensite [5]. It is important to note that selection of rational composition of surfacing consumable and post-surfacing heat treatment mode allows optimization of development of martensite transformation at loading, as in this case it is possible to achieve the highest level of wear resistance of the deposited parts.

New flux-cored wire VELTEK-N285S (Fe--Cr--Mn) was developed, which is largely devoid of the above drawbacks. Proportion of carbon, chromium and manganese is selected so as to achieve immediately after surfacing an increased stability of deposited metal austenite relative to $\gamma \rightarrow \alpha''$ transformation compared to the known surfacing consumables of this type. For this reason technology of surfacing is greatly simplified and cuttability is improved, thus promoting a wider application of the developed flux-cored wire. The required intensity of running of deformation martensite transformation in service is achieved as a result of heat treatment, which is performed after surfacing to relieve inner stresses.

Optimum mode of surfacing by 3.6 mm wire is as follows: I = 350--400 A; U_a = 35--40 V; v_s = 40--45 m/h. AN-26 and REKORD SK EN-760 fluxes were used. Here a good formation of the deposited metal layers and their joining with each other and with the base metal are achieved. Lacks-of-penetration, slag

Relative wear resistance of metal deposited with commercial wires and developed flux-cored wire

Surfacing consumable	Heat treatment mode	Relative abrasive wear resistance	Relative wear resistance at sliding friction
PP-Np-18Kh1G1M	Surfacing + annealing at 550 °C for 1 h	1.0	1.0
Sv-12Kh13	Same	1.2	1.3
Sv-06Kh18N9T	»	0.6	0.7
Developed flux-cored wire	Surfacing + annealing at 600 °C for 1 h	2.3	3.2

inclusions and cracks are absent (Figure 1). Slag crust separability is good. At surfacing with the developed flux-cored wire the deposited metal layers have an austenitic structure with dispersed carbides located inside the grains (Figure 2). No microcracks form in the deposited metal. A structure of austenite with troostite net is found near the line of fusion with the base metal (65G steel). Base metal has a troostite structure near the fusion line.

Hardness measurement across the section showed that it is equal to *HB* 217--220 near the deposited metal surface, and to *HB* 230--240 in the middle part, and at the transition zone it increases to *HB* 280--300, which is the result of carbon, chromium and manganese redistribution in the zone of fusion with the base metal.

As follows from the testing results, wear resistance of the metal deposited with the developed flux-cored wire at sliding friction by shoe--roller schematic and abrasive impact practically does not differ from that value at deposition with Np-30Kh10G10T wire (GOST 10543--98) and is much higher than that value when using wires PP-Np-18Kh1G1M (GOST 26101--84), Sv-12Kh13 and Sv-06Kh18N9T (GOST 224--70) (Table). Application of the developed flux-cored wire of Fe--Cr--Mn system provides a structure of metastable austenite, strongly hardening at cold working. The degree of its hardening is the same as with Np-30Kh10G10T wire, but maximum hardness is achieved during 1.5--2 times longer time, which is due to a lower intensity of deformation martensite transformation at application of the new wire. This results in longer time of the stress relaxation process alongside hardening, thus impeding crack initiation and propagation [6]. After annealing at 600 °C applied after surfacing to relieve inner stresses, a multitude of dispersed carbides is found in austenite, which also promote an improvement of wear resistance. According to the data of X-ray analysis, deformation martensite content on the worn surface after annealing of the deposited metal is 1.5--2 times higher than without it (30--35 wt.%), which is indicative of its partial destabilization.

Long-term industrial testing of crane wheels surfaced by the developed flux-cored wire, providing the effect of self-hardening in operation, confirmed the results of laboratory investigations and demonstrated an increase of fatigue life of these parts more than 3 times compared to wheels reconditioned by the commercial PP-Np-18Kh1G1M wire. The achieved result was similar to that obtained with Np-30Kh10G10T wire. However, the new material also offers indubitable technological advantages in surfacing. Measurement of hardness of the working surface of wheels, surfaced by the new flux-cored wire, showed that it increased from *HB* 217--220 to 450--470. This is indicative of realization of the self-hardening effect in the deposited metal during wheel operation, which ensures an improvement of their fatigue life. No increased wear of the rails is found at increase of crane wheel wear resistance.

Machining of crane wheels reconditioned by the new flux-cored wire using tools fitted with hard alloys does not involve any technical difficulties. Figure 3 shows the appearance of a surfaced and machined wheel. It should be noted that the metal deposited with the new wire is more difficult to machine than when PP-Np-18Kh1G1M wire is used. By the degree

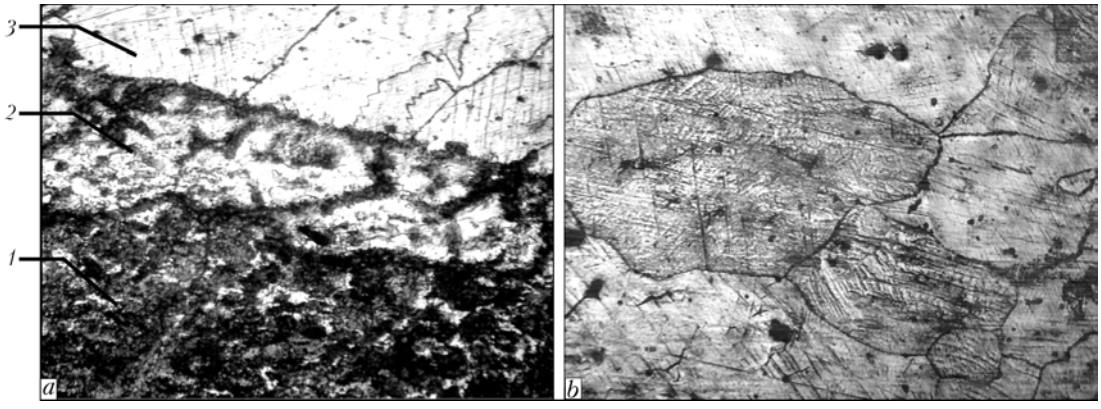

Figure 2. Microstructures (×550) of metal surfaced with the developed flux-cored wire: *a* ---- base metal and transition layer (*1* ---- base metal--troostite; *2* ---- transition layer--austenite with troostite net; *3* ---- deposited austenite layer); *b* ---- austenite structure of surface layer

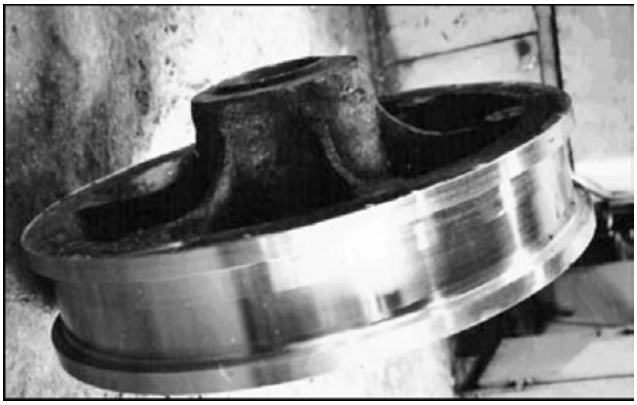

Figure 3. Appearance of deposited and machined wheel

of machinability it is close to the metal deposited with Sv-06Kh18N9T wire.

Thus, the developed flux-cored wire, providing the structure of metastable austenite in the deposited metal strengthened by dispersed carbides, features a good adaptability to fabrication in surfacing. Use of the new flux-cored wire owing to the effect of self-hardening in service allows an essential increase of fatigue life of the reconditioned parts.

The developed surfacing consumable can have a wide range of applications. It can be used not only for reconditioning crane wheels, but also wheels of railway rolling stock of enterprises, quarry wagons, various rollers, trunnions of steel-pouring ladles, rapidly wearing parts, exposed to low-aggressive media, for instance plungers in hydraulic presses, stop valves, and many other products, currently reconditioned by low-carbon surfacing consumable of different degrees of alloying. Cost effectiveness in this case is determined by costs (material, energy, labour, equipment downtime), which are much higher than the cost of the applied wire.

1. Bogachev, I.N., Mints, R.I. (1959) *Cavitation fracture of iron-carbon alloys*. Moscow; Sverdlovsk: Mashgiz.
2. Razikov, M.I., Iliin, V.P. (1964) *Welding and surfacing of cavitation-resistant steel 30Kh10G10*. Moscow: NIIMASh.
3. Bogachev, I.N., Mints, R.I. (1964) *Increase of cavitation-erosion resistance of machine parts*. Moscow: Mashinostroenie.
4. Tarasenko, V.V., Khomenko, G.V., Titarenko, V.I. et al. (2006) Experience of joint works of OJSC Zaporozhstal and EP Remmash in development and integration of new surfacing consumables. In: *Proc. of 2nd Sci.-Pract. Conf. on Improvement and Reequipment of Enterprises. Efficient Technologies of Repair and Recovery of Parts (in the frame of Int. Industrial Forum UkrIndustriya-2006)* (Dnepropetrovsk, 11 Oct., 2006). Dnepropetrovsk, 39–43.
5. Malinov, L.S., Malinov, V.L. (2001) Manganese-containing surfacing consumables. *The Paton Welding J.*, **8**, 30–32.
6. Malinov, L.S., Malinov, V.L. (2007) *Sparsely-doped alloys with martensitic transformations and strengthened technologies*. Kharkov: INTs KhFTI.

SEAM-TRACKING SYSTEM IN ANTICORROSION COATING UNITS

E.V. SHAPOVALOV and **V.A. KOLYADA**
E.O. Paton Electric Welding Institute, NASU, Kiev, Ukraine

A tracking system is developed which is designed for detection of weld reinforcement bead on a rotating pipe and controlling the polymer dosing at deposition of an anticorrosion polymer coating on the outer surface of welded pipes. System introduction will allow an essential improvement of uniformity of thickness of anticorrosion coating on pipes.

Keywords: *anticorrosion coating, longitudinal welded pipes, weld tracking, TV sensor, polymer dosing, communications controller*

At present steel pipes are the main element of industrial pipelines, which is promoted by their mass production, relatively low cost, high strength and adaptability to fabrication. Sound anticorrosion protection of welded pipes allows an essential improvement of pipeline performance. Under the conditions of mass production specialized units are used for application of a protective polymer coating on the outer surface of longitudinal welded large-diameter pipes [1]. Coating is applied automatically at rotation and simultaneous translational motion of the pipe at a low speed, whereas the linear speed of pipe surface motion at its rotation can be considerable (up to 0.5 m/s).

Pipe rotation is usually performed using rollers, which come into direct contact with the coated pipe surface. Here deformation of the polymer coating occurs in the area of the weld reinforcement bead, which usually is the cause for its non-uniform thickness. The following approach is used to solve this problem: when the reinforcement bead passes under the extruder for protective coating application, polymer dosing is increased, which results in a uniform thickness of the anticorrosion coating of welded pipes. In practice the value of linear speed of pipe surface movement is not constant, and depends on the errors in welded pipe manufacture, as well as other external factors, which does not allow controlling polymer dosing in keeping with the set program. Therefore, closed-loop control systems for polymer dosing with a weld sensor in feedback circuit are mainly used.

In the units for anticorrosion coating deposition on the outer surface of welded pipes closed-loop control of polymer dosing is most often performed using tactile sensors or point laser distance meters. Both determine the distance from the sensor to an individual point of the object. At any displacement of the pipe surface relative to such sensors, the amplitude of their output signals changes. Here the signal corresponding to weld reinforcement can be commensurate with the disturbances, arising as a result of pipe vibration or presence of mechanical defects on its surface. In practice this causes frequent «skipping» of the weld or false operation of polymer dosing control system.

To increase the reliability of weld detection on a rotating pipe, PWI developed a specialized tracking system, based on technical vision. Its main components are a TV sensor (TS) and communication controller (CC) (Figure 1). TS is mounted in front of the extruder for polymer application in the direction of pipe rotation. CC is integrated into the general control panel of the unit. System connection to the extruder is performed through two solid-state relays, which are part of CC. TS functioning is based on the principle of laser triangulation and is considered in greater detail in [2]. Laser beam, developed into a plane, forms a light trace on the pipe surface, which is recorded by a video camera. Its shape follows the pipe surface relief. A microcontroller built directly into TS is used for processing and analysis of images received by the video camera. As a result of analysis a decision is taken on the presence/absence of the weld under the TS. In case of its presence, also the co-ordinates of the center of weld reinforcement bead are determined in TS own system of co-ordinates and time markers are saved. At bead center crossing the origin of coordinate, TS based on the found co-ordinates and time markers, forms «Bead» output signal with its own marker, which is transmitted to CC through RS-485 interface.

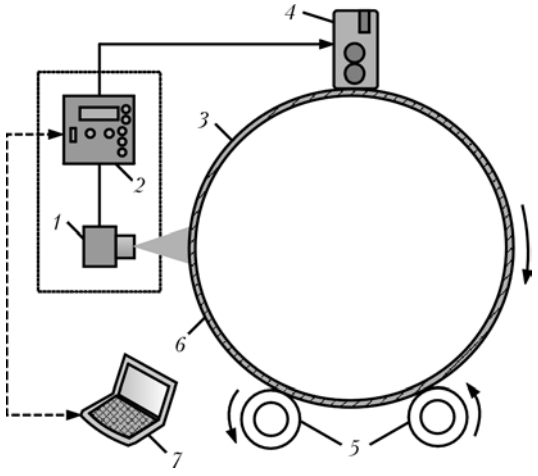

Figure 1. Schematic of integration of seam-tracking system in the unit for application of anticorrosion coating: *1* ---- TS; *2* ---- CC; *3* ---- rotating pipe; *4* ---- extruder for polymer application; *5* ---- pipe rotation rollers; *6* ---- weld reinforcement bead; *7* ---- external computer for parametrization of seam-tracking system

Figure 2. Front panel of communications controller

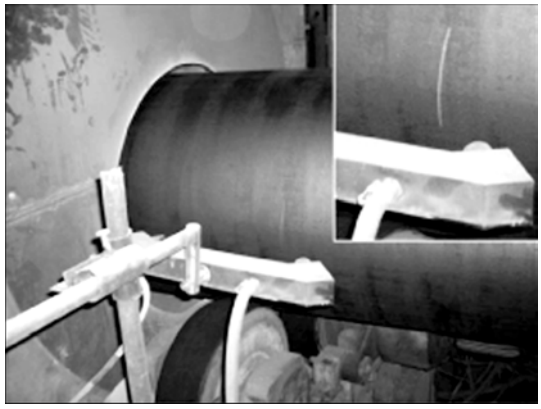

Figure 3. TV sensor scanning the surface of the rotating pipe

After receiving this signal, CC after a certain time interval of delay T_d relative to its time marker, forms «Polymer Feed» control signal with pulse duration T_p. By this signal CC solid-state relays switch-over and polymer dose is increased.

Forced air cooling of TS case and blowing of its viewing ports is envisaged in view of the high (up to 240 °C) pipe temperature and strong dust contamination of the working zone by powder primer. Respective adjustment knobs and liquid-crystal indicator located on CC front panel are used to set the values of time constants T_d and T_p (Figure 2). Liquid-crystal indicator has two displaying modes ---- main and additional one. Switching of these modes is performed by «Menu» button. In the main mode the current state of the tracking system and the set values of time constants T_d and T_p are displayed, in the additional mode ---- brief recommendations on fault handling are displayed on the liquid-crystal indicator. Monitoring of system conditions and displaying of the following text messages are performed:

- «Norm» ---- system is in the working mode, object being tracked (pipe) is in TS field of vision;
- «Object not found» ---- system is in standby mode, no object being tracked (pipe) is in TS field of vision;
- «No sensor reply» ---- critical error because of disturbance of the connection between TS and CC;
- «Sensor overheating» ---- system is in the working mode, temperature inside TS case is close to the critical one;
- «Working zone boundary» ---- system is in the working mode, distance between TS and pipe surface corresponds to the positive or negative boundary of TS working zone along a vertical, i.e. object being followed can move out of TS working zone during operation.

Respective LED indicators are used for visual support of «Bead» and «Polymer Feed» signals. System parametrization and adjustment are performed from an external computer through RS-232 interface. For protection from short-circuiting, fuses are envisaged in the circuit of CC relay connection to the extruder for polymer application.

To increase system reliability CC algorithmic support was complemented by the function of monitoring «Bead» signal period, which compares the period of TS forming this signal with an average period, calculated for the last several signals. If «Bead» signal does not come from TS during the calculated time, it is forcedly formed; now if the time of the above signal arrival does not correspond to the calculated average period, such a signal is ignored.

Seam-tracking system operates in real-time. TS and CC are fitted with watch dog timers, which ensure their restarting in the case of development of emergency situations. All the components of the above system have a galvanic decoupling.

Seam-tracking system is practically insensitive to pipe vibration, mechanical defects on its surface and outer light sources. The main technical characteristics of the system are given below:

TS frame frequency, Hz	60
Accuracy of detection of weld bead center, mm	±1
TS sensitivity (minimum admissible weld bead height), mm	0.5
Nominal distance from TS to pipe surface, mm	200
TS working zone, mm:	
along the vertical	±30
along the horizontal	±30
Time of CC relay switching, ms	1
Maximum load current on CC relay, A	2
Maximum load voltage on CC relay, V	28
Working temperature range, °C	–10–+85

Developed seam-tracking system was introduced into production at OJSC «Khartsyzsk Pipe Plant» (Ukraine) in two units for application of an anticorrosion polymer coating on the outer surface of large-diameter pipes. Figure 3 shows TS scanning the surface of a rotating pipe during application of an anticorrosion polymer coating. Tracking system allowed an essential increase of the reliability of detection of weld reinforcement and accuracy of execution of time constants, thus significantly improving the quality of pipe anticorrosion coating. Such systems can be used also in those fields of production automation, where recording of high-speed objects is required.

1. Ryabov, V.M., Usova, L.A. (1987) Factory-applied anticorrosive insulation for large-diameter pipes. *Metallurgist*, 31(**10**), 320–321.
2. Kiselevsky, F.N., Shapovalov, E.V., Kolyada, V.A. (2006) System of laser following of weld reinforcement. *The Paton Welding J.*, **1**, 42–44.

EXHIBITION «METALS OF SIBERIA: METALLURGY, MACHINE-BUILDING, METAL-WORKING, WELDING» IN NOVOSIBIRSK

Specialised industrial exhibition «Metals of Siberia: Metallurgy, Machine-Building, Metal-Working, Welding», one of the largest in the West Siberia, was held from 24 till 27 March in Novosibirsk at the International Exhibition Centre «ITE Siberian Fair». Despite the economical crisis and business decline, many manufacturers and suppliers of metal-working and welding equipment, tools, metal rolled stock, machine-tools and devices from different cities of Russia, from Germany, Italy, Finland and Switzerland presented their products and goods. Altogether, over 100 industrial enterprises and industrial equipment dealers took part in the Exhibition.

The exhibits included ferrous and non-ferrous metal rolled products, welding equipment and technologies, metal-working equipment and technologies, robotics, and industrial software products.

Modern welding equipment was demonstrated by companies «Promteks», «Sibmontazhkomplekt», «Shtorm-ITS» and «Uraltermosvar». Company «Shtorm-ITS» presented a series of German welding equipment, some of the samples of which having no analogues in the current market. Of special interest was a spot welding device presented by Company «Promteks». This device allows an almost instantaneous damage- and distortion-free welding of thin metal parts. Company «Evrotekhprom» exhibited a welding robot, which provides a high accuracy of positioning of the welding head during welding. Equipment, machine-tools and tools for metal-working, as well as engineering services constituted the major part of the exposition. Companies «Abamet», «Alpha Trend», Savelovsky Machine-Building Works, «Delkam-Novosibirsk», «Sovplim-Holding», Limited Liability Companies «Stanki RTM» and «Handtmann Russland», etc. demonstrated their products and equipment. The saturated business program of the Exhibition was dedicated to the key problems in the machine-building sector of Russia. Scientific-and Practical Conferences «Innovation Developments by Russian Machine-Tool Builders for Technical Re-equipment of Enterprises of the Siberian Region», «Problems of Increasing the Efficiency of Metal-Working in Industry at the Current Stage» and «Information Technologies in Industry» were held in the course of the Exhibition with a focus on the issues associated with supporting industrial enterprises during the crisis period, possibility of involving investments for science-intensive projects, interaction of research institutions with industrial enterprises, and practical application of advanced technologies.

The Annual VIII All-Russian Scientific-and-Practical Conference «Problems of Increasing the Efficiency of Metal-Working in Industry at the Current Stage» was held within the frames of the Exhibition, which served as a platform for sharing the experience between representatives of different scientific schools of the Siberian region. The event was organised by Open Joint Stock Company NPT and EI ORGSTANKINPROM (Novosibirsk), Limited Liability Company NPK MASHSERVISPRIBOR (Novosibirsk), and Journal «Obrabotka Metallov» (Novosibirsk), which jointly support the high status of the Conference. Specialists from the Novosibirsk State University, Kuzbass Technical University, Tomsk Polytechnic University, Yurga Technological Institute (branch) of the Tomsk Polytechnic University, I.I. Polzunov Altaisky State Technical University, and industry representatives took an active part in the Conference. This year the Conference consisted of two sessions ---- «Technology. Materials» and «Equipment. Tools». The papers presented at the sessions dealt with the problems of improvement of the technologies for mechanical and physical-engineering processing of metals, design of metal-working equipment and tools, increasing the efficiency of different types of tools, and optimisation of expenditures of industrial enterprises.

The contest of the welding skill aroused considerable interest at the Exhibition, with welders of the Novosibirsk enterprises and students of the corresponding schools and colleges participating in it.

Participation in such exhibitions with a wide business program promotes development of interaction between institutes of higher education and industrial enterprises, increase in competitiveness of domestic products, and attraction of investors to implementation of innovation research projects in different sectors of machine-building.

Drs A.A. Mokhovikov, D.A. Chinakhov

UNIVERSAL KL-115 MACHINE FOR EBW WITH 7-AXIS MOTION SYSTEM

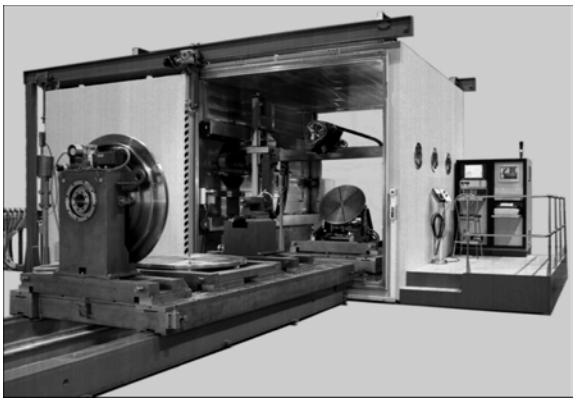

Vacuum chamber and slide doors have two shells, namely a stainless inner shell and outer shell of structural steel connected to each other by frames. The produced box section allows a significant lowering of the structure metal content with preservation of a high rigidity, that guarantees a high accuracy of the displacement mechanisms.

The cantilever mechanism of EB gun displacement allows moving the gun along *X, Y, Z* axes, as well as rotating it in *X*–*Y* (±90°) and *X*–*Z* (by 90°) planes.

Programmable CNC 7-axes motion control, simultaneous control of 4 coordinates.

Unique high voltage control regulator with vacuum tube detects and suppresses arcing, allowing continuous welding without discontinuties and defects.

Welding control with real time automatic seam tracking by RASTR secondary electron emission system.

Beam analysis system allows the operator to determine actual beam operating conditions prior to welding start and reduce weld parameter development time.

Lanthanum hexaboride cathodes are used for long life of more than 40 h at the power 60 kW, and prevent «beam walking» when the focus position is changed.

PC and programmable controllers are used.

Machine design

The vacuum chamber is a rectangular double-wall welded structure. Two sliding doors are moved letting workpiece to be loaded into the vacuum chamber for the welding. Movement mechanism of the EB gun has three moving axes: *X*–*X, Y*–*Y* and *Z*–*Z*. Accuracy of gun linear positioning along *X*–*X, Y*–*Y, Z*–*Z* axes is not less than ±0.1 mm. EB gun is mounted on the table along *Y*–*Y* axis and has two rotating axes: rotation ---- *QG* axis and tilt ---- *VG* axis. Accuracy of EB gun angular movement on *QG* and *VG* axes is better than 0.1°. Screws in ball-and-screw pairs, linear guides of all linear modules are covered by protective shields or encased to protect them from depositions.

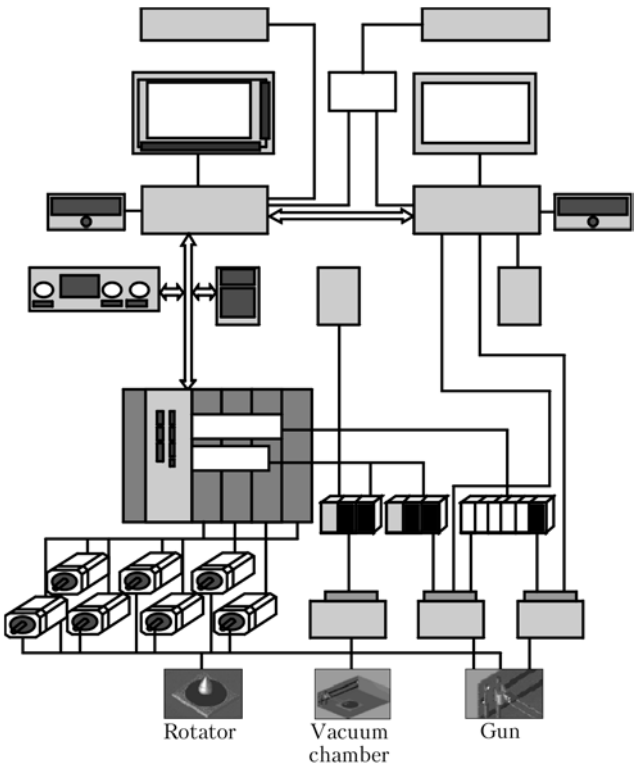

Machine is equipped with three rotators: with horizontal rotation axis, with vertical rotation axis and with tilt rotation axis. Two platforms are functionally designed for the placement of machine mechanisms, mounting of workpieces, their assembling, control of joints to be welded as well as for their transportation into the chamber. This allows assembling and fitting up of workpieces to be done on the one platform while welding of other workpieces is being done on the other platform.

Control system is based on open architecture principles of automation systems for machine tools.

Control system provides implementation of the following features:

• programmable CNC of 7-axes motion (3 linear gun axes, 2 rotary gun axes and 2 rotary rotator axes);
• any 4 axes of the 7 CNC axes selectable for coordinated contouring CNC of motions with linear and circular interpolations;
• full integration of all beam parameters with CNC control;
• operating in a fully automated mode, a semi-automated mode with user defined start and stop locations, and a manual mode including jog function;
• windows oriented GUI (User Graphic Interface) for programming, system diagnostics, data logging, seam tracking, seam/weld viewing, and real-time process control;
• sequencing blocks of programmed data together into master programs;
• automatic real time teaching and seam tracking via seam tracking system RASTR;
• off-line programming and remote communication;
• PLC control of vacuum system and power supply in all modes;
• diagnostic tools for trouble-shooting faults or errors;
• data logging of process control parameters.

Main technical parameters for KL-115 machine

Overall machine sizes (l × w × h), mm	15960 × 10390 × 3740
Weight, t	48
Vacuum chamber internal sizes (l × w × h), mm	4040 × 2950 × 2950
Working pressure in chamber, Torr	not lower than $1 \cdot 10^{-4}$
Time before working pressure in chamber and gun is obtained, min	max 25
EB gun movements with positioning accuracy of ±0.1 mm along coordinates *X*–*X*, *Y*–*Y*, *Z*–*Z*, mm	3000, 1800, 2000
Gun tilt angle in *X*–*Z* plane, deg	90
Gun rotation angle with 0.1° accuracy in *X*–*Y* plane, deg	not less than ±90
EB gun traveling speed along linear coordinates, mm/s	1.66–33.3

Electron beam gun and power supply

Power, kW	60
Accelerating voltage, kV	$60 \pm 0.5 \cdot 10^{-2}$
Beam current, mA	1–1000
Cathode life, h	40
Beam deflection angle, deg	±3.5

Technical parameters provided by the Buyer

Mains	380 V, 50/60 Hz
Consumed power, kV·A	max 250
Cooling water flow rate at temperature of 20 °C and pressure of 4 kg/cm^2, l/h	2630
Compressed air pressure, kg/cm^2	6

UNIVERSAL KL-118 MACHINE FOR EBW WITH 7-AXIS MOTION SYSTEM

Vacuum chamber and slide doors have two shells, namely a stainless inner shell and outer shell of structural steel connected to each other by frames. The produced box section allows a significant lowering of the structure metal content with preservation of a high rigidity, that guarantees a high accuracy of the displacement mechanisms.

The cantilever mechanism of EB gun displacement allows moving the gun along *X*, *Y*, *Z* axes, as well as rotating it in *X*–*Y* (±90°) and *X*–*Z* (by 90°) planes.

Programmable CNC 7-axes motion control with the capability of simultaneous control of 4 coordinates.

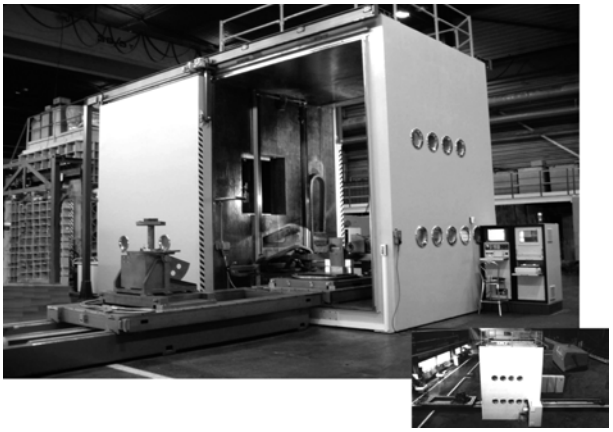

Unique high-voltage control regulator with vacuum tube detects and suppresses arcing, allowing continuous welding without discontinuties and defects.

Welding control with real time automatic seam tracking by RASTR secondary electron emission system.

Beam analysis system allows the operator to determine actual beam operating conditions prior to welding start and reduce weld parameter development time.

Lanthanum hexaboride cathodes are used for long life of more than 40 h at 60 kW power, preventing «beam walking» when the focus position is changed.

PC and programmable controllers are used.

Machine design and parameters

The vacuum chamber is a rectangular double-wall welded structure. Two sliding doors are moved letting workpieces to be loaded into the vacuum chamber for the welding. Movement mechanism of the EB gun has three moving axes: *X*–*X*, *Y*–*Y* and *Z*–*Z*. The accuracy of gun linear positioning along *X*–*X*, *Y*–*Y* and *Z*–*Z* axes is ±0.1 mm. EB gun is mounted on the table along *Y*–*Y* axis and has two moving axes: rotation ---- *QG* axis and tilt ---- *VG* axis. Accuracy of EB gun angular movement on *QG* and *VG* axes is better than 0.1°. Screws in ball-and-screw pairs, linear guides of all linear displacement modules are covered by protective shields or encased to protect them from depositions.

Machine is equipped with three rotators: with horizontal rotation axis, with vertical rotation axis and with tilt rotation axis. Two platforms are functionally designed for placement of machine mechanisms, mounting of workpieces, their assembling, control of assembled butt joints, and their transportation into the chamber. This allows saving the work time during assembling and fit up of workpieces on the one platform due to welding of other workpieces being done on the other platform.

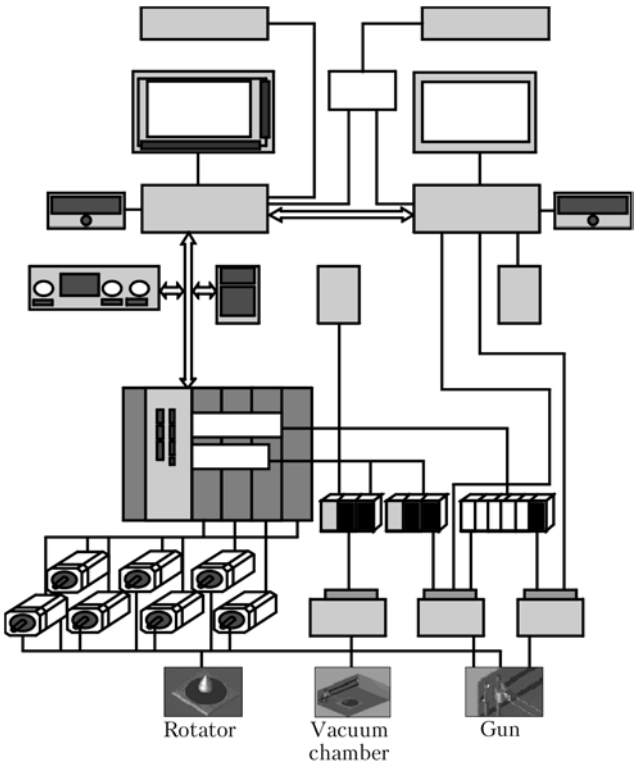

Control system is based on open architecture principles of automation systems for machine tools.

Control system provides implementation of the following features:

- programmable CNC of 7-axes motion (3 linear gun axes, 2 rotary gun axes and 2 rotary rotator axes);
- any 4 axes of the 7 CNC axes selectable for coordinated contouring CNC of motions with linear and circular interpolations;
- full integration of all beam parameters with CNC;
- operating in a fully automated mode, a semi-automated mode with user defined start and stop locations, and a manual mode including jog function;
- windows oriented GUI (User Graphic Interface) for programming, system diagnostics, data logging, seam tracking, seam/weld viewing, and real-time process control;
- sequencing blocks of programmed data together into master programs;
- automatic real time teaching and seam tracking via seam tracking system RASTR;

- off-line programming and remote communication;
- PLC control of vacuum system and power supply in all modes;
- diagnostic tools for trouble-shooting faults or errors;
- data logging of process control parameters.

Main technical parameters for KL-118 machine

Overall machine sizes (l × w × h), mm	15070 × 11690 × 6610
Weight, t	51
Vacuum chamber internal sizes (l × w × h), mm	3800 × 3600 × 4800
Working pressure in chamber, Torr	not higher than $1 \cdot 10^{-4}$
Time before working pressure in chamber and gun is obtained, min	max 25
EB gun movements with positioning accuracy ±0.1 mm along coordinates *X*–*X*, *Y*–*Y*, *Z*–*Z*, mm	2800, 2500, 3700
Gun tilt angle in *X*–*Z* plane, deg	90
Gun rotation angle with accuracy 0.1° in *X*–*Y* plane, deg	not less than 90
EB gun traveling speed along linear coordinates, mm/s	1.66–33.3

Electron beam gun and power supply

Power, kW	60
Accelerating voltage, kV	$60 \pm 0.5 \cdot 10^{-2}$
Beam current, mA	1–1000
Cathode life-time, h	40
Beam deflection angle, deg	±3.5

Technical parameters provided by the Buyer

Mains	380 V, 50/60 Hz
Consumed power, kV·A	max 300
Cooling water flow rate at temperature of 20 °C and pressure of 4 kg/cm^2, l/h	4566
Compressed air pressure , kg/cm^2	6

UNIVERSAL MACHINE FOR ELECTRON BEAM WELDING *MODEL 101*

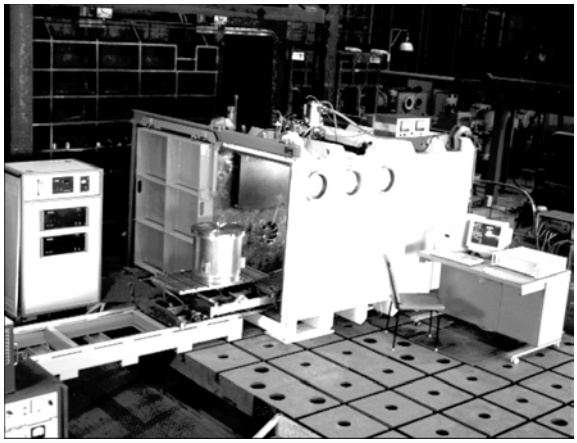

Universal production machine for EBW of a wide range of cylindrical and flat workpieces.

PC and programmable controllers are used.

Real-time seam tracking and monitoring of EBW process by RASTR-3 system on the basis of secondary electron emission.

Power source with the electron tube flashless system.

5, 15, 30 or 60 kW electron beam gun and power source at 60 kV.

Machine design

• Work chamber has two sliding doors. For loading and unloding, the workpiece table is moved out of the work chamber onto the runout platform. This is especially necessary for welding of large heavy workpieces with commensurately large clamping devices. The table accommodates a 2-axis-manipulator for welding of flat workpieces or a rotator for circumferential welding. The electron beam gun with an optical viewing system is mounted in one of the three openings on the upper cover of the chamber.

• The gun has an independent turbomolecular pumping system. The cathode area is isolated by a vacuum valve to keep the gun under vacuum when the work chamber is vented. Precision of the guidance and drive sysems equals that of the high-precision machine tools operation with tolerances in the hundredth-of-a-millimeter range.

Technical data for machine of model 101

Mains	50 kV·A, 380 V ± 10 %, 50–60 Hz
Cooling water flow rate at < 25 °C, l/min	23
Vacuum chamber inner dimensions, m	1.1 × 2.4 × 1.4
Time of pumping down at the vacuum of $2 \cdot 10^{-4}$ Torr, min	8
Workpiece weight, kg	max 500

Application. Welding of high-precision structures; welding and repair in gas turbine engine fabrication; welding of a wide range of power engineering products.

UNIVERSAL MACHINE FOR ELECTRON BEAM WELDING *MODEL 102*

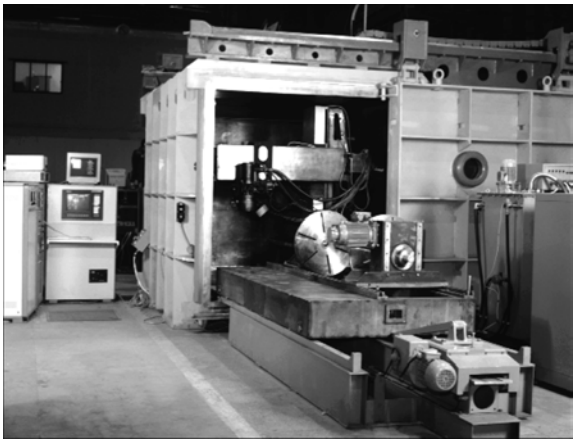

- Universal production machine for EBW of a wide range of cylindrical and flat workpieces.
- PC and programmable controllers are used.
- Real-time seam tracking and monitoring of EBW process by RASTR-3 system on the basis of secondary electron emission.
- Power source with the electron tube flashless system.
- Mobile type 15, 30 or 60 kW electron beam gun at 60 kV.

Machine design

The work chamber has two sliding doors. For loading and unloding, the workpiece table is moved out of the work chamber onto the runout platform. This is especially necessary for welding of large heavy workpieces with commensurately large clamping devices. The table accommodates the universal rotator with horizontal or vertical axis, and back centre. The EB gun 3-axis-manipulator has the travelling distance in *X*-direction ---- 2000 mm, in *Y*-direction ---- 800 mm and in *Z*-direction ---- 800 mm. Precision of the guidance and drive systems equals that of the precision machine tools operation with tolerances in the hundredth-of-a-millimeter range.

The gun can be mounted in any spatial position and has an independent turbomolecular pumping system. The cathode area is isolated by a vacuum valve to keep the gun under vacuum when the work chamber is vented.

Technical data for machine of model 102

Set power	130 kV·A, 380 V ± 10 %, 50–60 Hz
Cooling water flow rate at < 25 °C, l/min	20
Vacuum chamber inner dimensions, m	2 × 2 × 3
Time of evacuation at the vacuum of $2 \cdot 10^{-4}$ Torr, min	20
Workpiece weight, kg	max 1000

Application. Welding and repair in turbine engine fabrication; selection of welding technology for a wide range of workpieces.

Prof. Nazarenko O.K.
E-mail: nazarenko@technobeam.com.ua
http://www.nas.gov.ua/pwj/beam
http://paton.kiev.ua/eng/inst/ntkstructure/deplist/571.html

INFORMATION FOR CONTRIBUTORS TO
THE PATON WELDING JOURNAL

«The Paton Welding Journal» is an English translation of the monthly «Avtomaticheskaya Svarka» journal published in Russian since 1948.

THE PATON WELDING JOURNAL is a scientific journal publishing fundamental and applied papers and short notes in the area of:

- *weldability of structural materials*
- *welding different types of steels and cast irons*
- *welding non-ferrous metals, including aluminium, titanium, etc.*
- *joining dissimilar and composite materials*
- *welding refractory metals and alloys*
- *welding cryogenic materials*
- *arc welding*
- *flash-butt welding*
- *electron beam and laser welding*
- *explosion welding and cutting*
- *friction welding*
- *electroslag welding*
- *soldering and brazing*
- *advanced structural materials*
- *surfacing and coating deposition*
- *cutting*
- *computer technologies in welding*
- *strength of welded joints and structures*
- *residual stresses and strains*
- *calculation and design of welded joints and structures*
- *automation of welding fabrication*
- *estimation of residual life of welded structures*
- *welding for fabrication of unique structures*
- *welding and repair in thermal and nuclear power engineering*
- *advances in underwater welding, cutting and repair*

The journal accepts also advertisements and announcements of conferences and publications on related topics.

THE PATON WELDING JOURNAL is published monthly.

Subscription requests should be sent to the Editorial Office.

Manuscripts should be submitted in duplicate in English, and supplemented with a text file and figures on a diskette. An electronic copy may be submitted by e-mail.

The rules for submission of electronic copies are as follows:

- an electronic copy should be submitted on a diskette or by e-mail simultaneously with sending a hard copy of the manuscript;
- acceptable text formats: MSWord (rtf, doc);
- acceptable graphic formats for figures: EPS, TIFF, CDR. Figures created using software for mathematical and statistical calculations should be converted to one of these formats.

Manuscripts should be supplemented with:

- official letter signed by a chief manager of the institution where the work was performed. This rule does not apply to papers submitted by international groups of authors.

Title page:

- title of the paper and name(s) of the author(s);
- name of affiliated institution, full address, telephone and fax numbers, e-mail addresses (if available) for each author.

Abstract: up to 100 words, must be presented in English. Before the abstract text one should indicate in the same language: the paper title, surnames and initials of all authors.

Key words: their amount must not exceed eight word units. In the specific cases it is acceptible to use two- or three-word terms. These words must be placed under the abstract and written in the same language.

Text should be printed double-spaced on white paper (A4 format) with a 12-point font. Titles of the paper and sections should be typed with bold capitals.

Tables should be submitted on separate pages in the format of appropriate text processors, or in the text format (with columns separated by periods, commas, semicolons, or tabulation characters). Use of pseudo-graphic characters is not allowed.

List of references should be double-spaced, with references numbered in order of their appearance in the text.

Captions for figures and tables should be printed in the manuscript double-spaced after the list of references.

Pictures will be scanned for digital reproduction. Only high-quality pictures can be accepted. Inscriptions and symbols should be printed inside. Negatives, slides and transparencies are accepted.

Figures: each figure should be printed on a separate page of the manuscript and have a size not exceeding 160 × × 200 mm. For text in figures, use 10-point fonts. All figures are to be numbered in order of their appearance in the text, with sections denoted as (a), (b), etc. Placing figure numbers and captions inside figures is not allowed. On the back side, write with a pencil the paper title, author(s) name(s) and figure number, and mark the top side with an arrow.

Photographs should be submited as original prints.

Color printing is possible if its cost is covered by the authors.

For information about the rules and costs, contact the Executive Director.

No author's fee is provided for.

Publication in TPWJ is free of charge.

Manuscripts should be sent to:

Dr. Alexander T. Zelnichenko
Executive Director of
«The Paton Welding Journal»,
11, Bozhenko Str.,
03680, Kiev, Ukraine
International Association «Welding»
Tel.: (38044) 287 67 57, 529 26 23
Fax: (38044) 528 04 86
E-mail: journal@paton.kiev.ua
www.nas.gov.ua/pwj